Dynamics of Cyclones and Precipitation over the Middle East

by

Ali Raheem Tuaimah Al Nassar

Under the direction of Marta Alarcón Jordán (Universitat Politècnica de Catalunya)
and Josep Lluís Pelegrí Llopart (Institut de Ciències del Mar, CSIC)

A thesis submitted to the Universitat Politècnica de Catalunya in conformity with the requirements for the Doctoral degree, speciality in Computational and Applied Physics

Department of Physics
Universitat Politècnica de Catalunya

Barcelona, 4 July 2018

Dynamics of Cyclones and Precipitation over the Middle East

Ali Raheem Tuaimah Al Nassar

Doctorate in Computational and Applied Physics

Department of Physics
Universitat Politècnica de Catañunya

2018

Abstract

Precipitation is one of the most important, and also difficult to predict, elements of climate. This difficulty is associated with the transport of moisture through weather fronts that change their pathway, shape and intensity at different spatial and temporal scales. Despite this difficulty, a proper rainfall prediction is necessary both to quantify the resources and infrastructures necessary to bring water to farm fields and cities and to anticipate the occurrence of extreme precipitation episodes that may cause human death and huge economic losses.

The main objective of this dissertation is to investigate the influence of weather systems on the patterns and amount of precipitation over Iraq, from its variability at different temporal scales (daily to inter-decadal) to the contribution of severe precipitation events to total rainfall and the mechanisms underlying these extreme episodes. With this objective, we use monthly (1938-2016) and daily (2005-2016) precipitation records from a meteorological station in the city of Baghdad, ran by the Iraqi Meteorological and Seismology Organization. This station is located in the large central plains of Iraq, (33.33°N, 44.43°E) and 34 m elevation, where topographic variability is nearly absent.

Additionally, we use the temperature, humidity, geopotential height, horizontal and vertical velocity, horizontal divergence, relative vorticity and potential vorticity fields from the ERA-Interim global atmospheric reanalysis, available four times a day on a $0.75^{o} \times 0.75^{o}$ latitude-longitude grid from the European Centre for Medium-Range Weather Forecasts (ECMWF). These data, downloaded for a domain extending from 0°E to 60°E and from 10°N to 60°N, are then used to calculate the

equivalent potential temperature, precipitable water, moisture flux, moisture flux convergence, Q-vector divergence, relative vorticity and potential vorticity advection, as well as several instability indices (K, CAPE, SWEAT and LI).

The body of the work is split in four different sections. After an introductory chapter, in Chapter 2 we focus on the analysis of the monthly rainfall data for the 1938-2016 period. For most of our analysis we use natural years, running from 1 July to 30 of June, so that years are logically separated by the dry summer season. The mean annual precipitation is 135.8 ± 61.9 mm/yr and the mean monthly precipitation is 11.3 ± 18.7 mm (increasing to 17.1 ± 20.9 mm if we ignore the June-August dry months). Despite the linear trend for the entire period is small, there are decades (1950s and 1960s) of relatively high mean-annual precipitation (150-170 mm/yr) and other ones (1990s and 2000s) with substantially lower values (100-120 mm/yr). The monthly rainfall time series also shows the existence of substantial inter-annual variations, with annual precipitation values ranging between 29.3 and 307.7 mm (2012 and 1974, respectively). A probability density function of annual rainfall allows us to define arid and wet years – annual rainfall below/above the 25/75 percentiles – with mean values of 64.6 and 220.1 mm/yr, respectively. The seasonal cycle changes substantially between arid and wet years, with December-February receiving most rainfall (10-15 mm/month, with December displaying the highest variability) during the arid years, and November-April collecting most precipitation (30-40 mm/month, with highly variable March, April and November) during the wet years. The inter-annual changes in precipitation show no correlation with a global index for El Niño-Southern Oscillation.

In Chapter 3 we analyse a 12-year time series of daily data (2005-2016) from the Baghdad meteorological station. For this period the annual precipitation was 130.8 ± 67.1 mm/yr, with annual values varying between 29.3 and 278.1 mm in only two years (2012 and 2014, respectively). From the ERA-Interim data, and with the help of a numerical algorithm, we identify the contribution of cut-off lows to precipitation: 38 events (14 with rainfall over 20 mm) contributed to 43.4% of the total precipitation over Baghdad. Cut-off lows occur all year long but those happening between October and December account for one-third of the total annual precipitation. We find that most of the inter-annual variation in rainfall is associated with these cut-off lows, its contribution increasing from 31.3 mm during the three dry years to 512.3 mm during the three wet years (a 16-factor increase).

In Chapter 4 we have carefully considered the dynamics behind the 18-20 November 2013 extreme rainfall episode, the largest one since 1980. The middle and upper atmospheric conditions resulted from the development of an omega block into a Rex block. The eastern part of the cyclonic structure of the Rex block was experiencing horizontal divergence and the associated upward motions reached all the way from 1000 to 250 hPa. Simultaneously, the lower atmosphere (1000 to 700 hPa) exhibited intense southerly cool winds that brought large amounts of moisture into central Iraq. These moist airs were the result of substantial water evaporation and heat release from the Red Sea to the atmosphere, as evidenced by the concurrent cooling of its surface waters.

Finally, in Chapter 5 we again combine the daily Baghdad rainfall data with the ERA-Interim analysis to explore the weather patterns associated with the 20 extreme precipitation events for the 2005-2016 period. These events brought 805.2 mm (51.3%) of the total precipitation to the Baghdad station, distributed as follows: 7 events related with Rex block conditions (causing the highest precipitation, 324.1 mm or 40.3% of the total extreme-event precipitation), 7 episodes related with cut-off low (252.6 mm or 31.4%), 2 instances related with jet streaks (95.3 mm or 11.8%), and 4 events related with upper-air troughs (133.2 mm or 16.5%). We briefly characterize the synoptic conditions during these 20 episodes, with a more detailed description of one case of jet streak, upper-air trough and cut-off low.

Dinámica de Ciclones y Precipitación sobre el Medio Oriente

Ali Raheem Tuaimah Al Nassar

Doctorado en Física Computacional y Aplicada

Departament de Física
Universitat Politècnica de Catalunya

2018

Resumen

La precipitación es uno de los elementos climáticos más importantes y difíciles de predecir. La dificultad se asocia con el transporte de humedad por medio de los frentes meteorológicos que cambian su camino, forma e intensidad en diferentes escalas espaciales y temporales. A pesar de esta dificultad, es necesaria una predicción adecuada de la lluvia para cuantificar los recursos y las infraestructuras necesarias para llevar el agua a los campos agrícolas y las ciudades, y también para anticipar la ocurrencia de episodios de precipitación extrema que pueden causar muertes humanas y grandes pérdidas económicas.

El objetivo principal de esta disertación es investigar la influencia de los sistemas climáticos en los patrones y la intensidad de la precipitación en Iraq, desde su variabilidad a diferentes escalas temporales (desde diarias hasta interdecadal) hasta la contribución de los eventos de precipitación severa a la precipitación total y los mecanismos subyacentes a estos episodios extremos. Con este objetivo, utilizamos registros de precipitación mensual (1938-2016) y diaria (2005-2016) provenientes de una estación meteorológica en la ciudad de Bagdad, dirigida por la organización de meteorología y sismología iraquí. Esta estación se encuentra en las grandes llanuras centrales de Iraq, (33.33°N, 44.43°E) y 34 m de elevación, donde la variabilidad topográfica es casi inexistente. Utilizamos además la temperatura, humedad, altura geopotencial, velocidad horizontal y vertical, divergencia horizontal, vorticidad relativa y campos de vorticidad potencial provenientes del análisis atmosférico global ERA-Interim, disponible cuatro veces al día en una malla de 0.75º×0.75º de latitud-longitud, provenientes del Centro Europeo de Pronósticos Meteorológicos de Medio Alcance

(ECMWF). Estos datos, descargados para un dominio que se extiende de 0° a 60°E y de 10°N a 60°N, se usan para calcular la temperatura potencial equivalente, el agua precipitable, el flujo de humedad, la convergencia del flujo de humedad, la divergencia del vector Q , la vorticidad relativa y la advección de vorticidad potencial, así como varios índices de inestabilidad (K, CAPE, SWEAT y LI).

El cuerpo del trabajo se divide en cuatro secciones diferentes. Después de un capítulo introductorio, en el Capítulo 2 nos enfocamos en el análisis de los datos mensuales de lluvia para el período 1938-2016. Para la mayor parte de nuestro análisis usamos años naturales, desde el 1 de julio hasta el 30 de junio, para que los años estén lógicamente separados por la temporada seca de verano. La precipitación media anual es de 135.8 ± 61.9 mm/año y la precipitación media mensual es de 11.3 ± 18.7 mm (aumentando a 17.1 ± 20.9 mm si ignoramos los meses secos de junio a agosto). A pesar de que la tendencia lineal para todo el período es pequeña, hay décadas (1950 y 1960) de precipitación anual media relativamente alta (150-170 mm/año) y otras (1990 y 2000) con valores sustancialmente menores (100-120 mm/año). La serie temporal de lluvias también muestra la existencia de variaciones interanuales sustanciales, con valores de precipitación anual que oscilan entre 29,3 y 307,7 mm (2012 y 1974, respectivamente). La función de densidad de probabilidad de la precipitación anual nos permite definir los años áridos/húmedos (precipitación anual inferior/superior a los percentiles 25/75) con valores medios de 64.6 y 220.1 mm/año, respectivamente. El ciclo estacional cambia sustancialmente entre los años áridos y húmedos, con diciembre-febrero recibiendo la mayoría de las precipitaciones (10-15 mm/mes, con diciembre presentando la mayor variabilidad) durante los años áridos, y noviembre-abril recogiendo la mayoría de las precipitaciones (30-40 mm/mes, con marzo, abril y noviembre altamente variables) durante los años lluviosos. Los cambios interanuales en las precipitaciones no muestran correlación con un índice global de El Niño-Oscilación del Sur.

En el Capítulo 3 analizamos una serie temporal de 12 años de datos diarios (2005-2016) de la estación meteorológica de Bagdad. Para este período, la precipitación anual fue de 130.8 ± 67.1 mm/año, con valores anuales que varían entre 29.3 y 278.1 mm en solo dos años (2012 y 2014, respectivamente). A partir de los datos de ERA-Interim, y con la ayuda de un algoritmo numérico, identificamos la contribución de los *cut-off lows* a la precipitación: 38 eventos (14 con precipitaciones superiores a 20 mm) contribuyeron al 43-4% de la precipitación total sobre Bagdad. Los *cut-off lows* ocurren todo el año, pero aquellos que tienen lugar entre octubre y diciembre

representan un tercio de la precipitación anual total. Encontramos que la mayoría de las variaciones interanuales en las precipitaciones están asociadas a estos cut-off lows, con su contribución aumentando desde 31,3 mm durante los tres años secos a 512,3 mm durante los tres años húmedos (un aumento en un factor de 16).

En el Capítulo 4 hemos considerado cuidadosamente la dinámica detrás del episodio de lluvia extrema del 18-20 de noviembre de 2013, el mayot desde 1980. Las condiciones de la atmósfera media y alta resultaron del desarrollo de un bloque omega hacia un bloque Rex, con la parte oriental de la estructura ciclónica del bloque Rex experimentando intensa divergencia horizontal y fuertes movimientos ascendentes entre 1000 y 250 hPa. Simultáneamente, la atmósfera inferior (de 1000 a 700 hPa) exhibía intensos vientos fríos del sur que traían grandes cantidades de humedad al centro de Iraq. Estos aires húmedos fueron el resultado de una evaporación sustancial del agua, y la consecuente liberación de calor, desde el Mar Rojo hacia la atmósfera, como lo demuestra el enfriamiento simultáneo de sus aguas superficiales.

Finalmente, en el Capítulo 5, nuevamente combinamos los datos diarios de precipitaciones de Bagdad con el análisis ERA-Interim para explorar los patrones climáticos asociados con los 20 eventos de precipitación extrema para el período 2005-2016. Estos eventos trajeron 805.2 mm (51.3%) de la precipitación total a la estación de Bagdad, distribuidos de la siguiente manera: 7 eventos relacionados con las condiciones del bloque Rex (causando la precipitación más alta, 324.1 mm o 40.3% de la precipitación total del evento extremo), 7 episodios relacionados con *cut-off lows* (252.6 mm o 31.4%), 2 casos relacionados con *jet streaks* (95.3 mm o 11.8%) y 4 eventos relacionados con *upper-air troughs* (133.2 mm o 16.5%). Brevemente caracterizamos las condiciones sinópticas durante estos 20 episodios, con una descripción más detallada de un caso de *cut-off low*, *jet streak* y *upper-air trough*.

Acknowledgments

First and foremost, I thank Allah for bringing me his grace and mercy; without his blessings it would have not been possible that all my wishes and dreams became reality. I am forever grateful to my God.

I would like to express my special appreciation and thanks to my advisor Dr. Marta Alarcón Jordán, she has been a tremendous mentor to me. Her advice on both research as well as on my career has been priceless.

I want to express my sincere thanks and deepest gratitude and appreciation to my first co-director Dr. Pablo Sangrà, who died in 13 August 2016, a noble soul and excellent oceanographer and meteorologist, may his spirit fly in peace.

I would like to express my sincere gratitude to my co-director Dr. Josep Lluís Pelegrí for his continuous support to my PhD study and related research, for his patience, motivation, and immense knowledge. His guidance helped me all the time to overcome the numerous obstacles I have faced through my research, getting the best-quality results.

I would like to thank my fellow doctoral students for their feedback, and my friend Dr. Hussein K. A. Hussein for sending Arabic references. In addition, I would like to express my gratitude to the staff of UPC, especially to Elena (Oficina de Mobilitat Internacional), Alicia Sánchez Nabau and Roser Alonso Bargalló.

I am deeply thankful to my beloved family – my parents, my wife, my brothers and sister, and my daughter Zahraa and little boys Mohammed and Hussein – for supporting me spiritually throughout the writing of this thesis and in every facet of my life.

I acknowledge the European Centre for Medium-Range Weather Forecasts for making freely available the ERA-Interim reanalysis. We also wish to thank Dr. Climente Ramis and Dr. Agustí Jansà for many useful comments and Marc Gasser, Ignasi Vallès and Alex Antares for their help with the computer programs.

I also acknowledge the Department of Physics at the Universitat Politècnica de Catalunya (UPC), for the facilities and great working conditions they have provided to me, as well as the four projects funded by the Spanish government that have supported the work done as part of this thesis: Atmospheric bio-aerosols: levels, transport and impacts (BATMAN, reference CTM2017-89565-C2-2-P), New technologies for the study of the diversity and dynamics of aerobiological components and for their forecast based on meteorology (TECBIOMET, reference CGL2012-39523-C02-02), Western boundary retroflections: connecting latitudinal transports and gyre recirculations in the Atlantic Ocean (VA-DE-RETRO, reference CTM2014-56987-P), and Flujos de Carbono en un sistema de afloramiento costero (Cabo Blanco, NW de Africa): modulación a submesoescala de la producción, exportación y consumo de carbon (FLUXES, reference CTM2015-69392-C3-3-R).

Finally, I would like to express my gratitude to the Iraqi Ministry of Higher Education and Scientific Research and Mustansiriyah University for awarding me the scholarship and for the financial support during years of research at UPC.

Table of Contents

List of Tables

List of Figures

Chapter 1

Introduction

1.1 Iraq location and climate

Iraq is a country located in the heart of the Middle East extending between 29.5°N- 37.22°N and between 38.45° E-48.45º E (Figure 1.1). It is surrounded by Turkey to the north, Iran to the east, Saudi Arabia, Kuwait and the Persian Gulf to the south and east, and Syria and Jordan to the west. Baghdad, the capital, is located at the central part of Iraq. The main water resources of Iraq come from two great rivers that run through the country from north to south: the Tigris in the eastern part of the country and the Euphrates in the centre (Zakaria et al., 2012; Al-Ansari, 2013). Both rivers confluence at Al-Qurnah, a town located NW of Basra, to form the Shatt-al-Arab River in the south of Iraq (Figure 1.2).The length of these two large rivers, as they run through Iraq, are 1213 km for the Euphrates and 1418 km for the Tigris. In early May, the flow of the Euphrates can reach 50,000 $m^3 s^{-1}$, whereas the Tigris reaches up to 80,000 $m^3 s^{-1}$ in March and April (Jassim and Goff, 2006).

The morphology of Iraq is relatively simple, being summarized as divided into four topographic areas (Figure 1.2):

1. Mountainous region. It is located in the northern and north-eastern parts of Iraq, covering about 92,000 km^2, or about 20% of the total area of Iraq. Its altitude reaches 3609 m at the highest point in the Taurus and Zagros massifs, bordering with Turkey and Iran, which reach up to 3600 m in altitude. This is the rainiest region of Iraq, with yearly precipitation ranging from 400 to 1000 mm.
2. Mesopotamian plain. It is located in central and southern Iraq, spreading over about 132,500 km^2, or about 30% of the total area of Iraq. It is an alluvial plain extending from north of Baghdad to the Persian Gulf. There is high deposition of sediments by the Tigris and Euphrates Rivers, composed by large amounts of sand, clay and salts. The area is generally of low altitude and flat. Its yearly precipitation ranges from 50 to 200 mm.

3. Desert plateau. It comprises the largest region of Iraq, located in the western part of the country and occupying about 40% of the total area of Iraq. Its altitude is about 100-1000 m, and its yearly precipitation ranges between 50 and 200 mm.

Figure 1.1. Location of Iraq in the Middle East with political borders.

4. Undulating region: It is the lowest altitude region of Iraq, covering about 10% of the country. It is a transitional area between the sedimentary plain and the highlands region. It is located between the Tigris, north of Samarra, and the Euphrates, north of Hit. Its yearly precipitation ranges from 250 to 450 mm.

According to the Köppen's climatic classification (Khidher and Pilesjö, 2015), Iraq belongs to three main climatic regions, namely Mediterranean (Csa), steppe (Bsha), and desert (Bwha) climates (Figure 1.3). The Mediterranean climate region is located north of Iraq and includes the mountainous region. It is the rainiest region although, as in other regions, summer is characterized almost by absence of precipitation. The middle region of Iraq has characteristics of steppe climate. It is a semi-arid and continental climate, typically cold in winter and hot in summer, being characterized by limited rainfall, high evaporation rate and water scarcity (Omer, 2013). The south

of Iraq has characteristics of arid or dessert climate, with very low yearly precipitation. The boundaries of these regions vary depending on wet and dry years (Khidher and Pilesjö, 2015). During wet years, the Mediterranean and steppe climate regions expand further to the south (Figure 1.3). The variability between dry and wet years may be related to phase changes in both the North Atlantic Oscillation and the El Niño-La Niña modes of climate variability (Section 1.4).

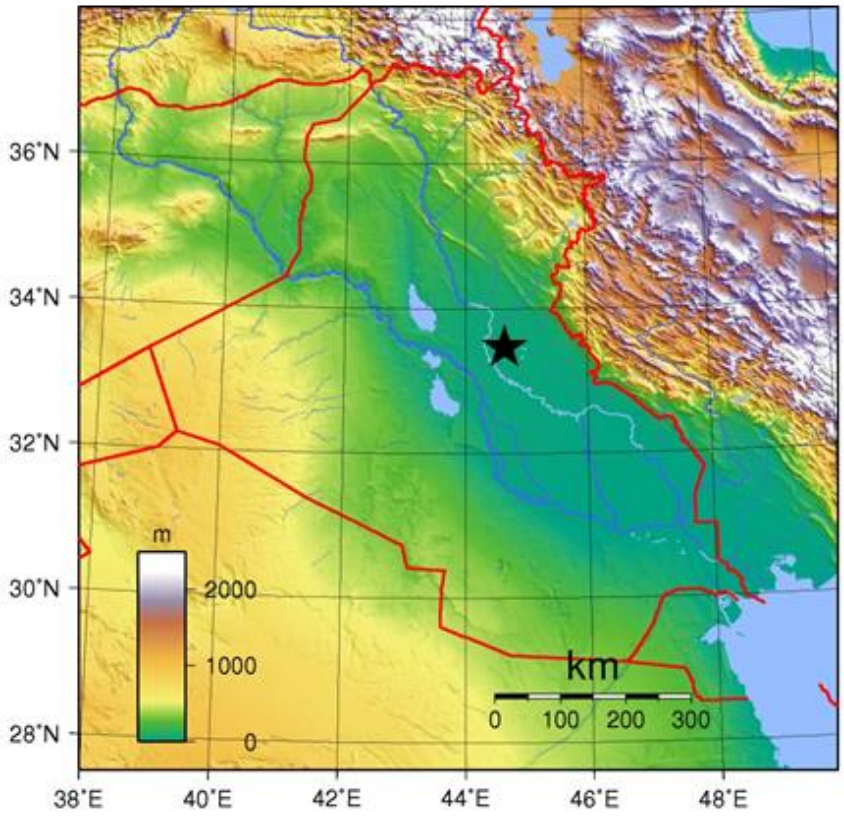

Figure 1.2. Relief of Iraq showing the different topographic areas. The location of Baghdad is indicated with a black star.

Extratropical low pressure systems, mostly of Mediterranean origin, cause precipitation during fall and winter (e.g. Al-Timimia and Al-Jiboori, 2013; Babu et al., 2011; Barthand and Steinkohl, 2004). In addition, the location of Iraq close to the Persian Gulf, Arabian Sea and Red Sea region favours the arrival of moisture flux from the south, which feeds the extratropical low pressure systems of distinct origin circulating over Iraq (Barlow et al., 2005; Vorhees, 2006). Iraq is strongly influenced in the summer by the northward displacement of the subtropical high pressure belt (Babau et al., 2011; Malinowski, 2002). This high pressure system is responsible of relatively high monthly mean maximum temperatures, ranging from 38 ºC in Rutba to 43 ºC in Baghdad. The prevailing winds are

north-westerly. The average annual rainfall is 154 mm, but it ranges from less than 100 mm over 60% of the country to 1200 mm in the northeast. The rainy season is restricted to the period from early October until the end of May (Al-Ansari and Knutsson, 2011). Dust storms are quite common in the desert and sedimentary plain regions, occurring mainly in the early summer months (Omer, 2011).

1.2 Iraq seasonal climate and precipitation regime

The amount of rainfall in Iraq varies from place to place and from time to time (Al-Rijaboa and Salih, 2013). As already mentioned, there is a marked seasonal variability, with the rainy season lasting from early in October until the end of May and a very dry summer season with no precipitation (Figure 1.4a) (Mohammed and Hadi, 2012). There is not a precise starting time for precipitation because it relies both on the arrival of lows – from the Mediterranean Sea (Cyprus and Black Sea lows) as well as from the Caspian Sea and from Sudan (Mohammed, 2009) – and on the occurrence of middle and upper troposphere disturbances, as it will be shown in this study.

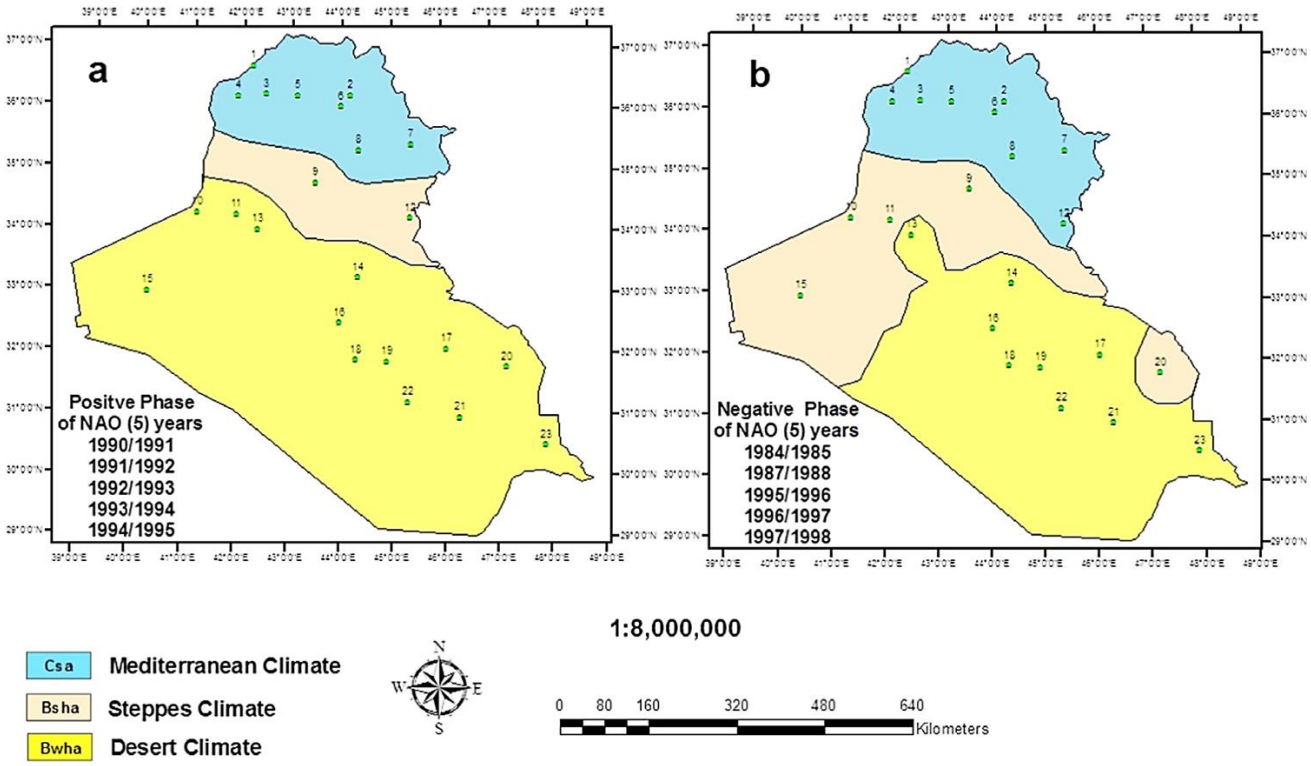

Figure 1.3. Climatic regions in Iraq using Köppen's classification during years of pronounced positive and negative NAO phases. Reproduced from Khidher and Pilesjö (2015).

Moreover, although the rainy season usually lasts longer than the dry season, often precipitation is scarce. The Iraqi climate is arid or semi-arid over most of the country so, even during the rainy season, monthly rainfall often does not exceed 1 mm. The situation is quite different in the mountainous region located north of Iraq, where precipitation may be important (Al- Dulimi, 2005; Hanson, 2007). Next, we briefly review the average seasonal variability of the precipitation regime.

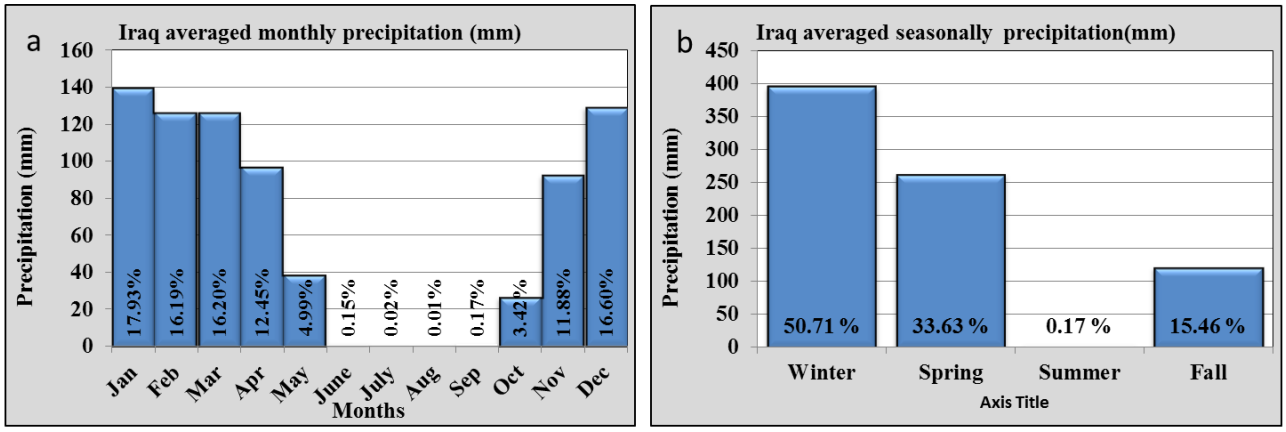

Figure 1.4. Iraq's (a) monthly- and (b) seasonally-averaged precipitation for the 1938-2013 period. The data comes from four meteorological stations located in northern (Mosul), southern (Basrah), western (Rutba) and central (Baghdad) Iraq.

The winter season – comprising December, January and February – is the wettest season of the year; the amount of rainfall accounts for almost 50% of the average annual precipitation (Figure 1.4b). There is also some regional variability, ranging from 51% in the city of Mosul, located in the mountainous northern region, to 41% in the Rutba desert region. During winter the polar front jet reaches its southernmost latitudes with maximum intensity, becoming a zonal conduit for the extratropical low pressure systems (Hansen, 2007).

Several climatological studies have pointed out that the recurrent passage of Mediterranean low pressure systems is responsible for the high amount of winter rainfall (Al-Timimia and Al-Jiboori, 2013; Babu et al, 2011; Barthand and Steinkohl, 2004). During the winter season, the surface Mediterranean waters are warmer than land, triggering the regular formation of low pressure systems in the eastern Mediterranean, i.e. a region of transient cyclogenesis that can get displaced eastward and affect Iraq (Babau et al., 2011). Barthand and Steinkohl (2004) proposed, as other sources of precipitation, the occurrence of cyclogenesis over the Zagros Mountains (between Iraq

and Iran) and the presence of air currents arriving from equatorial areas in Sudan and Ethiopia, the latter associated with the northward displacement of the Sudan low pressure centre (Sudan Low). In particular, Karamouz et al. (2008) and Salehvand et al. (2015) attributed the merging of the Sudan Low with the Mediterranean extratropical low pressure system as the main process responsible for heavy rain and floods in nearby Iran.

Nevertheless, the above studies did not focus on the disturbances of the middle and upper troposphere as other sources of precipitation. In this thesis, we will show that those disturbances are at the origin of the extreme precipitation events, at times when the winds in the lower atmosphere cause the convergence of moisture flux from the Persian Gulf, the Arabian Sea and the Red Sea into central Iraq. This coincides with some studies by Vorhees (2006) and Barlow et al. (2005), which pointed out that the amount of precipitation related with extratropical cyclones passing over Iraq can be strongly affected by the advection of moisture from the south. These authors related this moisture advection with convective variations convection in the eastern Indian Ocean and Southeast Asia during autumn and winter. As we will discuss in Section 1.4.2, this is related with the effects of El Niño shifting the surface circulation and large scale pressure systems (Vorhees, 2006; Mariotti, 2007).

Precipitation is scarce in winter due to the recurrence of a high pressure system that blocks the lows and leads to northwest winds. This high pressure system is the westward extension of the lower tropospheric semi-permanent high pressure area known as the Siberian or Asiatic High, which merges with the Arabian Peninsula High, Saharan High and Azores High to create a continuous lower tropospheric ridge (Hanson, 2007). The Arabian Peninsula High is initiated and maintained by radiative surface cooling over the large desert surface (Vojtesak et al., 1991), playing an important role in the winter climate (Vorhees, 2006).

The Mediterranean low pressure systems divert the westward outflow running in the northern side of the Arabian High. The amount and distribution of precipitation over Iraq is largely caused by this outflow, which feeds low level moisture from the Arabian Sea and Persian Gul (Vorhees, 2006). In this regard, it is assumed that the extratropical cyclones that move through Iraq (generally lows of Mediterranean and Caspian origin) draw their moisture primarily from the Mediterranean, Black and Caspian Seas. However, Barlow et al. (2005) concluded that the Persian Gulf and Arabian Sea “may

be equally or more important as moisture sources for Central-Southwest Asia, particularly for the Tigris-Euphrates basin."

During the spring season – comprising March, April and May – the extratropical low pressure systems still transit through Iraq, although much less frequently that in winter due to a northward shift of the polar frontal jet and to the strengthening of the Arabian Peninsula High (Hanson, 2007). This is reflected on the average mean precipitation for this season, which represents one third of the total annual precipitation (Figure 1.4b). Values vary between locations from 15.3% in the south (Basrah station) to 36.2% in the Rutba desert station.

The summer season – June, July, August and September – is the dry season, which is related to the northward displacement of the subtropical high pressure over Iraq. The absence of precipitation is linked to sinking motions of the subsiding air in the subtropical high belt (Babau et al., 2011). In addition, the descending branch of the Walker circulation associated with the Indian summer monsoon also affects the region, hence contributing to sinking motions and the absence of precipitation (Babau et al., 2011). Several studies have shown the strong influence of the Indian monsoon over the region during summer (Vorhees, 2006; Hanson, 2007). At low levels, it is related with a thermal trough that stretches from western North Africa to Southeast Asia and results in large-scale south-westerly flow, known as the southwest monsoon period.

The autumn season – September to November – is a transitional period between summer (warm, dry and stable air) and winter (cold, rainy and unstable air). Rainy events usually develop from middle October to the end of November, as the low pressure systems arrive mainly from the Mediterranean and the upper and middle tropospheric disturbances affect Iraq (Al-Dulimi, 2005). This short time span results in relatively low precipitation records when compared with others seasons (Figure 1.4b). It accounts for only about 15% of Iraq's average annual precipitation, though there is some regional variability. In the south part of Iraq (Basrah station) it may represent one third of the average annual precipitation whereas in the centre (Baghdad Station), north (Mosul Station) and west (Rutba station) of Iraq the autumn's rainfall does not exceed 22%.

This autumn season is a transition period between the southwest monsoon (summer) and the northeast monsoon (winter) periods (Vorhees, 2006; Hanson, 2007). During this period, thermal trough and associated heat lows formed during the summer period collapse due to a decrease in insolation (Vorhees, 2006; Hanson, 2007). The Asiatic High begins to form leading to a shift of the

prevailing winds from the southwest to the northeast. An important feature is that the polar front jet shifts south as the northern hemisphere begins cooling, leading to an increase of extratropical cyclones and the start of the rainy season.

1.3 Inter-annual variability of the precipitation regime

The precipitation regime in Iraq has substantial inter-annual variability (Mohammed and Hadi, 2012; Al-Timiri and Al-Jiboori, 2013), consisting in alternating periods of several years of rainy and dry years (Figure 1.5). A drought is a climatic phenomenon that occurs when the annual precipitation is substantially less than the annual average, often taken to lie below one standard deviation under the calculated mean (obviously, this definition causes a drought to depend on the period of calculation). Droughts are one of the main causes of desertification and environmental problems, its largest impact affecting the arid and semi-arid areas, such as Iraq. Additionally, the lack of moisture and rain affects the vegetation cover and leads to the disintegration of soil. The consequence is that the soil turns more susceptible to wind erosion, and there are more occurrences of dust storms (Sissakian et al., 2013; Al-Salihi and Mohammed, 2015).

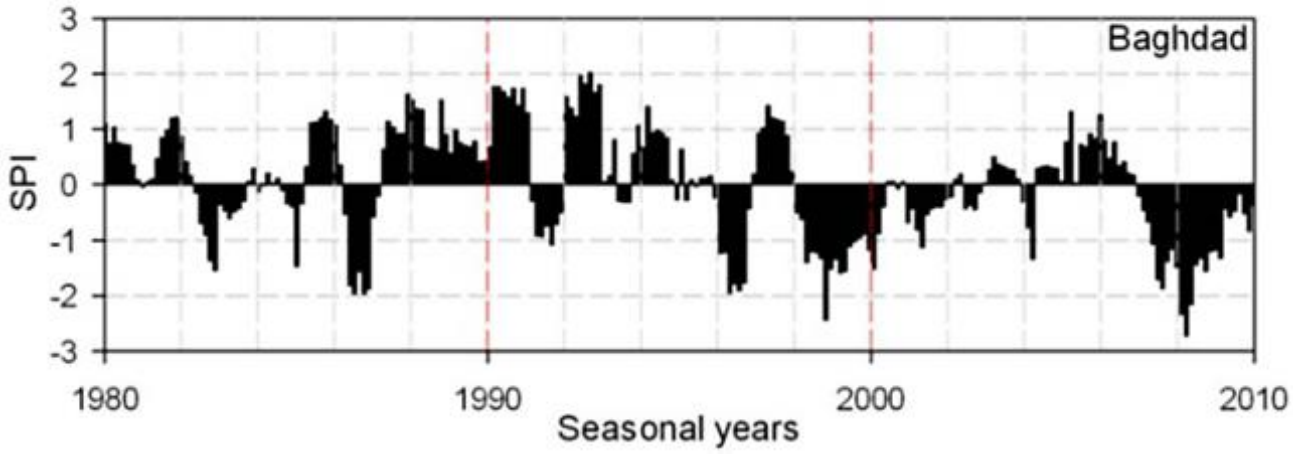

Figure 1.5. Time series of the standardized precipitation index (SPI) for Baghdad's station. Reproduced from Al-Timimi and Al-Jiboor (2013).

The amount of annual precipitation depends on the local orographic conditions but is largely controlled by several factors: type, intensity, speed, trajectory and moisture content of the extratropical low pressure systems passing over Iraq (Hadi, 2013). These combined factors are responsible for the variation in annual precipitation between years, i.e. from very scarce to abundant

waters. There are three principal processes affecting the amount of precipitation in Iraq: the frequency of the Mediterranean low pressure systems affecting the region, the strength and occurrence of jet streams at upper atmospheric levels, and the influence of the European trough (Hadi, 2013). As we discuss next, these three processes are closely related.

The main process affecting the inter-annual variation of precipitation in Iraq is the recurrence of Mediterranean low pressure systems (Al-Amiri, 2012; Aldsaa and Habib, 2007). As mentioned above, the rain in Iraq is also subject to the influence of other secondary cyclones such as those lows related with the Sudan, Caspian Sea and Zagros Mountains, whose variability will also affect the interannual regime (Aldsaa and Habib, 2007; Al-Amiri, 2012).

The strength and occurrence of the jet stream is another process that controls the inter-annual precipitation regime (Zangana, 2007). Iraq is influenced by the polar jet stream, the subtropical jet stream and the merging of both. In this study we will show that the perturbations of the polar jet stream – such as Rex Block, cut-off lows and troughs – can lead to extreme precipitation events with inter-annual variability. Additionally, it has been observed that the recurrence of the extratropical low pressure systems is related with the appearance and disappearance of the polar jet stream (Zangana, 2007; Aldsaa and Habib, 2007; Al-Amiri, 2012). The percentage of the contribution of polar jet stream to the total annual precipitation amount has been estimated to be 71% in northern Iraq, 61% in central Iraq, and 49.5% in southern Iraq (Zangana, 2007).

A third process that can play an important role on the inter-annual variability of precipitation is related with the European Trough (Hadi, 2013). This trough originates at the 500 hPa mid tropospheric level and extends from the Island of Novaya Zemlya in the Arctic Ocean to the middle of the Mediterranean Sea. The effects of this trough over the Mediterranean low pressure systems, which may affect Iraq, are reviewed by Hadi (2013). This author points out that the eastern part of the European Trough is a convergence area, thus increasing the absolute rotational motion of the Mediterranean low pressure systems. Therefore, those Mediterranean low pressure systems coinciding with the eastern part of the European Trough will deepen and increase their strength, causing heavy rain when moving from the Eastern Mediterranean towards Iraq. However, since the European Trough block the westerly winds, those Mediterranean low pressure systems reaching the European trough from the west will shift their path northeast and will not affect Iraq. Finally, the

Mediterranean low pressure systems originated at the southwestern part of the European Trough will decay and gradually fade, affecting Iraq much less than those arriving from the west.

Al-Timimi and Al-Jiboor (2013) investigated the inter-annual variability of the precipitation regime over Iraq for the period 1980-2010 in order to identify the occurrence and variability of drought periods. They examined the time series of the standardized precipitation index (SPI) – which quantifies the precipitation deficit for multiple time scales (McKee et al., 1993) – from data collected at 39 meteorological stations distributed across Iraq (Figure 1.5). They identified frequent non-uniform drought periods in an irregular repetitive manner, with dry years in the Baghdad station occurring in 1983, 1987, 1989, 1990, 1998, 1999, 2000, 2001, 2002, 2003 2004, 2005, 2007 and 2008 (Figure 1.5). In particular, year 2008 was the driest year during the entire period, with 30% of Iraq suffering an extreme drought, 36% under severe drought, 22% under moderate drought and 12% near normal. As we will discuss next, this variability in inter-annual precipitation is linked to variations at global scale, which affect the three processes mentioned above.

1.4 Global scale climate variations and precipitation regime in Iraq

The inter-annual variability in precipitation and surface air temperature in Iraq has been linked with variations in global-scale patterns, such as the North Atlantic Oscillation (NAO), the El Niño – La Niña (EN-LN or ENSO oscillation), the Madden-Julian Oscillation (MJO) and the Indian Ocean Zonal Mode (IOZM) (Cullen et al., 2002; Vorbees, 2006; Hanson, 2007; Khidher and Pilesjö, 2015). Vorhees (2006) investigated the relation between these global patterns and the autumn-winter precipitation anomalies in southwest Asia, including Iraq. The NAO and ENSO appear as the most relevant global-scale climate indices affecting the precipitation regime in Iraq (Cullen et al., 2002; Vorhees, 2006; Hanson, 2007; Khidher and Pilesjö, 2015) (see Table 1.1 from Vorhees, 2006). Hence, we will next focus on the processes and effects associated with these two climatic indices.

1.4.1 North Atlantic Oscillation and the precipitation regime in Iraq

The North Atlantic Oscillation (NAO) is the most prominent and recurrent large scale climate variation in the Northern Hemisphere. It is a dominant mode of the climate variability in the Atlantic sector, which can dictate much of the climate patterns in the Northern Hemisphere (Hurrell et al., 2003). The NAO is divided into three phases: positive, negative, and neutral. As depicted in Figure 1.6, the positive (negative) phase occurs when the Azores High and Icelandic Low are stronger

(weaker) than average. The NAO phases tend to be most accentuated during northern winter although they can occur any time throughout the year (Hurrell et al., 2003; Hanson, 2007).

Table 1.1. Variations in global climate patterns and associated fall and winter precipitation anomalies in southwest Asia, as proposed by Vorhees (2006). IOZM, MJO and NAO respectively stand for Indian Ocean Zonal mode, Madden-Julian Oscillation and North Atlantic Oscillation.

	Fall	**Winter**
El Niño	Wet	Dry
La Niña	Dry	Wet
Positive Phase IOZM	Wet	Inconclusive
Negative Phase IOZM	Inconclusive	Inconclusive
MJO convective component in the eastern Indian Ocean	Dry	Dry
MJO subsidence component in the eastern Indian Ocean	West: Wet East: Dry	West: Wet East: Dry
Positive Phase NAO	Dry	Dry
Negative Phase NAO	Varied	Wet

The positive and negative phases NAO can produce large anomalies in the mid-latitude westerly and subtropical trade winds, as well as in the precipitation and surface air temperatures. During the positive phase, there is an enhancement of the westerly flow over the North Atlantic, and the extratropical low pressure systems and storm pathways over the North Atlantic tend to move north. The effects are higher precipitation and warmer conditions in northern Europe whereas cold and dry conditions prevail in southern Europe, the Mediterranean Basin and western Asia. During the negative phase, the extratropical low pressure systems tend to move south. The consequences are higher precipitation and warmer conditions in southern Europe, the Mediterranean Basin and western Asia. As shown in Table 1.1 and detailed next, a positive (negative) NAO phase is therefore related with a negative (positive) precipitation anomaly over Iraq (Cullen et al., 2002; Whorhees, 2006; Hanson, 2007; Khidher and Pilesjö, 2015).

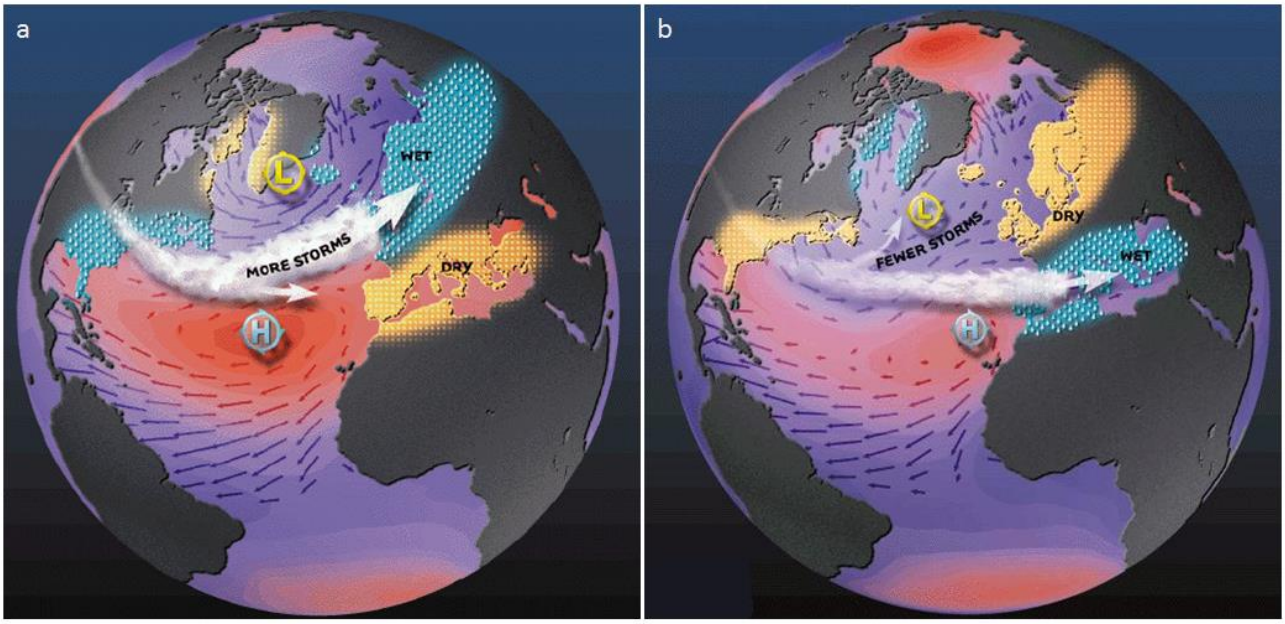

Figure 1.6. Schematics of sea-surface pressure and wind patterns during (a) positive and (b) negative NAO phases; reproduced from Columbia (2018).

Khidher and Pilesjö (2015) recently investigated the effects of NAO on the Iraqi climate. In accordance with Cullen et al. (2002) and Vorhees (2006) (Table 1.1), these authors concluded that the mean annual precipitation over Iraq increases (decreases) during a negative (positive) NAO phase. They also observed some dependence on seasonality, such as weak NAOs during autumn, strengthening during winter until a spring maximum, and vanishing in summer. Regarding spatial variability, they observed that the correlation between NAO and precipitation is more pronounced in the south of the country than in the middle and northern regions (Figure 1.3).

Although the above authors inferred a negative correlation between NAO and precipitation over Iraq, this correlation is not too strong. Khidher and Pilesjö (2015) argue that the amount of rainfall over Iraq does not entirely originate from the Mediterranean extratropical low pressure systems, but rather depend on other factors that are not related to the NAO. In particular, independent from the NAO index, the strength of the Mediterranean cyclones will increase when the Sudan and Mediterranean cyclones merge. Their results also show that there were no significant differences between the negative and the positive phases of the NAO in many Mediterranean cyclones moving towards Iraq. However, there were indeed differences in the strength and track of the Mediterranean cyclones. During the negative phase of NAO, cyclones move south and there is an increase in

precipitation over central and southern Iraq, whereas during the positive phase of the NAO, cyclones shift north, away from central and southern Iraq (Khidher and Pilesjö, 2015). As pointed out by Khidher and Pilesjö (2015), this will reduce rainfall over central and southern Iraq, leading to an increase in droughts; Hansen (2007) also found the correlation between NAO and precipitation over Iraq to be significant during spring, though it was not statistically significant during all other seasons.

1.4.2 ENSO and the precipitation regime in Iraq

One of the most studied climate variations is the ENSO global teleconnection, which extends all over the world. The ENSO variability has three phases: El Nino (EN), neutral, and La Nina (LN). Details of the development and cycle of ENSO can be found in Ropelewski and Halpert (1987) and Philander (1990). There are evidences, such as those pointed out by Vorhees (2006), Hansen (2007) and Marioti (2007), suggesting that ENSO can have significant consequences on the southwest Asia precipitation regime. These authors concluded that precipitation was enhanced during EN. They proposed that this is related to an increase in the number of days with onshore winds from the Arabian Sea and tropical Africa. This will increase the availability of moisture flux for the extratropical low pressure systems passing over Iraq (Vorhess, 2006). This onshore moisture flux is generated along the north-western flank of the high pressure anomaly over the Indian and western Pacific Oceans. Mariotti (2007) indicated that the impact of ENSO on the precipitation over southwest Asia is greatest during the transition autumn and spring seasons.

1.5 Objective and outline of the dissertation

The main objective of this thesis is to study what is the contribution of extreme precipitation events to total rainfall over Iraq – both in average and during wet/dry periods – and to investigate the characteristic weather patterns that lead to these abnormal episodes. This is done using monthly (1938-2016 period) and daily (2005-2016 period) data from several meteorological stations (mainly the Baghdad station) ran by the Iraqi Meteorological Organization and Seismology, as well as the ERA-Interim global atmospheric reanalysis available from the European Centre for Medium-Range Weather Forecasts (ECMWF) for a rectangular area centered over Baghdad, spanning (12°N-45°N) in latitude and (15-70°E) in longitude.

The specific objectives may be formulated as the following 10 questions:

1- What are the mean conditions and temporal variability of precipitation over central Iraq?

2- How these conditions change at inter-decadal scales? Can we talk of arid and wet periods?

3- What do we learn from the annual-precipitation histograms? How does precipitation changes between average, arid and wet years?

4- What do we learn from the monthly-precipitation histograms? How these histograms change between average, arid and wet years?

5- Is there any relation between monthly precipitation in central Iraq and the El Niño-Southern Ocean oscillation?

6- What is the contribution of extreme precipitation cut-off lows to annual precipitation?

7- How the contribution of rainy cut-off lows to the total annual precipitation changes between arid and wet years?

8- What are the physical processes in the lower, middle and upper atmosphere necessary for the occurrence of extreme precipitation events?

9- During severe rainfall incidents, where does the moisture comes from and how it gets to central Iraq?

10- Besides cut-off lows, are there other meteorological patterns involved in the extreme precipitation episodes?

After this introductory chapter (Chapter 1), we will proceed with the statistical analysis of the monthly (Chapter 2) and daily (Chapter 3) rainfall data, with special attention to the high precipitation events, their contribution to the total rainfall, and their inter-annual variability. In Chapter 4 we will explore the dynamic and thermodynamic characteristics of cut-off lows, with particular attention on the Rex block event that led to the highest precipitation for the entire 2005-2016 period. In Chapter 5 we will look at another three extreme rain episodes that display other type of synoptic structures: a cut-off low episode (non Rex block type), an upper-air trough incident, and a jet streak event. Chapter 6 closes the dissertation with the general conclusions and the answers to the above questions, as well as with several proposals on future work.

Chapter 2

Long Term Statistical Analysis for Baghdad Area

2.1 Introduction

In this chapter we use monthly precipitation data from the Baghdad meteorological station, ran by the Iraqi Meteorological Organization and Seismology. Our objective is triple. First, we explore the temporal distribution of rainfall, with special attention to the seasonal cycle and the inter-annual, decadal and long-term variations. Second, we examine how the annual and monthly precipitation is distributed for arid and wet years, defined in terms of the 25 and 75 percentiles of total annual rainfall. Finally, we investigate if the inter-annual variations correlate in some way with the NINO3.4 index, a global climatic mode that has been reported to affect the Middle East region.

2.2 Data set

The Baghdad meteorological station is located at 34 m elevation in the central plains of Iraq (33.33°N, 44.43°E), in an area of small topographic variability. A monthly rainfall time series from January 1938 to December 2016 – the longest one in Iraq – is available from the Iraqi Meteorological Organization and Seismology. This series, however, has data missing from January 2003 till December 2004 because of the Iraqi War (Fig. 2.1). The homogeneity of this 75-year annual precipitation series has been verified using the Von Neumann and Thom tests (Messeguer-Ruiz and Sarricolea, 2017). Additionally, we will use the monthly time series of the NINO3.4 index, available from the Royal Netherlands Meteorological Institute (KNMI, 2018).

2.3 Annual precipitation

The total rainfall for the 76-year period was 10,527 mm. To calculate the annual precipitation values, however, we introduce the concept of natural year from 1 July through 30 June. This follows from the precipitation cycle, associated with the totally dry summers; for instance, the natural year 1938 corresponds to the period between 1 July 1938 and 30 June 1939. This reduces the number of

annual precipitation values to only 75 natural years, 1939-2016, with 2003, 2004 and 2005 missing (Fig. 2.1). The total precipitation for the 75 natural years was 10,187 mm (135.8 ± 61.9 mm/yr).

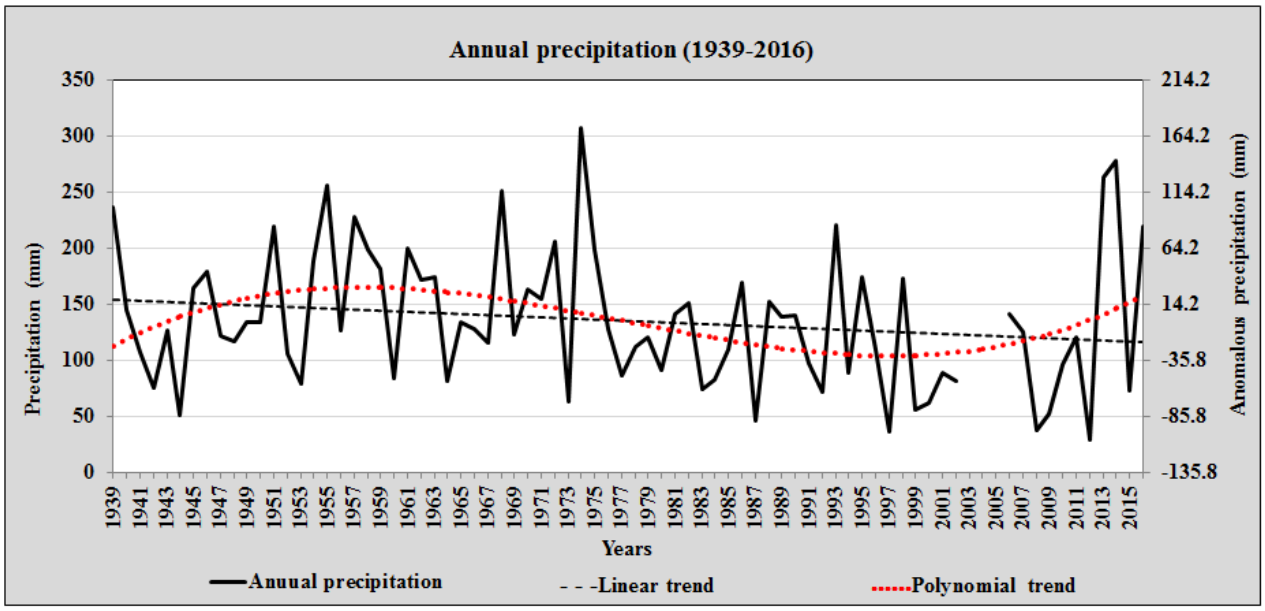

Figure 2.1. Annual precipitation (mm) over Baghdad during natural years (July through June) for the 1939-2016 period; a natural year in the abscissa is denoted by the year of the January-June semester so the actual data corresponds to the period between July 1938 and June 2016. The left ordinate represents the actual annual precipitation values while the right ordinate gives the anomalies (actual precipitation less the annual-mean value, 135.8 mm). The linear and third-order polynomial adjustments are shown with black and red dotted lines, respectively.

The annual-rainfall time series illustrates the existence of substantial intra-annual variability. Maximum annual precipitation corresponds to 1974 (307.7 mm), 2014 (278.1 mm) and 2013 (263.6 mm). In contrast, minimum annual precipitation occurred in 2012 (29.3 mm), 1997 (36.6 mm) and 2008 (37.6 mm). There are 43 years below the annual average (135.8 mm) and 32 years are above the annual average (Fig. 2.1).

There is a weak negative linear trend in the annual precipitation values, -0.5 mm/yr. However, this long-term trend depends largely on the interval of years used for the calculation. For example, for 1950-2000 the amplitude of the negative trend increases to about -2 mm/yr, while for 2000-2016 the trend turns into a relatively high positive value, close to 5 mm/yr. This clearly represents a long-term variability that can only be captured through a higher polynomial trend. A third order

polynomial appears as appropriate to capture this interdecadal variability (Fig. 2.1), reflecting the relatively high precipitation during the 1950s and 1960s and the relatively low rainfall during the 1980s, 1990s and early 2000s.

2.3.1 Frequency and cumulative frequency of annual precipitation

We use natural years to obtain the annual-precipitation histograms (Fig. 2.2a). The distribution is unimodal though skewed towards high values. This is reflected by the difference between the interval of highest precipitations – 69% of the annual precipitation is between 60 and 180 mm – and the interval between the mean value minus and plus one standard deviation, 73.9-197.7 mm. Further, there are 22% of years with precipitation over 180 mm in contrast with only 9% of the years with rain below 80 mm.

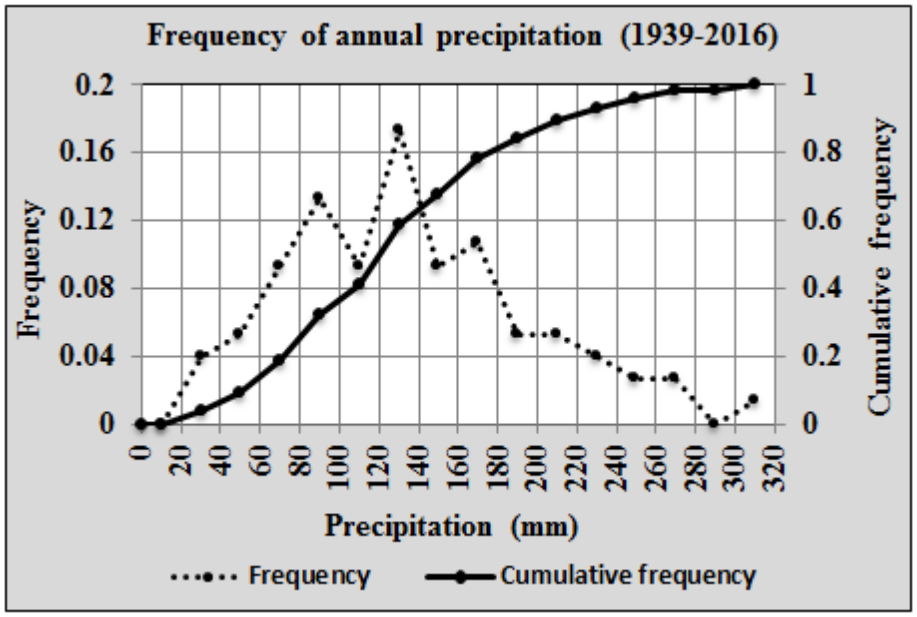

Figure 2.2. Frequency (dotted line) and cumulative frequency (solid line) of annual precipitation during natural years (July through June) for the 1939-2016 period. The abscissa values indicate the precipitation intervals used for the calculations.

2.3.2 Definition of arid and wet years

To define the arid and wet years, we use the 25 and 75 annual-precipitation percentiles, respectively; hereafter we will use the arid-wet nomenclature to refer to those years below/above the 25/75 percentiles, and will reserve the "dry" and "rainy" adjectives to refer to the meteorological seasons.

This represents 19 years with precipitation less than 88 mm, hereafter arid years, and 19 years with rainfall above 174 mm, henceforth wet years (Fig. 2.3). The amount of rain during the 19 dry years was 1227 mm (12.0% of the total) while the amount of rain during the 19 wet years was 4181 mm (41.0% of the total).

The 1950s corresponds to the wettest period, both in terms of the total decadal precipitation and the number of wet years, and there were no wet years during the 1980s and 2000s. In contrast, there were arid years during all decades, with the 1960s being the period with less decadal precipitation and more dry years. Surprisingly, the wettest and most arid years do not belong to these decades: the wettest year was 1974 (307.7 mm) and the most arid one was 2012 (29.3 mm) (Fig. 2.1).

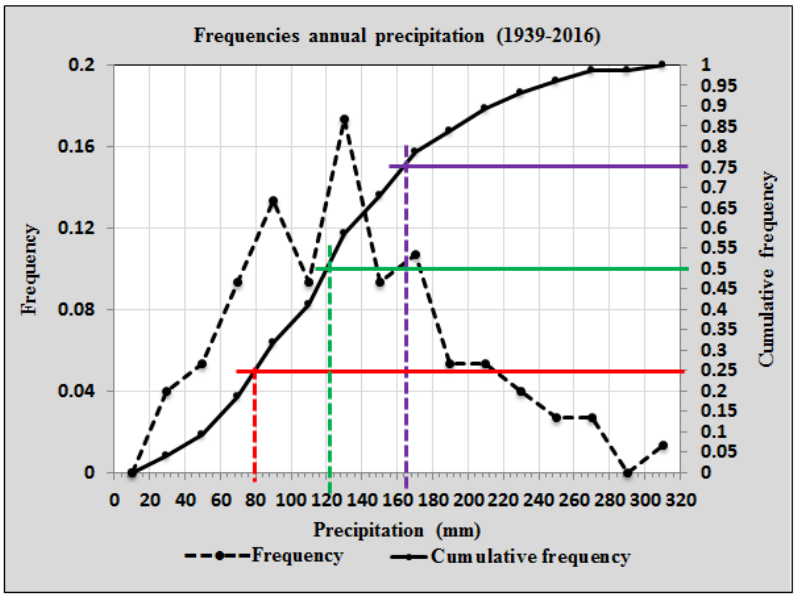

Figure 2.3. Frequency (dotted line) and cumulative frequency (solid line) of annual precipitation but showing the percentiles used to define the arid and wet years. The abscissa values indicate the precipitation intervals used for the calculations.

The distinction between wet and arid years allows assessing the differences between these times and the average conditions during the entire 75-year period. In Section 2.5 we will use this division to explore how the seasonal and monthly distributions vary between arid and wet years. Here we simply use the annual rainfall to differentiate the annual-mean characteristics during arid and wet years. This is nicely done with the help of chronological cumulative precipitation plots (Fig. 2.4).

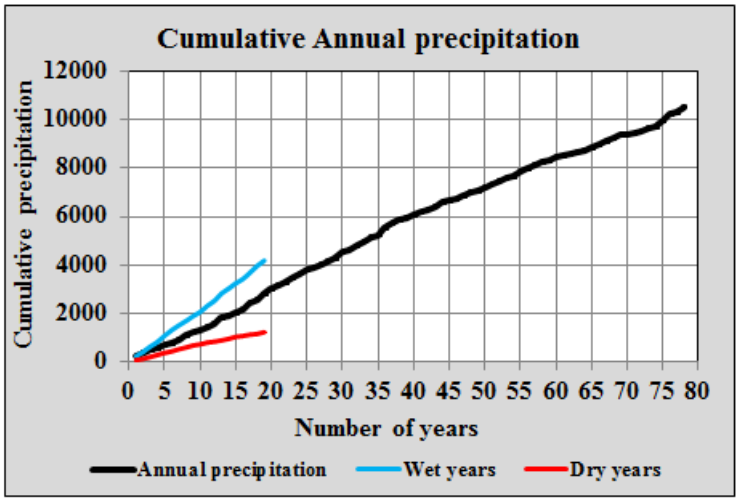

Figure 2.4. Cumulative annual precipitation, with values being integrated in chronological order, for natural years: all years (black line; notice that the average annual rainfall value for the 1939-2016 period has replaced years 2003, 2004 and 2004 with no data), arid years (red line) and wet years (blue line); notice the total number of years is 78 but there are only 19 wet and 19 dry years.

The cumulative precipitation as a function of the number of years is substantially larger/smaller for the wet/arid years as compared with the average from the entire dataset. The average conditions represent 10,187 mm of rain in 75 years, giving a slope of 135.8 mm/yr. In contrast, the arid years account for 1227 mm of rain, or 64.6 mm/yr, which is 12.0% of the total precipitation; the wet years account for 4181 mm of rain, or 220.1 mm/yr, or 41% of the total rainfall

The individual years do not signify substantial changes in the cumulative slope (Fig. 2.4). However, this slope does change at inter-decadal time scales. The maximum slope (150 mm/yr) corresponds to the first 40 years (1938-1977), thereafter decreasing to smaller values (120 mm/yr) during 20 years (1978-1997) and even less (100 mm/yr) during the following 15 years (1998-2012; recall there is no data for 2002-2004), to finally return to the original trend (150 mm/yr) between 2013 and 2016.

2.4 Monthly precipitation

The time series of monthly precipitation values during 1938-2016 is shown in Figure 2.5. There is data for a total of 924 months (there are 24 months of missing data because of the 2003-2004 Iraqi War). Rainfall took place during 614 months (66.4%) although monthly precipitation exceeding 1 mm occurred only on 494 months (53.4 %) and monthly rainfall in excess of 10 mm happened in

296 cases (32%). The peak monthly rainfall occurred in November 2013 (172.7 mm), largely due to one individual episode that will be carefully analysed in Chapter 4.

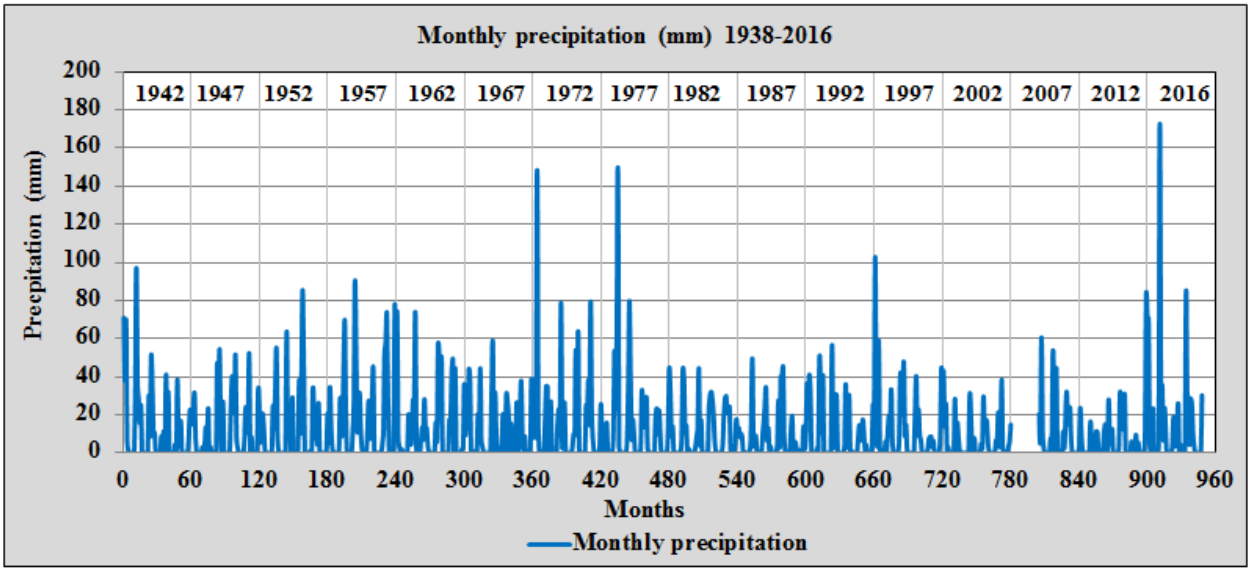

Figure 2.5. Monthly precipitation values (mm) over Baghdad for the 1938-2016 period. The lower abscissa represents the months while the corresponding years are indicated in the upper abscissa.

The mean monthly precipitation for the entire period was 11.3 ± 18.7 mm; this value increases to 17.1 ± 20.9 mm if we disregard the three (June-August) summer months. Considering only the rainy months, there are 391 months (63.6%) with precipitation below the 17.1-mm mean monthly value and 223 months (36.3%) with rainfall above this mean value. This confirms a relatively large asymmetry, with a relatively small number of months that contribute most to the total precipitation.

The monthly precipitation histogram (924 months) shows that most months correspond to either no precipitation or rainfall in the 0-20 mm interval. There were 310 instances (33.5%, including 210 values for summer months and 100 values for rainy months) with no precipitation, and 415 cases (44.9%, including 21 values for summer months and 394 values for rainy months) for precipitation in the 0-20 mm range (Figs. 2.6a).

The monthly cumulative-frequency distribution highlights the large number of months with zero or low precipitation values (Fig. 2.6b). In this figure, the cumulative plot uses rain intervals of 20 mm; a higher-resolution plot, would evidence that during 50% of the study period the monthly rain was less than 8 mm and during 75% of the study period it was less than 19 mm (not shown).

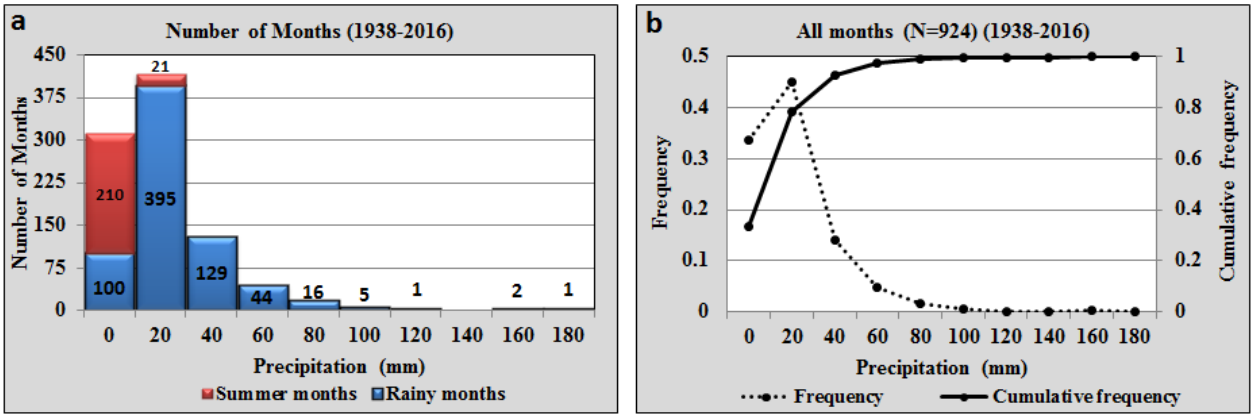

Figure 2.6. (a) Precipitation histograms for Baghdad between 1938 and 2016 (924 months); the red/blue bars represent months corresponding to the rainy/wet seasons (231/693). (b) Frequency (dotted line) and cumulative frequency (solid line) of monthly precipitation. In both panels, the abscissa values indicate the precipitation intervals used for the calculations, with the first bar corresponding to no rain, the second to 0-20 mm rain, the third one to 20-40 mm, and so on.

The monthly precipitation values also demonstrate the existence of a clear seasonal cycle. Peak rain takes place in January (29.5 mm), moderate rain (above the mean monthly value of 11.3 mm) happens between November and April, and heavy rain (exceeding the 75 percentile, 19 mm) occurs between December and March (Fig. 2.7)

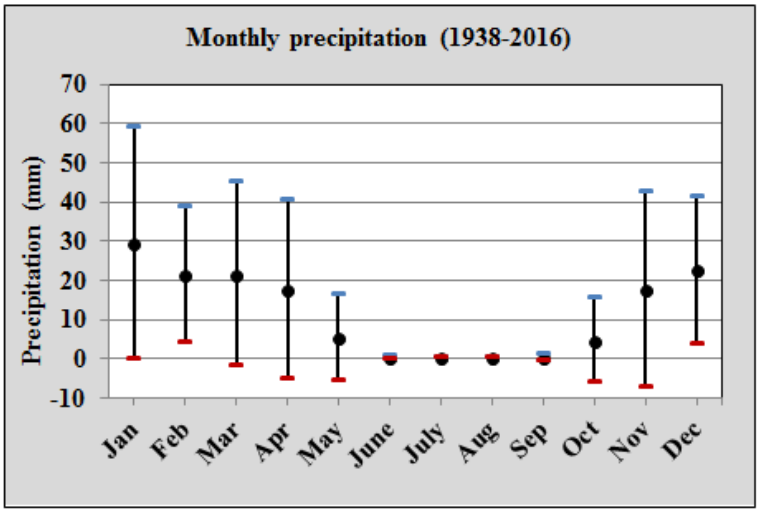

Figure 2.7. Monthly precipitation values (mm) over Baghdad for the 1938-2016 period; the black points indicate the mean values, the blue dash correspond to the mean value plus one standard deviation, and the red dash to the mean values minus one standard deviation.

We can construct an anomaly-precipitation (or deseasonalized) time series by subtracting the mean monthly values to the original time series (Fig. 2.8, top panel). This time series shows that the monthly rainfall is rather asymmetric around the mean value, with relatively few high positive anomalies as compared with numerous moderate negative anomalies.

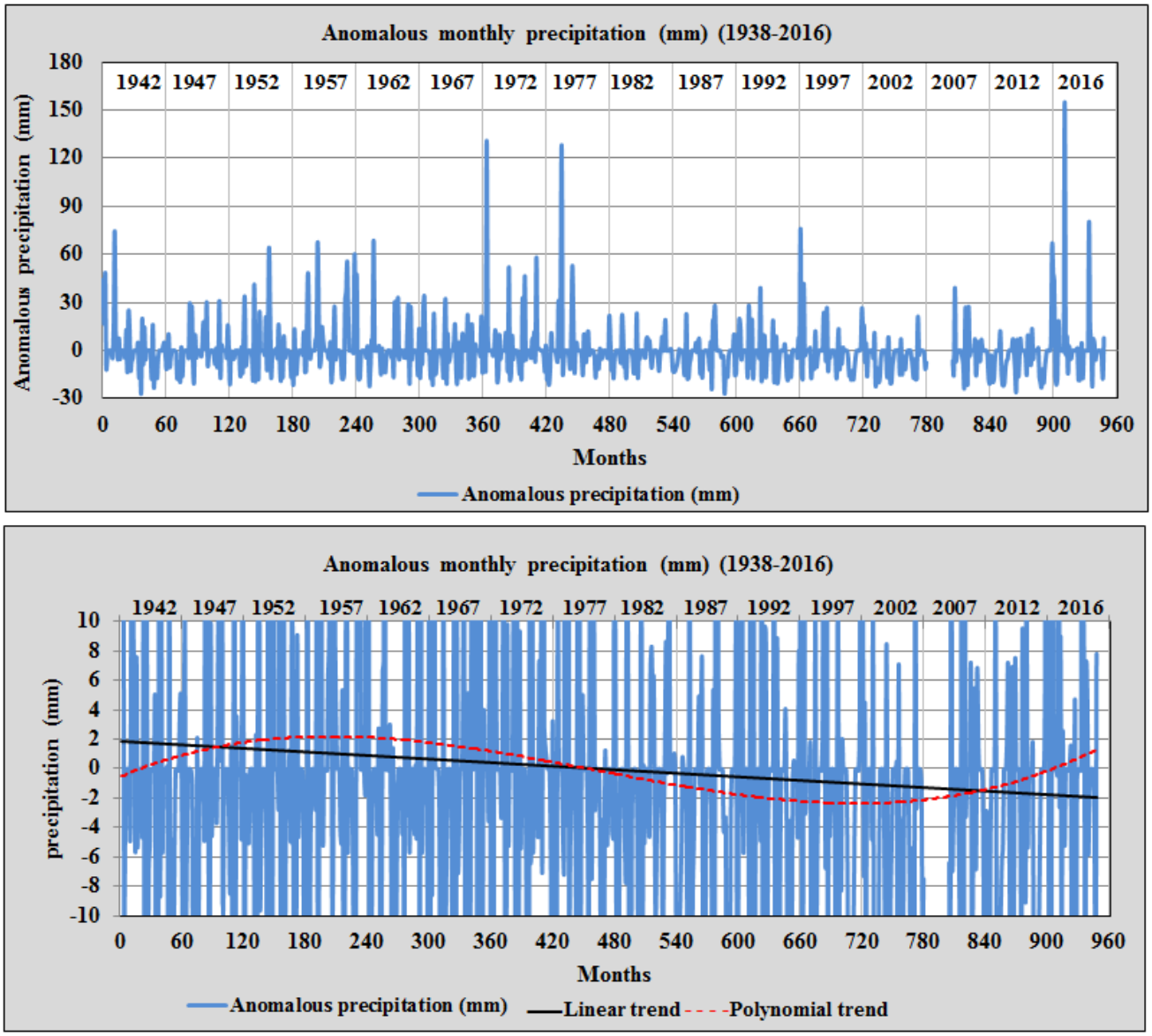

Figure 2.8. Deseasonalized anomaly-precipitation time series (mm) over Baghdad for the 1938-2016 period. The bottom panel reproduces the top values but for a limited rainfall range, with the linear and third-order polynomial adjustments shown with black and red dotted lines, respectively.

We may also calculate the linear trend for this deseasonalized time series (Fig. 2.8, bottom panel). As expected, the long-term linear trend is identical to the one calculated with the annual mean values (-0.5 mm/yr) and the third-order polynomial mimics the inter-decadal variations observed with the annual values, with high values in 1950-1970 and low values during the 1980-2016.

2.5 Monthly precipitation during arid and wet years

We examine next the differences in monthly precipitation between arid and wet years. The rainfall histograms are fairly similar for values less than 50 mm (the major difference corresponds to the interval between 10 and 20 mm, much more frequent during the dry years) (Figs. 2.9, upper panels). However, during the wet years, there were many months with rainfall over 50 mm.

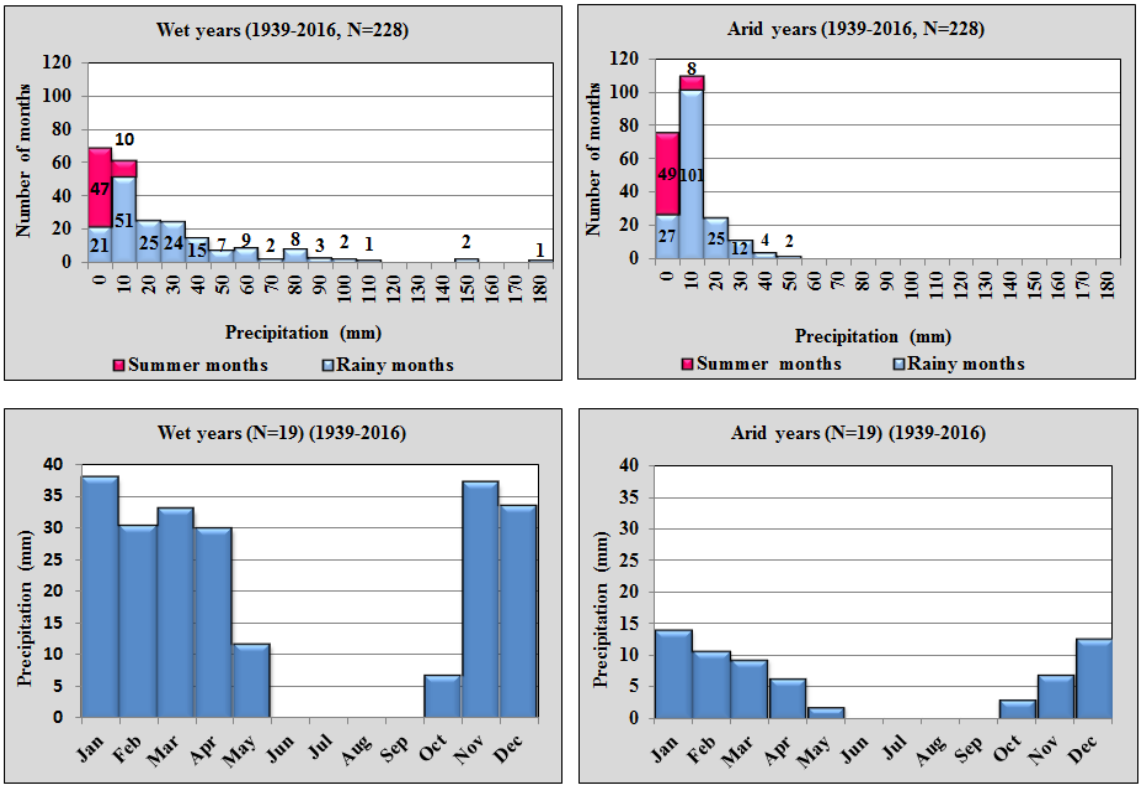

Figure 2.9. Precipitation during (left panels) wet and (right panels) arid years. The top panels show the precipitation histograms (228 months for wet years and 228 for arid years): the red bars represent the summer dry months (June-August) and the blue bars consider all rainy months; the abscissa values indicate the precipitation intervals used for the calculations, with the first bar corresponding to no rain, the second to 0-10 mm rain, the third one to 10-20 mm, and so on. The bottom panels show the corresponding mean monthly precipitation values.

The seasonal cycle for the arid and wet years displays large differences. The November-April rainfall exceeds 30 mm/month during wet years but it is less than 15 mm during dry years (Figs. 2.9, bottom panels). The largest difference occurs in November, with rainfall being over five times larger during wet than on arid years.

The inter-annual variability in monthly precipitation may be assessed through the standard deviation (SD) values (Figs. 2.7 and 2.10). A comparison of the values for arid, wet and entire years shows substantial differences in magnitude, with maximum SD during wet years and minimum during arid years. When using the entire dataset, the largest SD corresponds to January while for the arid years the SDs are nearly equally large for the December-February period and for the wet years they peak during March, April and November.

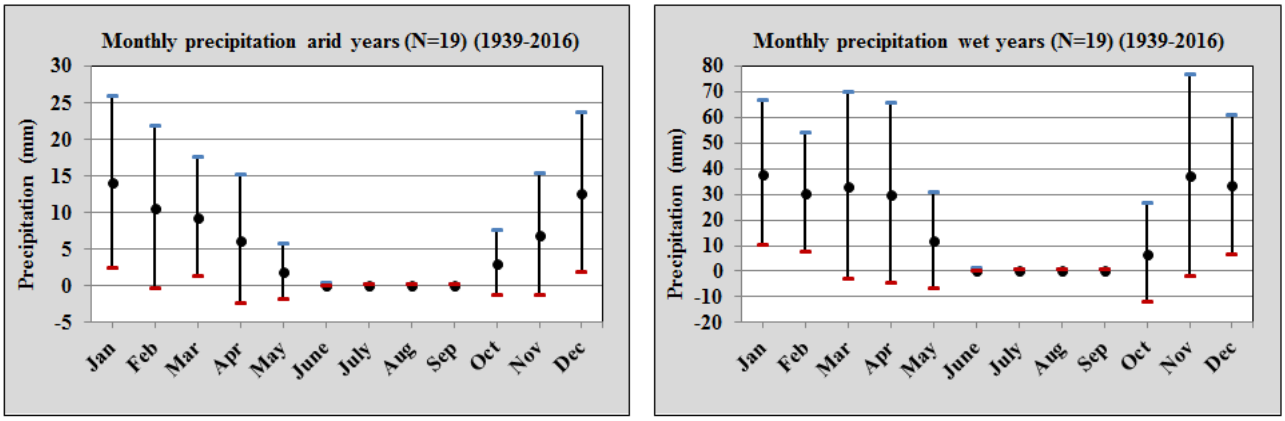

Figure 2.10. Mean monthly precipitation values (mm) during (left panel) arid and (right panel) wet years; the number of months was 228 for both the arid and wet years. Black points correspond to mean monthly precipitation, blue dashes to mean monthly precipitation plus one standard deviation, red dashes to mean monthly precipitation minus one standard deviation; for each month there are N=19 years. Notice the change in vertical scale between both plots.

Finally, we plot together the frequency and cumulative frequency distributions for both the arid and wet periods (Fig. 2.11). The frequency distributions essentially reproduce the histograms in the plot panels of Figure 2.9 though their joint plot emphasizes the differences, particularly the fact that the number of months in the 0-10 mm interval is nearly twice as large during arid than wet years. In contrast, the number of months above 20 mm is much larger during the wet years.

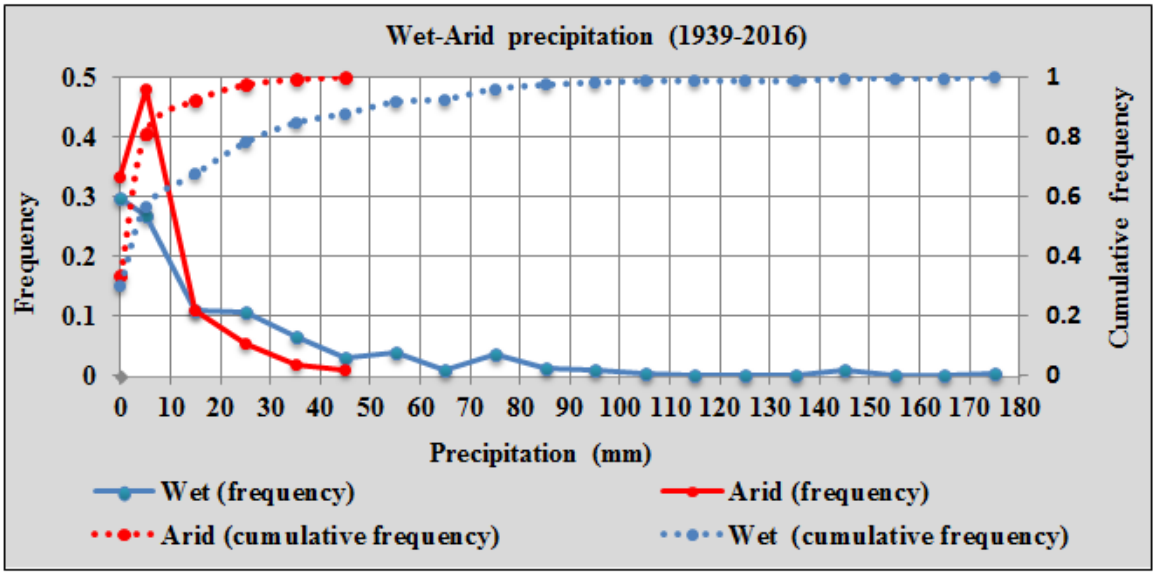

Figure 2.11. Frequency (dotted line) and cumulative frequency (solid line) of monthly precipitation for arid and wet years: the number of months was 228 for the wet years and 228 for the dry years with months; the red lines correspond to the arid years and the blue lines to the wet years. The abscissa values indicate the precipitation intervals used for the calculations.

The cumulative frequency curves –with the help of the 25, 50 and 75 percentiles (Fig. 2.12) – emphasize the difference between the arid and wet years (Fig. 2.11). The 50-percentile is about 3/7 mm for arid/wet years, and the 75-percentile increases to some 8/24 mm. In order to reach the 97-percentile we must account for precipitations up to 30/90 mm during arid/wet years.

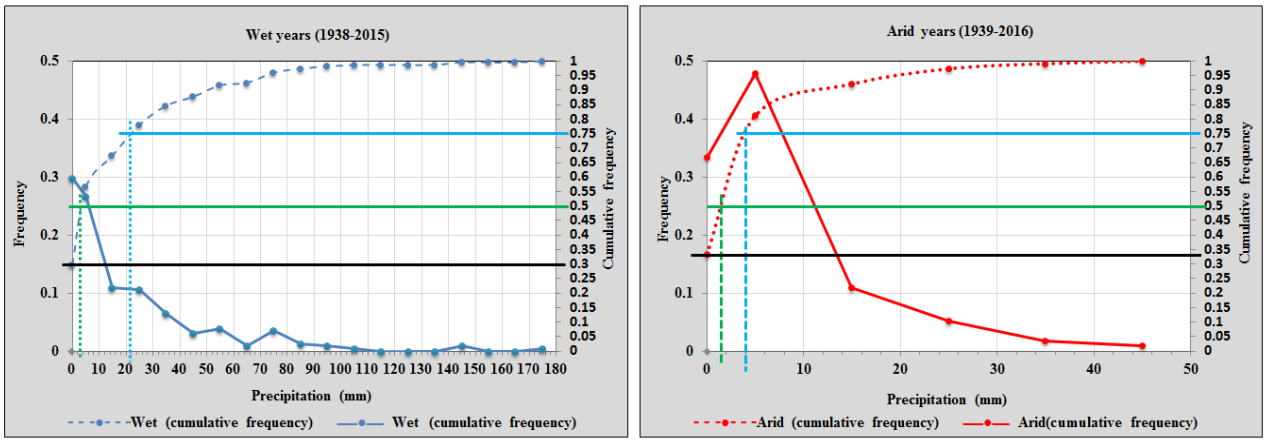

Figure 2.12. Frequency (dotted line) and cumulative frequency (solid line) of annual precipitation for (left panel) wet and (right panel) arid years, with the 0.25, 0.5 and 0.75 cumulative frequency percentiles. The abscissa values indicate the precipitation intervals used for the calculations

2.6 Seasonal precipitation

We may finally group the rainfall per season (winter: December-February; spring: March-May; summer: June-August; autumn: September-November) and plot the corresponding time series (Fig. 2.13). The major feature is the different amount of seasonal precipitation, being generally largest during winter (accounting for 51% of the total precipitation), followed by spring (32%) and much less during autumn (17%). During the 1960s, however, the spring precipitation reached values nearly as large as during winter.

Other remarkable characteristics of the seasonal time series are the linear trend and the variability. The trend is negative during both winter and spring but positive during fall. The winter variability remains fairly constant throughout the entire period but the spring and autumn variability show substantial inter-decadal changes.

In order to explore the long-term trends, we produce highly smoothed time series with the help of a third-order polynomial (Fig. 2.13). The winter time series shows little inter-decadal variations but the spring time series displays a period of high precipitation during the 1950s to 1970s and low rainfall during the 1990s and 2000s, which coincide with highest and lowest variability. The autumn values remain fairly small during the entire time series except for the last few years, when rainfall increases by one order of magnitude.

The arid and wet years show up remarkably well in the seasonal time series, with most arid/wet years, corresponding to situations of relatively low/high winter and spring values. The major exceptions correspond to 1957, 2013 and 2015, which were wet years because of the anomalously high autumn rainfall.

2.7 Correlation with el NINO3.4

Several studies have pointed at a possible relation between global atmospheric patterns and the amount of precipitation over the Middle East (Tsvieli and A. Zangvil, 2005, 2007; Krichak et al., 2015). This would occur through the reinforcement of a low-level low-pressure centre over the Arabian Peninsula and northeast Africa, what has been termed the Red Sea Trough (Bitan and Sa'aroni, 1992).

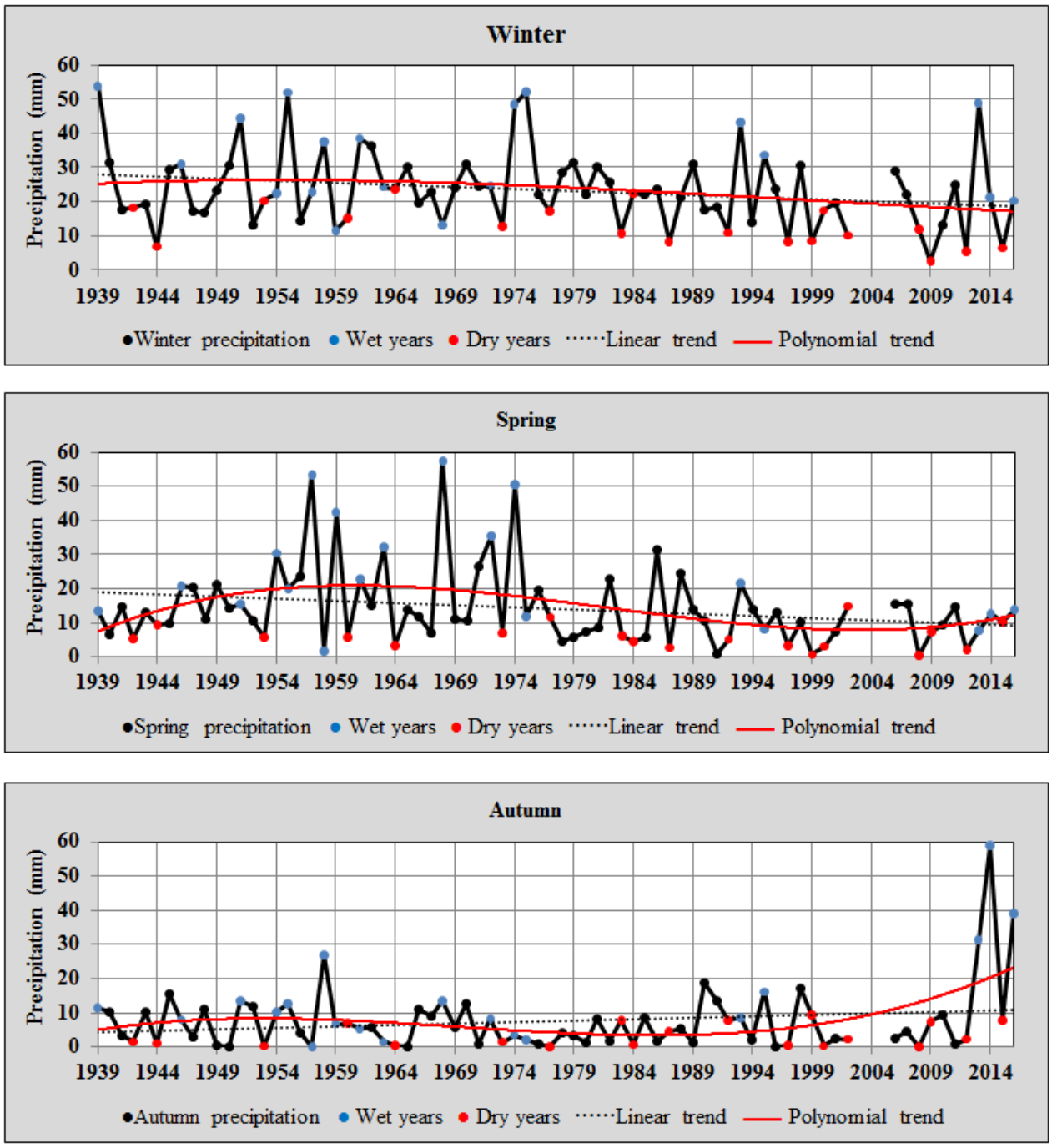

Figure 2.13. Seasonal precipitation (mm) histograms for Baghdad during1938-2015,the red points represent the dry years, blue points correspond to the wet years, the black dash points represent the linear trend and the red polynomial trend (third ordered).

The late fall and early winter enhancement of the Red Sea Trough is of particular interest because during these months the warm waters of the Red and Arabian Seas are a potential source of humidity to the lower atmosphere, as it will be shown in Chapter 4. For this reason, we will also use a monthly precipitation time series that only retains the October-through-February values.

Hence, in order to explore if there is a correlation between precipitation over Baghdad and the predominant middle-latitude global-scale climatic mode – El Niño-Southern Oscillation – we will calculate the correlation between the monthly time series of precipitation values and the monthly NINO3.4 indices (KNMI, 2018). Actually, we use four variations of the monthly precipitation time series to carry out this calculation: the entire original monthly rainfall values, the "decimated" time series with the precipitation values only for the period October to February, the entire "deseasonalized" monthly rainfall values, and the deseasonalized and decimated precipitation time series (the deseasonalization of the time series has been discussed in Section 2.3).

In Figures 2.14 we show the original and decimated time series and in Figure 2.15 we present the deseasonalized and decimated-deseasonalized time series, in all cases together with the monthly NINO3.4 values. In Table 2.1 we present the values for the Pearson correlation, a measure of the degree of linear association between both variables, together with its significance with a probability of P=0.95. The results show no significant correlation for any case.

Table 2.1. Pearson correlation and significance between the monthly time series of NINO3.4 and four different time series of monthly precipitation over Baghdad: original, decimated (October through February), deseasonalized and decimated-deseasonalized.

Precipitation monthly time series	Number of data points	Pearson correlation	Significance (P>0.9)
Original	924	-0.005	No
Decimated	385	0.014	No
Desasonalized	924	-0.025	No
Decimated and deseasonalized	385	-0.003	No

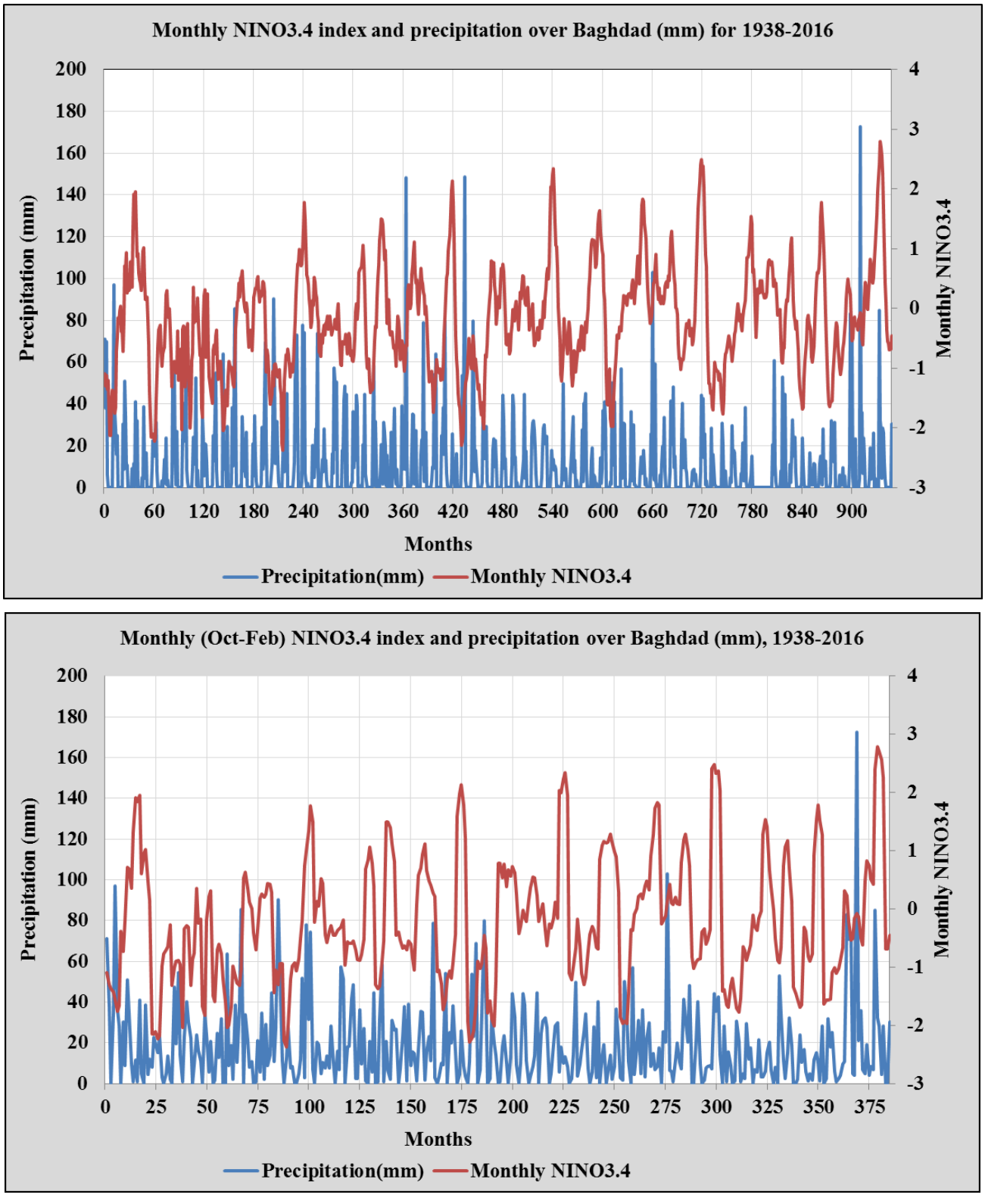

Figure 2.14. Monthly time series for el NINO3.4 index and precipitation over Baghdad for the 1938-2016 period, (top panel) considering the entire monthly time series and (bottom panel) considering only the decimated monthly data (October through February).

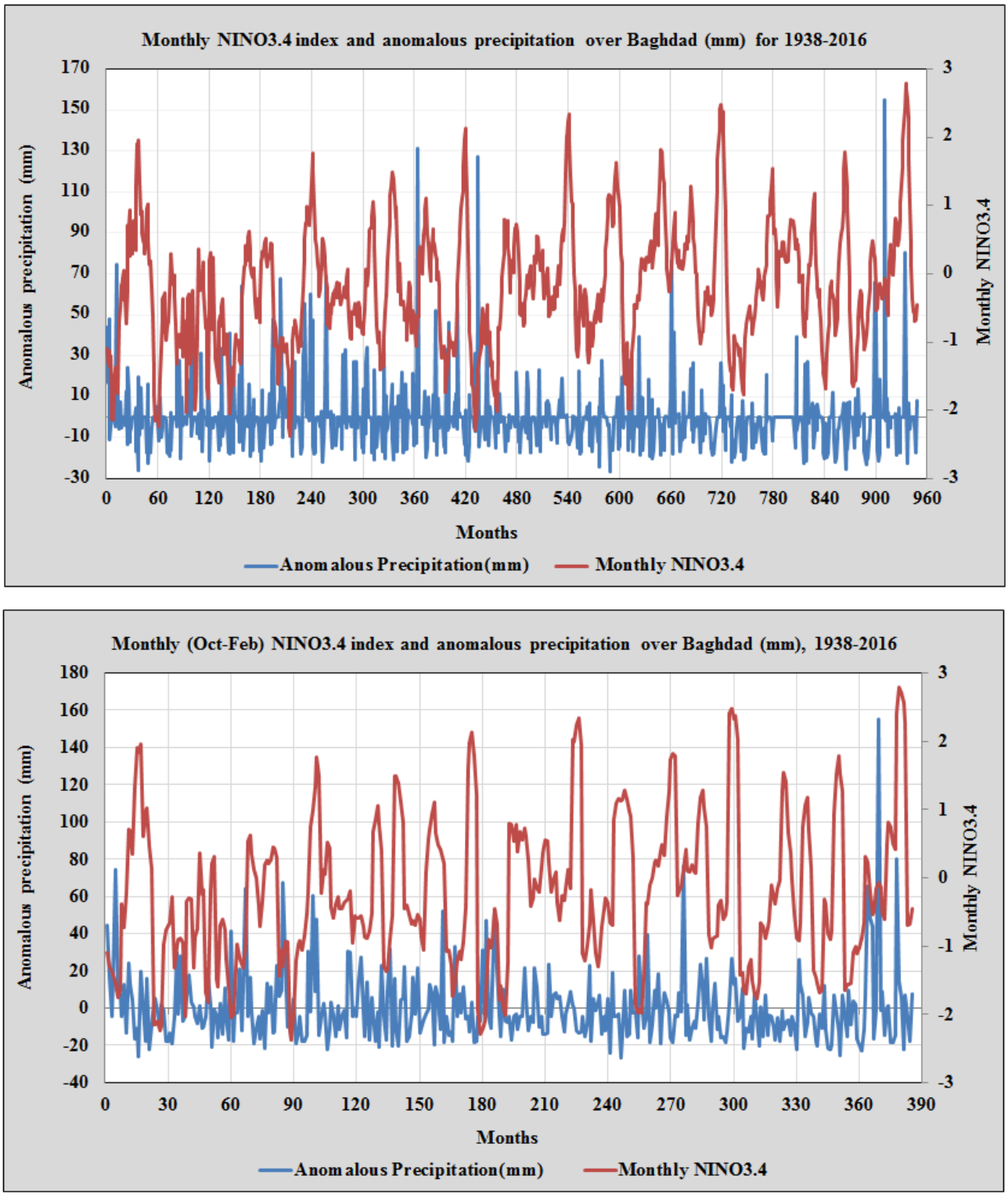

Figure 2.15. Monthly time series for el NINO3.4 index and deseasonalized precipitation over Baghdad for the 1938-2016 period, (top panel) considering the entire monthly time series and (bottom panel) considering only the decimated monthly data (October through February).

2.8 Concluding remarks

We have analysed a 76-year time series of monthly precipitation, from January 1938 to December 2016 (except 2003 and 2004), from a meteorological station in the city of Baghdad. The data allows exploring the monthly distribution of precipitation as well as the seasonal, inter-annual and decadal changes in rainfall in central Iraq. We reach the following conclusions:

(a) The annual precipitation is calculated for natural years, from 1 July to 30 June, logically separated by the dry summer season. With this consideration we find that the annual precipitation for the 75-year period (30 June 1938 to 31 July 2016 without 2002-2004) is 135.8 ± 61.9 mm/yr, with 43/32 years with rainfall below/above this mean value.

(b) The mean monthly precipitation for the entire period was 11.3 ± 18.7 mm. This value increases to 17.1 ± 20.9 mm if we ignore the three dry summer months (June-August), which never recorded any rainfall. Disregarding the summer months, there are 391 months (63.3%) with monthly rainfall below the mean and 223 months (36.3%) with monthly precipitation above the mean.

(c) There is substantial inter-decadal variation in annual and monthly rainfall. The 75-yr annual-rainfall record shows a relatively small linear trend (-0.5 mm/yr), which decreases even further when considering the winter and spring seasons (-0.13 and -0.11 mm/yr, respectively) but changes sign when considering the autumn season (0.08 mm/yr). However, these trends are very much dependent on the period considered, with the 1950s and 1960s being relatively wet years (150-170 mm/year) while the 1990s and 2000s where relatively arid (100-120 mm/yr).

(d) Besides the long-term trend in annual precipitation, there are also substantial inter-annual rainfall changes. The years with maximum precipitation were 1974, 2013 and 2013 (307.7, 278.1 and 263.6 mm), while those with minimum rainfall were 2012, 1997 and 2008 (29.3, 36.6 and 37.6 mm), with 43/32 years below/above the annual average. We calculate the precipitation density distribution and use the 25- and 75-percentiles (88 and 174 mm) to identify the conditions for arid and wet years (19 years for either one). The arid years account for a total of 1227 mm of rain, or 64.6 mm/yr, which is 12.0% of the total precipitation; the wet years account for 4181 mm of rain, or 220.1 mm/yr, or 41% of the total rainfall.

(e) The seasonal precipitation cycle also shows remarkable changes between average, wet and arid conditions, both in terms of mean values and variability. In average, January is the wettest month (29.5 mm/month) and also the one that experiences the largest inter-annual variations; November-December and February-April represent intermediate conditions and May and October correspond to low rainfall. During the arid years, the December-February period receives the largest amount of rain (10-15 mm/month) and experiences the highest variability. During the wet years, November-April collects the maximum precipitation (30-40 mm/month), with March, April and November showing the greatest variability.

(f) A careful comparison of the monthly rainfall shows no correlation with the NINO3.4 indices, neither using the original, decimated, deseasonalized nor decimated-deseasonalized data.

Chapter 3

Cut-off Lows over Iraq: Contribution to Annual Precipitation

3.1 Introduction

The Middle East and Northern Africa regions represent a vast region – roughly between 15°N and 35°N and from the Atlantic to the Indian Oceans – of arid and semiarid conditions, with annual precipitation less than 200 mm (Terink et al., 2013). These conditions have become more extreme during the last three decades because of severe droughts, with major negative effects on local and national economies (Ghulam et al., 2008; Asakereh, 2017). Further, climate projections for the coming years predict a continued decrease in precipitation and an increase in desertification (IAU, 2012).

The decline of mean precipitation in the Middle East, however, contrasts with the presence of extreme meteorological and flooding events with large economic impact (Easterling et al., 2009). The precipitation in Iraq is characterized by high temporal and spatial variability (UN-Iraq 2010, 2013), as it happens for the entire Mediterranean region (Reiser and Kutiel, 2010; Lionello et al., 2012). The country's mean annual precipitation is 154 mm (Al-Ansari and Knutsson, 2011) though rainfall changes largely with latitude and elevation, from less than 100 mm over about 60% of the country to some 1200 mm to the northeast. Rainwater is almost entirely restricted to October through May when the Mediterranean depressions enter Iraq (Al-Ansari and Knutsson, 2011; Lionello et al., 2012). However, the amount of rain varies considerably at inter-annual and decadal scales, with relatively moist 1970s and considerably dry 1990s (Mohammed and Hadi, 2012; Al-Rijabo and Salih, 2013). An extreme drought took place in 2008 – the most severe for the 1980-2010 period – followed by heavy rainfalls and short storms in the central and southern Iraq (Al-Timimi and Al-Jiboori, 2013).

Several studies on precipitation in Iraq have looked at the spatial and temporal distributions of rainfall, with emphasis on the character of the monthly-precipitation distributions (Al-Mansoty, 2005; Alghazali and Alawadi, 2014). Using data for 36 meteorological stations during the 1981–

2010 period, Al-Salihi et al. (2014) observed a negative annual-rainfall trend in 32 sites, with most of the decrease occurring in winter and spring. In contrast, there is a substantial lack of studies on daily precipitation and on the weather systems responsible for the high precipitation events that occasionally affect Iraq. Designers and decision makers need a proper knowledge of the spatial and temporal distribution of rainfall, including an improved short- and long-term forecast of its trends and variability (Mohammed and Hadi, 2012; Al-Suhili and Khanbilvardi, 2014; Hussein et al., 2005). In particular, the development of water resource facilities and farming capabilities in the Middle East has to consider that rainfall often occurs as extreme flooding. This requires identifying what is the contribution of the extreme flooding events and which are the atmospheric conditions that lead to these situations.

Here we explore the extreme precipitation events during the last 12 years, focusing on those cases that correspond to a cut-off low, with special attention on the 19 November 2013 episode that led to the maximum rainfall for the entire period. We will use different sources of information, including in situ and reanalysis data, in order to assess what were the dynamical conditions that promoted the anomalously high humidity during the episode.

This chapter is organized as follows. Section 3.2 presents the datasets and methods, Section 3.3 describes the temporal variability of the rainy events, and Section 3.4 identifies those extreme precipitation cases that responded to cut-off low atmospheric systems. We close summarizing the contribution of cut-off lows for Iraq's hydrological regime.

3.2 Data and methods

Iraq is located in the heart of the Middle East, extending from 29.50°N to 37.22°N and between 38.45°E and 48.45ºE. It is found adjacent to the shallow Persian Gulf, with very saline year-long waters and very warm summer waters (Yao, 2008), and relatively close to the eastern Mediterranean and Red Seas. Following Köppen's classification, Iraq can be divided into three main climates: subtropical-desert in the south and central regions, subtropical-steppe in central-northern Iraq, and dry-summer subtropical in the northern mountainous regions (Pannell, 2002; Walker, 2005; Peel et al., 2007). Here we will focus on the large central plains, where topographic variability is absent and long data records are available.

3.2.1 In situ precipitation

Daily precipitation records for 12 years – 1 January 2005 to 31 December 2016 – come from the Baghdad meteorological station, run by the Iraqi Meteorological and Seismology Organization. This station is located in the large central plains (33.33°N, 44.43°E; 34 m elevation), where topographic variability is absent. The homogeneity of the annual precipitation series has been verified using the Von Neumann and Thom tests (Messeguer-Ruiz and Sarricolea, 2017).

Data from three other Iraqi meteorological stations (Basra, Mosul and Rutba) are available for selected periods. These data are complemented with satellite images in the visible spectrum, downloaded from the National Aeronautics and Space Administration (NASA) web page (https://earthdata.nasa.gov/worldview.)

3.2.2 Radiosonde data

Daily radiosonde data from the Baghdad station is available for the days previous, during and after the November 2013 flooding (except for 18 November due to a balloon failure). These data can be used to draw skew-T log-P diagrams, as well as to calculate several atmospheric instability indices. These are the Lifted (LI), Showalter (SI), Total Totals (TT), SWEAT, K and CAPE indexes, as well as the precipitable water (PW) content. The definitions, common usages and threshold values for these indexes are shown in Table 3.1.

3.2.3 Reanalysis fields

The temperature, humidity, geopotential height, horizontal and vertical velocity, horizontal divergence, relative vorticity (RV) and potential vorticity (PV) fields come from the ERA-Interim global atmospheric reanalysis, available four times a day on a $0.75^{o} \times 0.75^{o}$ latitude-longitude grid from the European Centre for Medium-Range Weather Forecasts (ECMWF). These data has been downloaded for a domain extending from 0°E to 60°E and from 10°N to 60°N. Other inferred variables are equivalent potential temperature (EPT), PW, moisture flux (MF), moisture flux convergence (MFC), Q-vector divergence, RV and PV advection, and the instability indexes; the divergence and advection values are calculated using centered finite differences.

Table 3.1. Definitions of precipitable water (PW) and atmospheric indexes computed using both the Baghdad station soundings and the ERA-Interim reanalysis. Its principal use and common threshold values are specified.

Skew-T indexes	Definition	Common usage	Thresholds
Precipitable water (PW, mm) (Peixoto and Oort 1992)	Integral of the humidity between 1000 and 700 hPa.	Amount of moisture in the lower troposphere	High moisture content: 45-50 mm; very high moisture content: > 50 mm
Convective available potential energy (CAPE, J kg-1) (Weisman and Klemp 1986)	Integral of the positive area in a skew-T log-P diagram	Likelihood of storm formation	Moderate instability: > 1000 J kg-1 (Lorente et al., 2008); 1000-2500 J kg-1 (NOAA, 2017)
K (KI, °C) (George 1960)	Temperature differences between 850 and 500 hPa combined with the differences in dewpoint temperature at 850 and 700 hPa, $KI = (T_{850} - T_{500}) + T_{d,850} - (T_{700} - T_{d,700})$	Convective potential	High probability of thunderstorms: > 25°C (Lorente et al., 2008); > 30°C (NOAA, 2017)
SWEAT (Miller 1972)	$SWEAT = 12\ T_{d,850} + 20\ (TT - 49) + 2\ V_{850} + V_{500} + 125\ (\sin\theta + 0.2)$, where V_{850} and V_{500} stand for the wind speed at 850 and 500 hPa, and θ is the change in wind direction from 850 to 500 hPa	Probability of storms	Possible severe thunderstorms: > 200 J kg-1 (Lorente et al., 2008) ; 300-400 (NOAA, 2017)
Lifted index (LI, °C) (Galway 1956)	Difference between the environment temperature at 500 hPa minus the temperature of an air parcel at 850 hPa risen to 500 hPa, $T_{500} - T_{850/500}$	Stability of the atmosphere	Thunderstorms possible: < 0°C (Lorente et al., 2008); -2-0°C (NOAA, 2017)
Showalter (SI, °C) (Showalter 1953)	Difference between the environment temperature at 500 hPa minus the temperature of an air parcel at 850 hPa, the air parcel is lifted moist adiabatic to the lifted condensation level (LCL) and then dry adiabatic to 500 hPa, $T_{500} - T_{850/500}$	Stability of the atmosphere	Thunderstorms possible: < 4°C (Lorente et al., 2008); -2-1°C (NOAA, 2017)
Total totals (TT, °C) (Miller 1972)	Lapse rate between 850 and 500 hPA, $TT = (T_{850} - T_{500}) + (T_{d,850} - T_{500})$	Static stability between 850 and 500 hPa	Isolated moderate thunderstorms : > 44°C (Lorente et al., 2008); 44-45°C (NOAA, 2017)

The moisture flux is vertically-integrated between 1000 and 700 hPa (VIMF, with units of kg m^{-1} s^{-1}) and its horizontal convergence is then calculated (VIMFC, with units of kg m^{-2} s^{-1}) (Van Zomeren and van Delden, 2007, Krichak et al., 2015):

$$\mathrm{VIMF} = -\frac{1}{\mathrm{g}} \int_{p_{1000}}^{p_{700}} (q\vec{u})\, \mathrm{d}p \,,$$

$$\mathrm{VIMFC} = -\frac{1}{\mathrm{g}} \int_{p_{1000}}^{p_{700}} \left[\frac{\partial(qu)}{\partial \mathrm{x}} + \frac{\partial(qv)}{\partial \mathrm{y}}\right] \mathrm{d}p \,,$$

where $\vec{\mathrm{u}} = (\mathrm{u}, \mathrm{v})$ is the horizontal wind velocity vector with components in the west-east and south-north directions (x, y), p is air pressure, q is specific humidity, ρ is air density and g is gravity acceleration; the integrals are calculated between the 1000 and 700 hPa pressure levels, p_{1000} and p_{700}. Note that in these definitions the VIMF is a vector while the VIMFC is a scalar.

3.2.4 Sea and air surface temperature

The foundation (free from daily variation) sea surface temperature (SST) is available since January 2007 from the Operational Sea Surface Temperature and Ice Analysis (OSTIA) system run by the UK Met Office. For our analysis we have examined the 0.05° resolution daily SST data in the central Persian Gulf (26°N, 52°E) and northern Red Sea (25°N, 36°E). These marine regions represent potential sources for low-level humidity; the selected sites are representative for these regions and yet are located far enough from coastal areas that could be influenced by upwelling. The data used corresponds to the week previous to seven cut-off low events that brought extreme flooding to the Baghdad area; a one-week period is adequate to assess the arrival of air masses from the marine regions to central Iraq.

Additionally, we use temperature data for Basra (from the Iraqi Meteorological and Seismology Organization) and climatological temperature data for Kuwait City (from the Kuwait Meteorological Service, http://www.met.gov.kw/) to estimate the monthly-mean air surface temperature (AST) for the northern Persian Gulf. The procedure consists in calculating the mean climatological temperature difference between the two stations (Kuwait City is cooler than Basra by 7.1°C) and

using this difference to obtain the monthly-mean AST for the northern Persian Gulf since January 2007.

3.2.5 Cut-off low detection

We use an index as defined by Scherrer et al. (2006) and Davini (2013), which is a bidimensional extension of the original method by Tibaldi and Molteni (1990), set to identify reversals in the sign of the geopotential-height latitudinal gradient at 500 hPa. The algorithm is applied to the 6-hourly data, using the 1200 UTC data, in the region 0-60ºE and 10-75ºN as extracted from the ERA-Interim reanalysis. The procedure works automatically to identify all instances with a cut-off low pattern. Once the pattern is detected, the geopotential distribution is visually inspected, first, to check if the cut-off low center was situated near or over Iraq (inside the square 35-50°E and 25-40°N) and, second, to verify whether the situation corresponded to a precipitation event. Some examples of cut-off lows detected by the algorithm, with and without precipitation, are shown in Figure 3.1.

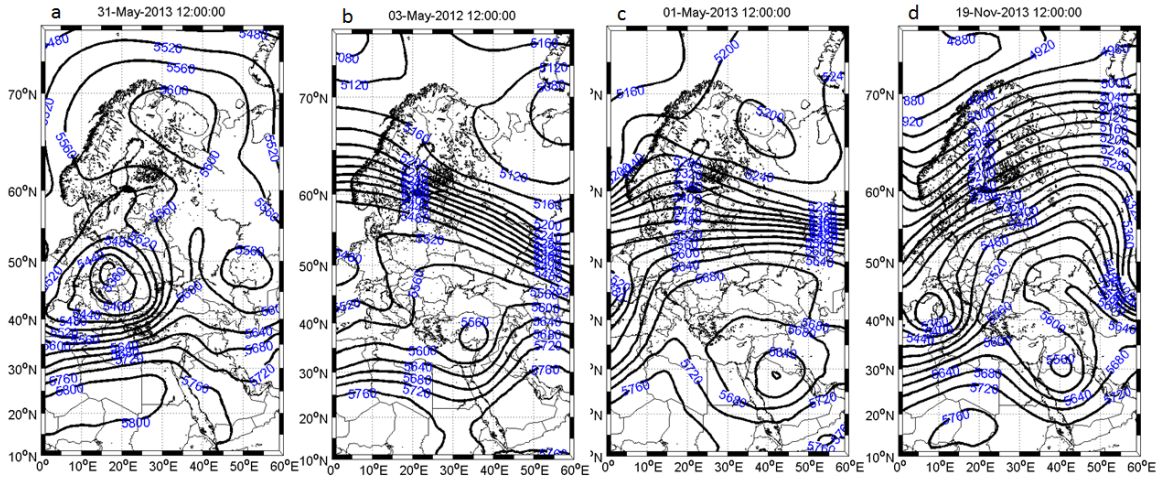

Figure 3.1. Examples of cut-off low detection for the following situations: (a) not affecting the Middle East, (b) affecting the Middle East but not bringing precipitation over Baghdad, (c) affecting the Middle East bringing low precipitation over Baghdad, (d) affecting the Middle East with high precipitation over Baghdad.

3.3 Seasonal and inter-annual hydrological variations

The daily-precipitation 12-year time series from the Baghdad station shows that rain occurred as isolated events, for a total of 204 incidences (Figs. 3.2a,b and Table 3.2); these rainy events were

nearly absent during the summer season, with one single instance of rain in 12 yrs. The annual precipitation rate for this 12-year period is 130.8 ± 67.1 mm/yr. Rain fell during 421 days (9.6% of the days), with daily precipitation exceeding 1 mm only on 145 occasions (3.3%). We have gathered rainy days into events or episodes, with each individual episode defined as a group of days when rain fell continuously, for a total of 204 events. There were 20 extreme events, defined to equal or exceed the 90 precipitation percentile (20 mm), which accounted for 51.3% of the precipitation during the entire period (Fig. 3.2b and Table 3.2).

Table 3.2. Precipitation events for the Baghdad station (mm) during 2005-2016. A total of 20 extreme events, with precipitation over 20 mm, are shown in bold letters; the 14 extreme events detected as cut-off lows are indicated as C.

No.	Date	Precip. (mm)	No.	Date	Precip. (mm)	No.	Date	Precip. (mm)
1 C	**21-24 Jan 2005**	**20.4**	69	26-27 Mar 2010	5.5	137	30 Mar 14	<0.1
2	2-8 Feb 2005	6.4	70	7 Apr 2010	1.4	138	12-17 Apr 2014	12.6
3	**7-11 Mar 2005**	**60.6**	71	17-18.Apr 2010	1.8	139	21 Apr2014	<0.1
4	25-26 Apr 2005	10.8	72	22 Apr 2010	1.5	140	27-28 Apr 2014	1.7
5	2 May 2005	2.2	73	27-28 Apr 2010	6	141	9 May 2014	<0.1
6	29 Oct 2005	<0.1	74	1 May 2010	12.6	142	12 May2014	<0.1
7	6 Nov 2005	<0.1	75	15 May 2010	<0.1	143	21-23 May 2014	<0.1
8	15-16 Nov 2005	7.8	76	4 Oct 2010	<0.1	144	1 Jun 2014	<0.1
9	**6-11 Jan 2006**	**34.7**	77	1 Nov 2010	2.5	145	12-16 Oct 2014	2.9
10	20 Jan 2006	0.3	78	10-12 Dec 2010	14.6	146	19-20 Oct 2014	0.9
11	23-25 Jan 2006	17.7	79	30-31 Dec 2010	17.4	147	27-29 Oct 2014	0.8
12	**1-3 Fab 2006**	**33.4**	80	3-4 Jan 2011	0.4	148	01-03 Nov 2014	0.7
13	26 Fab 2006	0.7	81	8-9 Jan 2011	1.9	149	16 Nov 2014	<0.1
14 C	**1-2 Apr 2006**	**20.8**	82	14-15 Jan 2011	7.8	150	20-21 Nov 2014	4.0
15	11-12 Apr 2006	5.0	83	24-25 Jan 2011	0.7	151	24-26 Nov 2014	14.3
16	17 Apr 2006	17.0	84	28-30 Jan 2011	7	152	09 Dec 2014	<0.1
17	26 Apr 2006	1.8	85	1-2 Feb 2011	7.5	153	13-14 Dec 2014	2
18	6 May 2006	2.2	86	7-8 Feb 2011	17.5	154	22-23 Dec 2014	0.9
19	10-15 Oct 2006	1.4	87	7-8 Mar 2011	<0.1	155	26-27 Dec 2014	1.0
20	23-31 Oct 2006	9.8	88	12 Mar 2011	0.2	156	7-10 Jan 2015	7.9
21	4-6 Nov 2006	2.4	89	22-25 Mar 2011	12.2	157	15 Jan 2015	0.3
22	15-17 Dec 2006	4.5	90	**19-22 Apr 2011**	**29.1**	158	29-30 Jan 2015	<0.1
23	22-23 Dec 2006	10.6	91	29-30 Apr 2011	1.9	159	15-16 Feb 2015	<0.1
24	5-8 Jan 2007	7.2	92	16-18 May 2011	0.3	160	19-21 Feb 2015	5.3
25 C	**11-12 Jan 2007**	**24.6**	93	8 Jun 2011	<0.1	161	2 4Feb 2015	1.6
26	30 Jan 2007	0.4	94	25-29 Oct 2011	6.1	162	8-9 Mar 2015	0.2
27	2-3 Feb 2007	2.3	95	19 Nov 2011	0.8	163	12-13 Mar 2015	<0.1
28	15-16 Feb 2007	15.5	96	30-31 Dec 2011	2.5	164	19-21 Mar 2015	19.4

29	21-22 Feb 2007	1.0	97	25 Jan 2011	0.3	165	28-29 Mar 2015	6.5
30	1 Mar 2007	8.0	98	30-1 Feb 2012	12	166	4 May 2015	4.5
31	15-17 Mar 2007	6.9	99	7 Feb 2012	0.5	167	9-10 May 2015	<0.1
32	10-11 Apr 2007	17.3	100	17-18 Feb 2012	<0.1	168	26-27 May 2015	<0.1
33	26-30 Apr 2007	6.7	101	25 Feb 2012	0.7	169	30 Aug 2015	<0.1
34	16-17 May 2007	7.3	102	1-4 Mar 2012	1.0	170	6 Oct 2015	<0.1
35	1 Dec 2007	2.0	103	10-12 Apr 2012	5.4	171	19-21 Oct 2015	<0.1
36	5 Jan 2008	1.1	104	21 Oct 2012	6.0	172 C	**25-29 Oct 2015**	**84.9**
37	10-11 Jan 2008	7.3	105	24-26 Oct 2012	4.7	173 C	**4-6 Nov 2015**	**21.8**
38	22-26 Jan 2008	15.1	106	10-12 Nov 2012	8.3	174	9 Nov 2015	2.5
39	30-31 Jan 2008	0.2	107 C	**17-19 Nov 2012**	**35.0**	175	16-17 Nov 2015	7.4
40	6-8 Feb 2008	0.1	108 C	**22-23 Nov 2012**	**37.3**	176	30 Nov2015	0.4
41	14 Feb 2008	2.6	109	27 Nov 2012	2.6	177	3 Dec 2015	0.5
42	24-26 Feb 2008	7.6	110	4 Dec 2012	0.5	178	12-14 Dec 2015	1.1
43	11-13 Mar 2008	1.6	111	18-19 Dec 2012	2.6	179	17 Dec 2015	0.3
44	17 May 2008	<0.1	112 C	**24-25 Dec 2012**	**67.5**	180	23 Dec 2015	2.6
45	18 Oct 2008	0.3	113	7-9 Jan 2013	0.1	181 C	**29 Dec15 – 1 Jan16**	**23.7**
46	25-30 Oct 2008	16.3	114	**27-28 Jan 2013**	**49.7**	182	7-9 Jan 2016	1.5
47	28-29 Nov 2008	5.8	115	**30-1 Fab 2013**	**21.0**	183	17-18 Jan2016	0.5
48	22-23 Dec 2008	1.1	116	6 Fab 2013	1.4	184	22-25 Jan 2016	2.3
49	11 Jan 2009	4.8	117	22-23 Fab 2013	3.5	185	6-7 Feb 2016	4.7
50	10 Feb 2009	1.4	118	1-6 May 2013	16.1	186	10 Feb 2016	1.1
51	1-3 Mar 2009	0.3	119	12-15 May 2013	2.5	187 C	**21-23 Feb 2016**	**21.3**
52	9 Mar 2009	10	120	19-20 May 2013	4.8	188	26-27 Feb 2016	1.2
53	13 Mar 2009	1.1	121	30-2 Nov 2013	12.4	189	3 Mar 2016	0.2
54	4-9 Apr 2009	11.1	122 C	**7-10 Nov 2013**	**74.3**	190	14 Mar 2016	<0.1
55	25 Apr 2009	<0.1	123 C	**18-20 Nov 2013**	**89.6**	191 C	**25-28 Mar 2016**	**25.9**
56	9 May 2009	<0.1	124	28-29 Nov 2013	0.4	192	7-14 Apr 2016	11.7
57	19 Sep 2009	2.1	125	3-5 Dec 2013	16.6	193	27 Apr 2016	<0.1
58	24 Oct 2009	5.4	126	12-13 Dec 2013	0.4	194	29 Apr 2016	<0.1
59	27 Oct 2009	6.2	127	29-31 Dec 2013	3.9	195	5-7 May 2016	3.8
60	16-18 Nov 2009	15.1	128	1 Jan 2014	0.1	196	10-11 May 2016	<0.1
61	12 Dec 2009	9.2	129	4-5 Jan 2014	2.2	197	25 Oct 2016	<0.1
62	16 Dec 2009	0.2	130	9-10 Jan 2014	12.7	198	3-4 Nov 2016	<0.1
63	29-31 Dec 2009	0.6	131	17 Jan2014	17.8	199	30 Nov 2016	<0.1
64	14-15.Jan 2010	0.6	132	26-28 Jan 2014	3.0	200	1 Dec 2016	0.1
65	18-20 Jan 2010	0.5	133	2-3 Feb 2014	6.8	201	14 Dec 2016	0.5
66	3-6 Feb 2010	13.6	134	15 Feb 14	<0.1	202	18 Dec 2016	0.1
67	19 Feb 2010	3.9	135	2-3 Mar 2014	6.9	203 C	**23-25 Dec 2016**	**29.6**
68	25-28 Feb 2010	10.6	136	8-14 Mar 2014	16.7	204	27 Dec 2016	<0.1

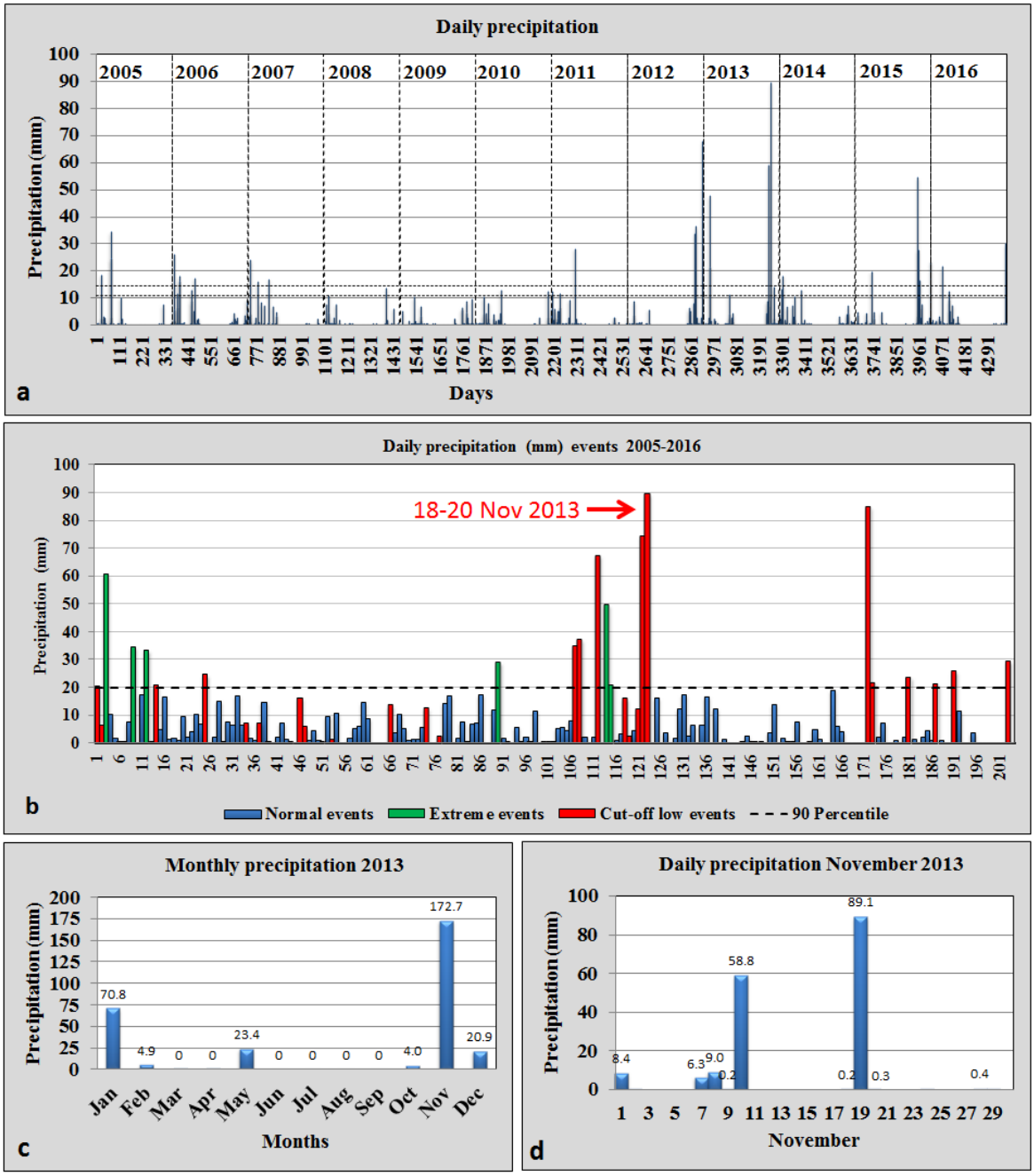

Figure 3.2. Precipitation data (mm) over Baghdad for the 2005-2016 period: (a) time series with daily precipitation values, (b) sequence of precipitation events over Baghdad: cut-off lows are in red, extreme events (over the 90-percentile) are in green except for the red-colored cut-off lows, and all other rainy events are in blue; (c) monthly values during 2013, and (d) daily values during November 2013.

The precipitation time series (Fig. 3.2a) also illustrates the existence of substantial seasonal (Fig. 3.3a) and intra-annual (Fig. 3.3b) variability. Peak rain values occurred during November although moderate rain (above the mean monthly value of 10.9 mm/month) took place between October and April. Hence, for calculating the annual precipitation figures, we set July-to-June natural years that recognize this Mediterranean rainy season (Xoplaki et al., 2004) and identify them through the year of the second semester, e.g. natural year 2006 corresponds to the period between 1 July 2005 and 30 June 2006; this reduces the number of annual histograms to only 11 natural years (Figs. 3.3b,d). Maximum natural annual precipitation corresponded to 2013 (263.6 mm), 2014 (278.1 mm) and 2016 (219.4 mm), for a mean precipitation of 253.7 mm (Fig. 3.3b), so we combine these three years to characterize the wet conditions. In contrast, minimum natural annual precipitation occurred in 2008 (37.6 mm), 2009 (52.2 mm) and 2012 (29.3 mm) for a mean precipitation of 39.7 mm (Fig. 3.3b), so again we pool these three years to portray the arid-year conditions. Notice that this selection of three wet and three arid years is equivalent to thresholds of 25 (95.1 mm) and 75 (167.9 mm) percentiles.

The daily precipitation time series demonstrates the exceptionality of the 19 November 2013 event (Figs. 3.2a,b; see also Table 3.2). This episode, the largest flood for the entire time series, took place as part of a series of events that began in autumn 2012, following a severe drought in Iraq that lasted for some 30 years (1980-2011) (Al-Timimi and Al-Jiboori. 2013). The precipitation during November 2013 (172.7 mm) represented 62.1% of the total annual precipitation for the natural 2014 year (and 58.2% of the calendar 2013 year) (Fig. 3.2c). Further, more than half the November precipitation (89.1 mm) took place on 19 November, representing 30.2% of Baghdad's during the 2014 natural year (Fig. 3.2d).

The data illustrate how the extreme values recorded in Baghdad were also anomalously large as compared with other locations in the country. No rain was recorded to the north of the country (Mosul station) and substantially smaller values were recorded to the west (20 mm in Rutba, with peak precipitation also on 19 November) and south (40 mm in Basra, with peak values on 18 November) (Fig. 3.4). These measurements confirm that the extreme precipitation was fairly localized, with maximum values in the eastern part of the country, and lasted no more than 48 hours.

These observations somewhat contrast with cloud coverage over the Middle East, which increased rapidly between 17 and 19 November 2013 (Fig. 3.5). On 19 November the extension of the clouds

was largest, covering portions of the southern Arabian Peninsula as well as all Iraq and part of Iran. On 20 November the cloud coverage was still large but had disappeared from most of the Arabian Peninsula and southern Iraq.

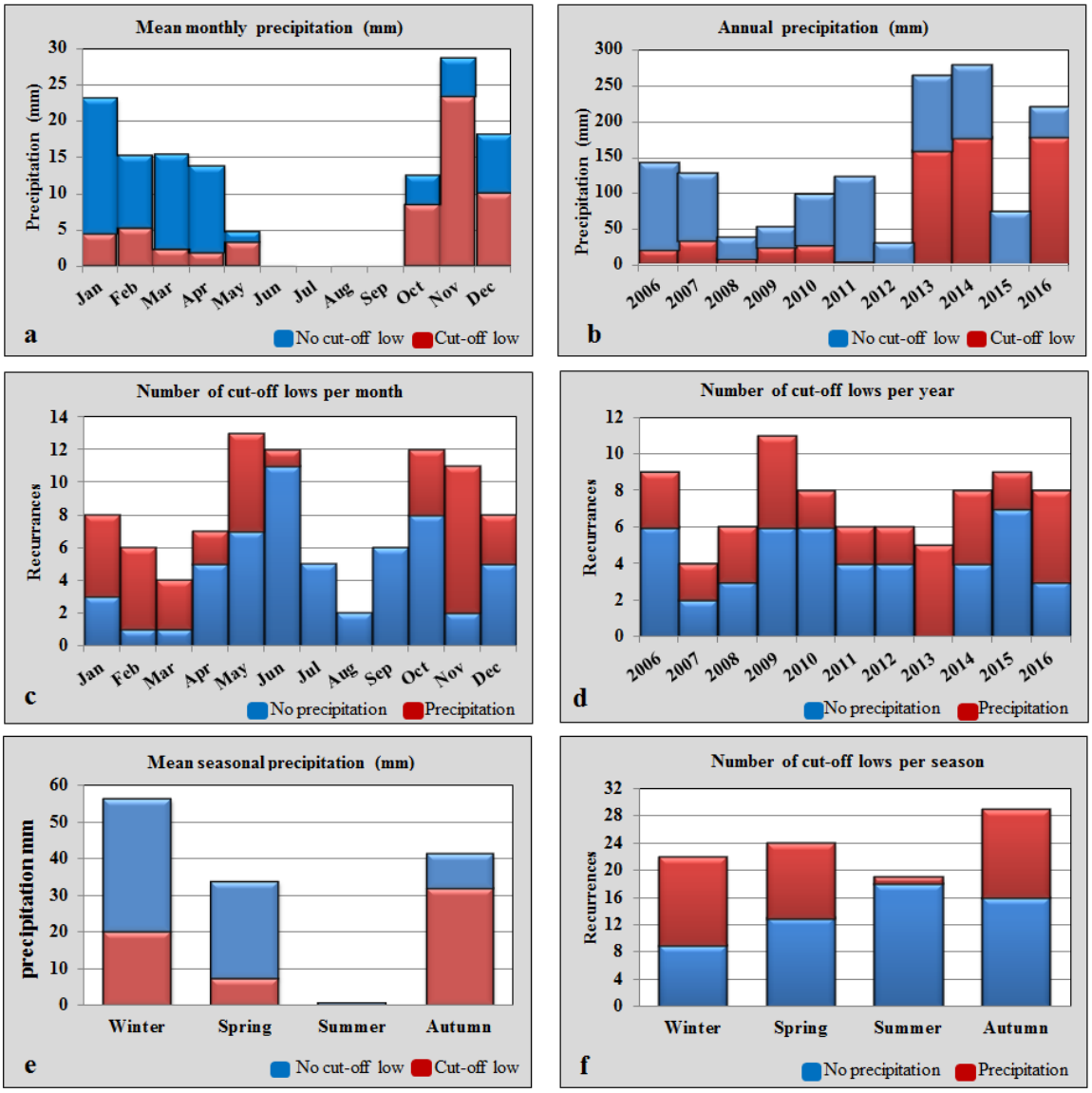

Figure 3.3. Precipitation histograms for Baghdad during 2005-2016 (panels b and d represent the natural annual values, hence representing the period from 1 July 2005 to 30 June 2016). (a) Monthly and (b) annual precipitation values (mm), distinguishing the fraction associated with cut-off low events. Number of cut-off low events (c) per month and (d) per year, with and without precipitation. (e) Seasonal precipitation (mm), distinguishing the fraction associated with cut-off lows. (f) Number of cut-off lows per season, indicating those with and without precipitation.

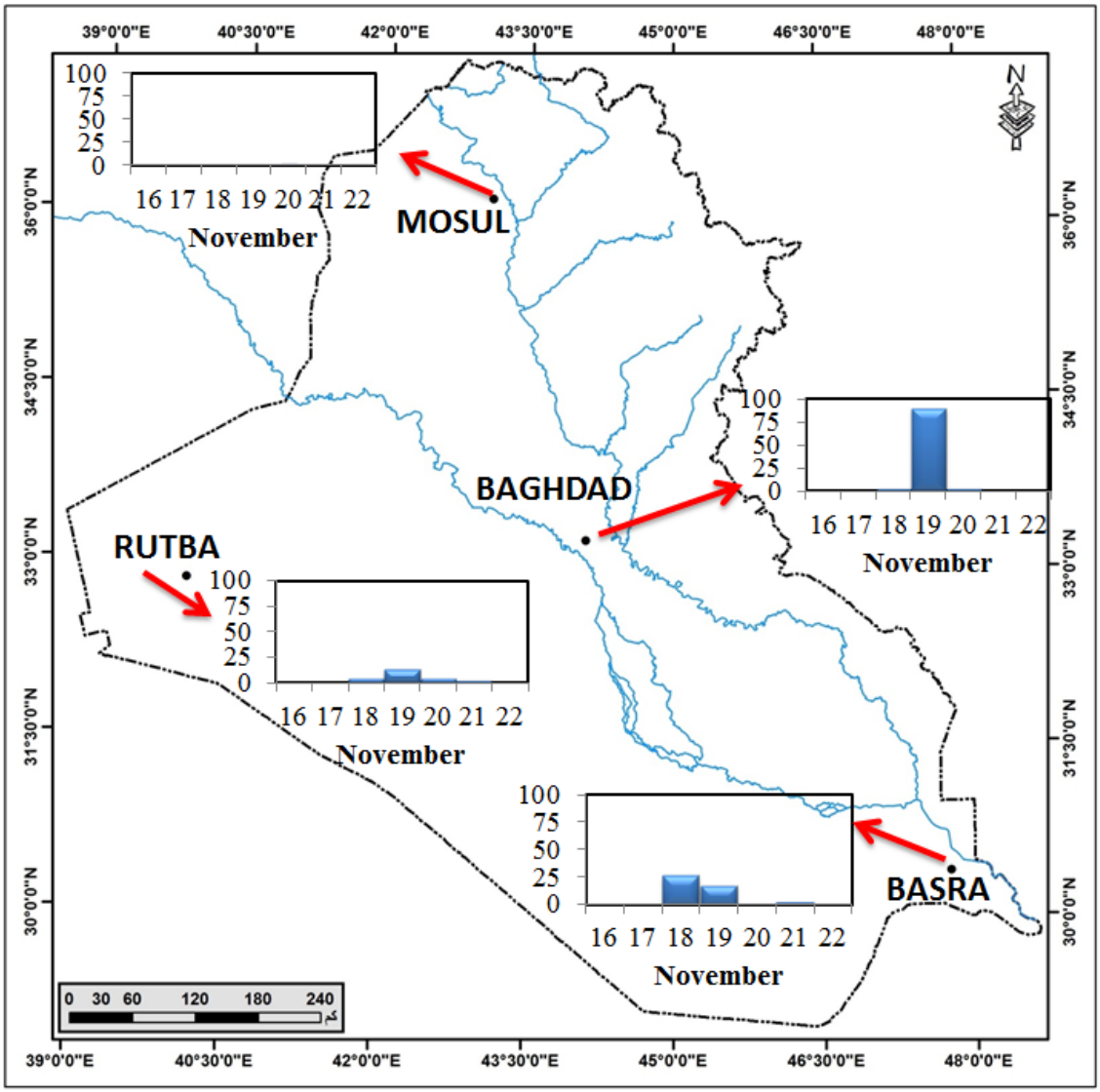

Figure 3.4. Precipitation histograms (mm) in four different Iraqi stations during the 16-22 November 2013 period.

3.4 Cut-off low contribution to extreme events

The cut-off low detection algorithm allows investigating the frequency of this pattern and its contribution to rainfall (Fig. 3.2b). From all cut-off lows automatically identified, a total of 94 affected Iraq during the study period with 38 of them causing precipitation and 14 leading to extreme rainfall. The number of cut-off low events influencing Iraq ranged between 3 and 10 per natural year (Fig. 3.3d). The number of cut-off low rainy events was less than doubled for the wet years as compared with the arid years: nor for the entire year (14 versus 9 events) neither for the

autumn months (9 versus 5 episodes); however the amount of rain brought by these rainy events was 16 times less during the arid than during the wet years, 31.3 mm as compared with 512.3 mm.

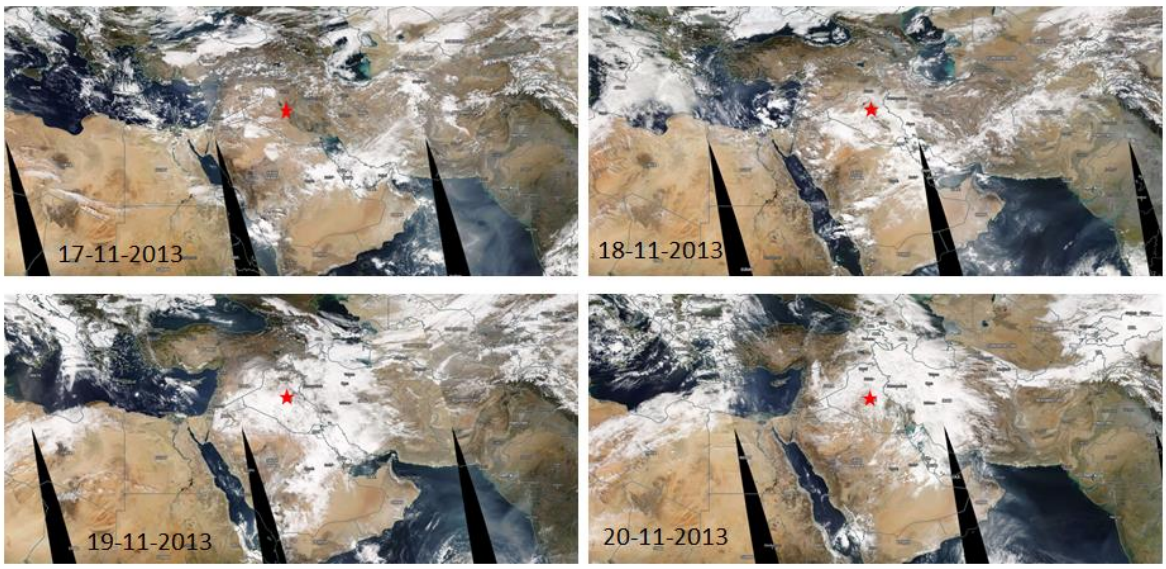

Figure 3.5. Satellite images for the Middle East between 17 and 20 November 2013, in the visible spectrum (downloaded from NASA, https://earthdata.nasa.gov/worldview).

The monthly frequency of all cut-off lows is bimodal, with the largest mode centered in May and June and a second mode in October and November; however, the cut-off low conditions associated with rain dominated in May and November (Fig. 3.3c). If we group the cut-off lows per season (Dec-Feb, Mar-May, June-Aug, Sep-Nov), it turns out that the number of cut-off lows remains fairly constant between seasons (Fig. 3.3f) though the amount of rain associated with these events is much larger during autumn (Fig. 3.3e), all the rain falling in October and November (Fig. 3.3a).

Most cut-off lows lasted only 1-3 days, though some events persisted longer, up to seven days (Fig. 3.6). As a result, the 38 rainy cut-off low events over Baghdad led to 118 rainy days (21.6% of the total number of wet days), although these events brought 43.4% (681.9 mm) of the total rainfall. There were major differences between the arid and wet years. The total rain for the arid years was of 119.1 mm, with a contribution of 31.3 mm (26.3%) from cut-off lows. During 2008, the driest natural year of the time series, the contribution of cut-off lows to the annual precipitation was only 0.3 mm. In contrast, during the wet years the total rain was 761.1 mm, with an input of 512.3 mm (67.3%) from cut-off lows. In 2014, the wettest year of the time series, the rainfall associated with

cut-off lows was 63.4% of the total (176.3 out of 278.1 mm); this fraction increased even more during 2016, with a cut-off low contribution of 80.9% (out of a total of 219.4 mm).

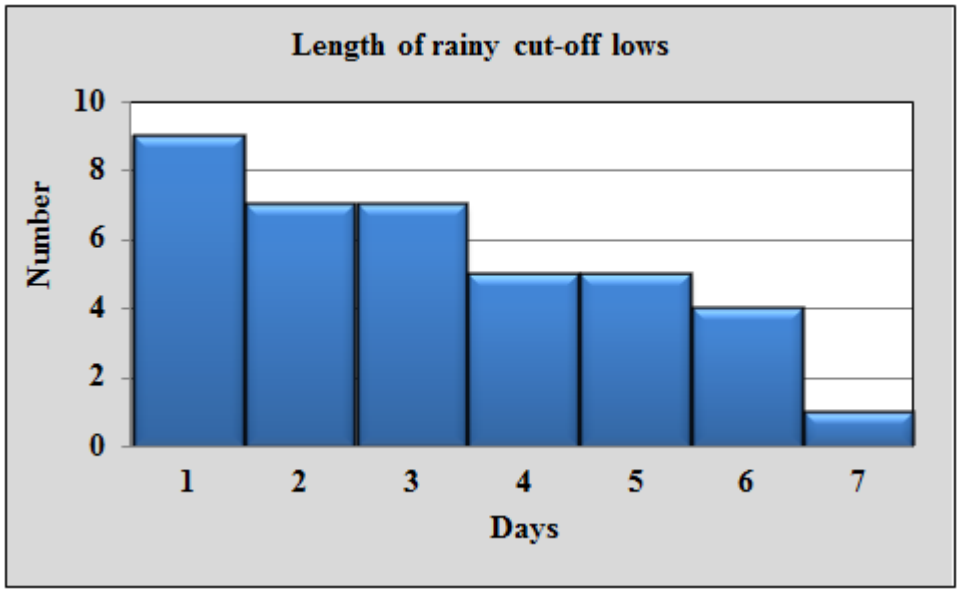

Figure 3.6. Histogram for the number of days that rainy cut-off lows remained over the Middle East during the 2005-2016 period.

The daily- and event-precipitation histograms help quantify the differences between arid and wet years (in the event-precipitation histograms the abscissa corresponds to the total precipitation during an event, Fig. 3.7). The shape of the arid- and wet-years daily-precipitation histograms is fairly similar for values less than 4 mm: during the arid years, 74% of the rainy days had precipitations ≤ 1 mm, 14% had precipitations between 1 and 4 mm, and 11% had precipitations between 4 and 14 mm; during the wet years these values were 61%, 17% and 12%, respectively (Figs. 3.7a,b). However, during the wet years there were 8% of days with rainfall over 14 mm (4% exceeding 30 mm) as compared with none during the arid period.

The different impact of cut-off lows on rainfall during arid and wet years shows up in the event-precipitation histograms that distinguish the cut-off low contribution (Figs. 3.7c,d). The number of cut-off lows was 10 out of 32 rainy events during the arid years (25%), and 15 out of 69 rainy events during the wet years (22%). Despite the similar proportions, the influence of the cut-off lows to rain was very disparate: the cut-off lows contribute mostly to high-rain events (being the sole contribution to events over 20 mm) and instead have a residual contribution to low-rain events; in

contrast, during the arid years, the cut-off lows have a moderate contribution to events with less than 10 mm. Specifically, considering the 0-4, 4-14 and >14 mm intervals, the number of events during the arid years was 7, 2 and 1, while for the wet years they were 2, 1 and 12.

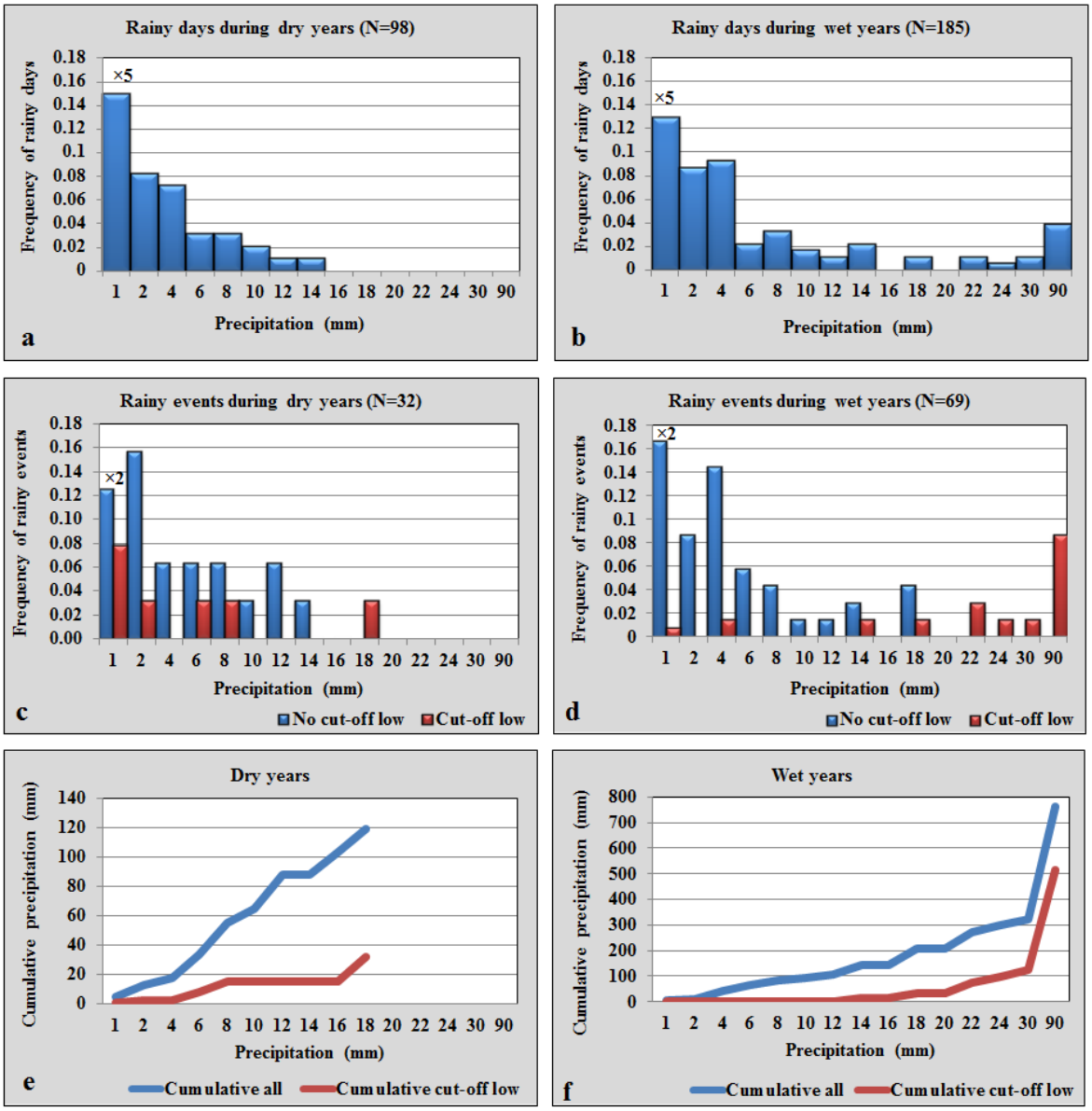

Figure 3.7. Precipitation histograms for Baghdad during (a, c, e) arid and (b, d, f) wet years; the number of rainy days (rainy events) was 116 (30) for the arid years and 185 (69) for the wet years. Frequency of (a, b) days and (c, d) events with precipitation, with the red bars represents cut-off lows and the blue bars all other types of events. (e, f) Cumulative precipitation of events with precipitation; the red line corresponds to cut-off lows and the blue line considers events of all types.

We may use these event-precipitation data to draw cumulative precipitation histograms for both arid and wet years (Figs. 3.7e,f). We have drawn two curves for each histogram, one accounting for all rain and the other including only rain associated with cut-off lows: these events represent a relatively minor contribution to total rainfall except for the large increment resulting from extreme precipitation events (over 30 mm) during the wet years, when a 249 mm rainfall increase (from 512 to 761 mm) was entirely caused by cut off lows.

In Figure 3.8 we present the distribution of geopotential height at three different pressure levels (850, 500 and 250 hPa) for six cut-off lows that recorded extreme precipitation: two in November 2012, October and November 2015, and March and December 2016 (all except the December 2016 event belong to the wet-years compiled in Figure 3d; a seventh event, in November 2013, is analyzed in next section). These distributions (for the day that best displayed the cut-off low pattern) are shown together with the horizontal divergence at 250 and 850 hPa, and the pressure vertical velocity at 500 hPa, In all cases, the cut-off low was located on top of the Baghdad area, displaying divergence. This was accompanied by low-level air (and moisture, not shown) convergence and upward vertical velocities at intermediate heights.

In order to best describe the cyclogenesis that led to cut-off lows rainy events, in the following section we focus on the November 2013 flood, presenting the daily synoptic situation for a period ranging from two days before the event to one day after the event, as calculated using the ERA-Interim reanalysis. The variables used are geopotential height, EPT, horizontal velocity, PV and PV-advection, and RV and RV-advection.

3.5 Concluding remarks

We have analyzed a 12-year time series of daily precipitation values over Baghdad in order to identify the seasonal and inter-annual changes in rainfall, the number of precipitation events, and the relative contribution of cut-off lows. Summer had no rain and autumn and winter were the wettest seasons; the contribution of rainy cut-off low episodes was largest in autumn, followed by spring. The mean annual precipitation was 130.8 ± 67.1 mm/yr, with minimum/maximum values of 59.1/296.7 mm for the calendar years of 2009/2014. However, because of the lack of summer rain, we integrate the precipitation for natural years running from 1 July to 30 June and labeled by the final year (e.g. natural year 2006 runs from 1 July 2005 to 30 June 2006). This shows that there were three years (2008, 2009 and 2012) with extreme low precipitation (mean value of 39.7 mm) and

three years (2013, 2014 and 2016) with precipitation much greater than the annual average (mean value of 253.7 mm); the minimum and maximum corresponded to 2012 and 2014 with 29.3 mm and 278.1 mm, respectively.

We have identified a total of 94 cut-off lows affecting Iraq, with 38 of them bringing rain over the Baghdad area and 14 leading to extreme precipitation (over 20 mm). The persistence of the cut-off low rainy conditions is very short, typically 1-3 days. These rainy events lasted only 118 days (21.6% of the total number of rainy days) but brought 43.4% of the total amount of rain.

Our data shows that cut-off lows can take place all year long, more often in May-June and October-November, when the Red Sea Trough (a low-level cyclonic circulation) sets over the Middle East (see Section 4.3), and less frequently between July and September, when the Atlantic subtropical high-pressure system extends into the Arabian Peninsula and inhibits the generation of cyclones (e.g. Bitan and Sa'aroni, 1992). The amount of rain associated with cut-off lows between October and December – when the surface waters of the Red Sea and Persian Gulf are still warm and, hence, can release water vapor to the atmosphere – accounts for about one third of the total annual precipitation (41.0 out of 130.8 mm/yr).

The contribution of cut-off lows to the total precipitation also shows large inter-annual variations. The fraction of rain associated with cut-off lows did not change substantially between arid and wet years but the total amount of rain accompanying these events increased by a factor of 16, from 31.3 mm during the three arid years to 512.3 mm during the three wet years (with nearly 400 mm corresponding to six extreme cut-off lows, each discharging over 30 mm). This is because rainy cut-off lows bring little water (< 10 mm) during arid years while they bring high rain (> 14 mm) during wet years. These data confirm that extreme-rain cut-off lows are the principal reason turning an arid into a wet year.

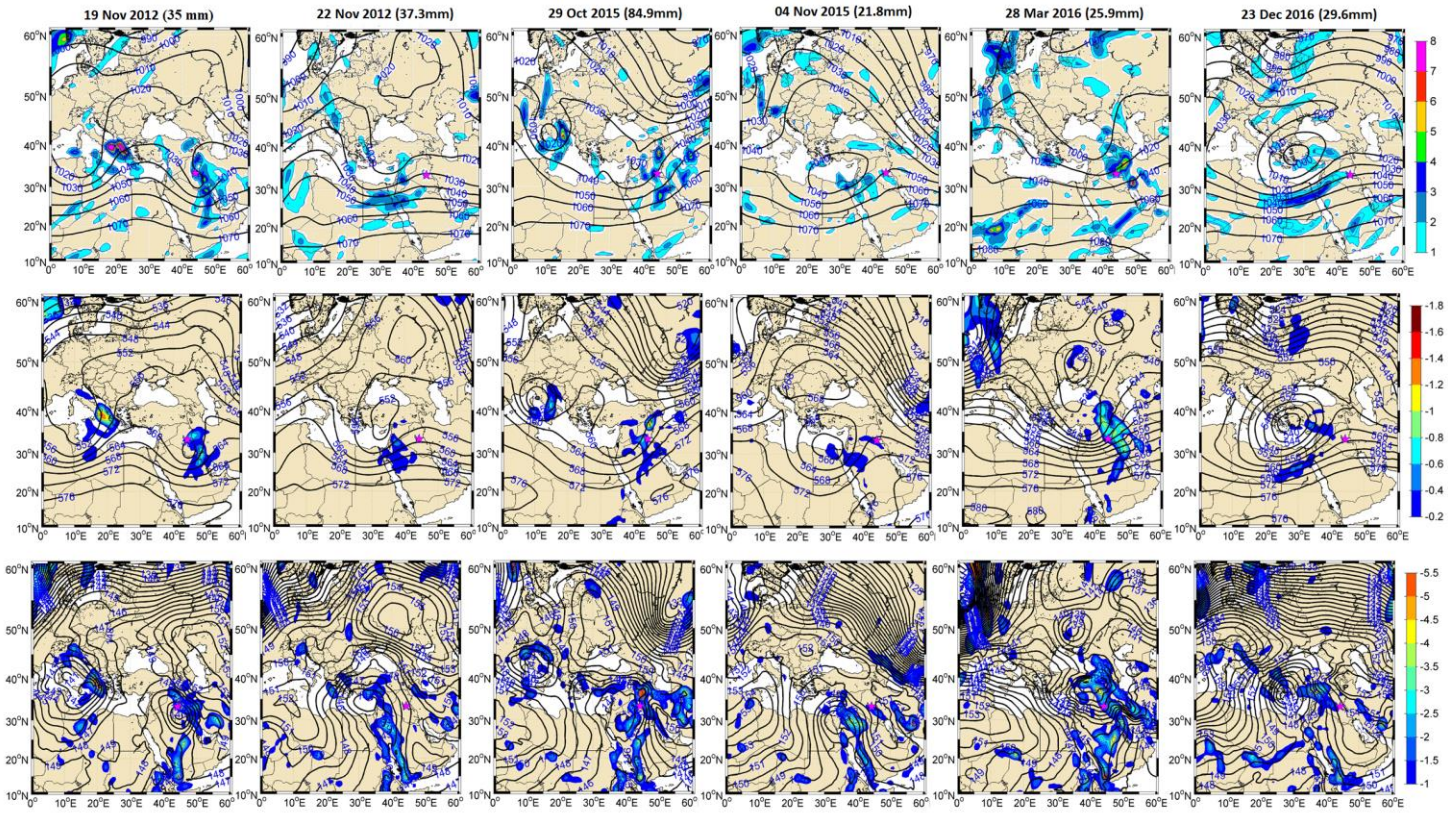

Figure 3.8. Dynamic conditions during extreme precipitation cut-off lows over Iraq. From left to right: 19 November 2012, 22 November 2012, 29 October 2015, 4 November 2015, 28 March 2016 and 23 December 2016, all times are 1200 UTC. (Top panels) Horizontal divergence (colored with intervals of 10-5 s-1) and geopotential height (black contours with intervals of 5 dam) at 250 hPa. (Middle pannels) Pressure vertical velocity (colored with intervals of 0.2 Pa s-1) at 700 hPa and geopotential height (black contours with intervals of 4 dam) at 500 hPa. (Bottom panels) Horizontal divergence (colored with intervals of 0.5 × 10-5 s-1) and geopotential height (black contours with intervals of 1 dam) at 850 hPa; note the change in the color bar as compared with the top panels, with the reddish colors now representing negative convergent values.

Chapter 4

Case Study: the November 2013 Episode

4.1 Introduction

In this chapter we focus on the flash-floods of 19 November 2013. Section 4.2 will explore the dynamic (synoptic situation, horizontal divergence and vertical flows) and thermodynamic (convective instability) conditions that characterize the episode. In Section 4.3 we explore the source of moisture to the lower atmosphere during this episode and what are the lower-atmosphere conditions responsible for bringing these humid air masses to central Iraq. We close (Section 4.4) summarizing the main factors that caused this extreme precipitation episode.

4.2 The November 2013 episode

4.2.1 Synoptic situation

We begin presenting the daily fields of geopotential height for the 17-20 November 2013 period, at high (250 hPa), middle (500 hPa) and low (850 hPa) levels, accompanied by the PV distribution at the upper level (1 PV unit = 1 PVU = 10^{-6} m^2 s^{-1} K kg^{-1}), the equivalent potential temperature at the middle level, and the wind fields in the lower level (Fig. 4.1). Notice we have selected the 850 hPa level in order to minimize the influence of the orography on our maps, as the mountain ranges in the northern and eastern Iraq reach heights well above the 3000 m.

On 17 November, the geopotential maps at 250 and 500 hPa show an omega block pattern, with high values over central Europe and low values on both ends of the Mediterranean Sea. The EPT and PV fields illustrate the penetration of high-PV cold streaks along both margins of the omega high (Figs. 4.1a,e). The 850 hPa geopotential height indicates a low-level cyclonic circulation centered near (27°N, 39°E) with southeast flow, which introduced air from the Red Sea and Persian Gulf into central Iraq (Fig. 4.1i). In 18 November, the geopotential and PV contours at 250 hPa show that the omega block pattern evolved towards a Rex block pattern with its high and low geopotential values oriented in the northwest-southeast direction. This was caused by a deepening of

the eastern trough, as well as to a slight shift of the blocking anticyclone to the southwest. The 250 and 500 hPa geopotential maps illustrate the evolution of the eastern trough towards a cut-off (Figs. 4.1b,f). At this time, the 850 hPa cyclone deepened over the northern Arabian Peninsula, causing strong low-level winds from the Persian Gulf and Arabian Sea (Fig. 4.1j); the penetration of this low-pressure wedge appears correlated with the deepening of the eastern trough at the mid and high levels.

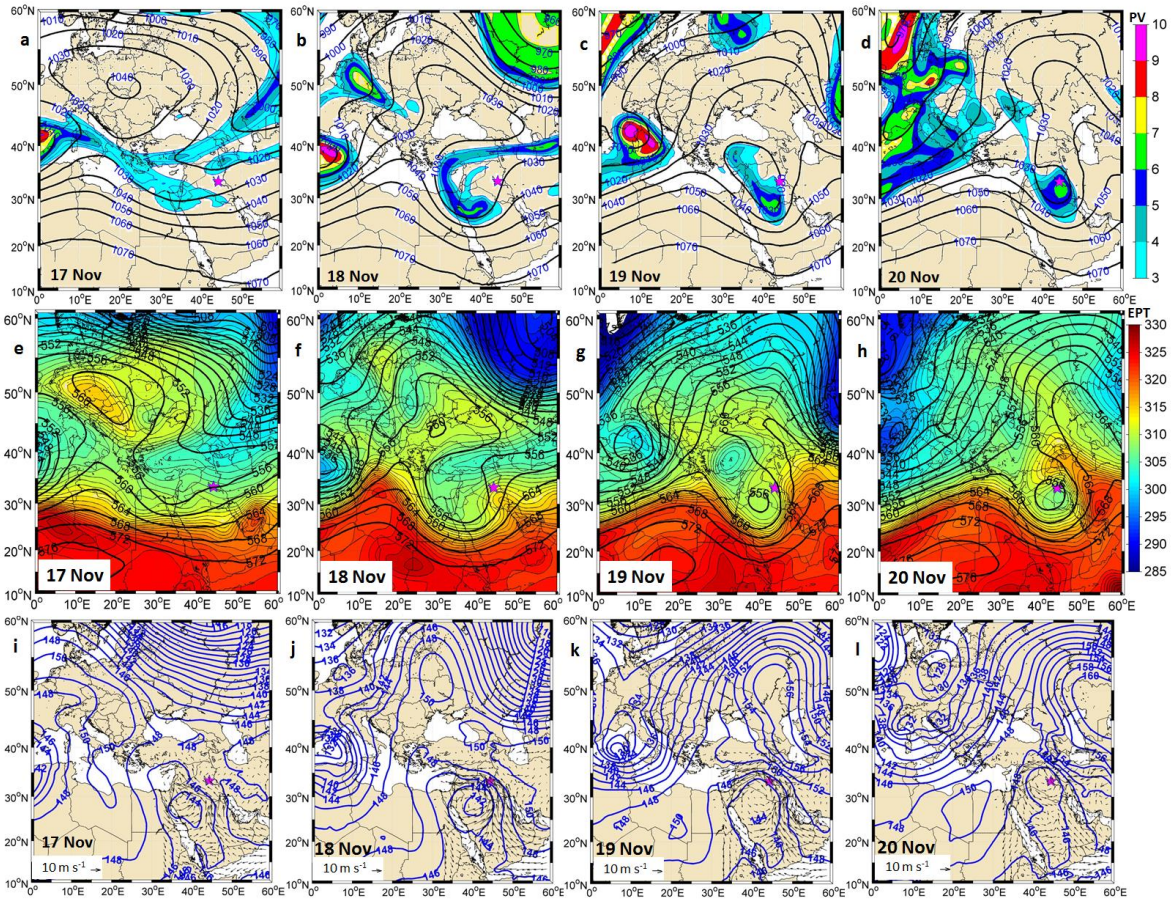

Figure 4.1. (Top panels) PV (colored with intervals of 1 PVU) and geopotential height (solid contours with intervals of 10 dam) at 250 hPa for 17-20 November 2013, 1200 UTC. (Middle panels) EPT (colored with intervals of 5 K) and geopotential height (solid contours with intervals of 4 dam) at 500 hPa. (Bottom panels) Geopotential height (solid contours with intervals of 2 dam) and wind vectors solely for the Iraq region (arrows, units of m s^{-1}; the reference arrow denotes 1 m s^{-1}) at 850 hPa for 17-20 November 2013, 1200 UTC.

On 19 November, the cut-off low stretched southeast at the 250 and 500 hPa levels, into the Arabian Peninsula, becoming vertically aligned on top the 850 hPa low. This low-level cyclonic feature, together with the anticyclone found between the Black and Caspian Seas, favored the appearance of intense southeasterly winds, from the Persian Gulf into central Iraq (Figs. 4.1c,g,k). Finally, on 20 November, the cyclonic feature remained vertically aligned over central Iraq tough the low-level winds from the Persian Gulf had weakened considerably (Fig. 4.1l).

4.2.2 Horizontal divergence and vertical flow

We want to identify those regions that, for the period 18-20 November, underwent low-level horizontal divergence and vertical convection. For this purpose we plot the distributions of PV (P) at 250 hPa and RV (ζ) at 500 hPa together with their horizontal advection ($\vec{u} \cdot \nabla P$ and $\vec{u} \cdot \nabla \zeta$) (Fig. 4.2). The cyclogenesis during the flood day is revealed by the peak PV and RV advection values on 19 November over central Iraq (Figs. 4.2b,e).

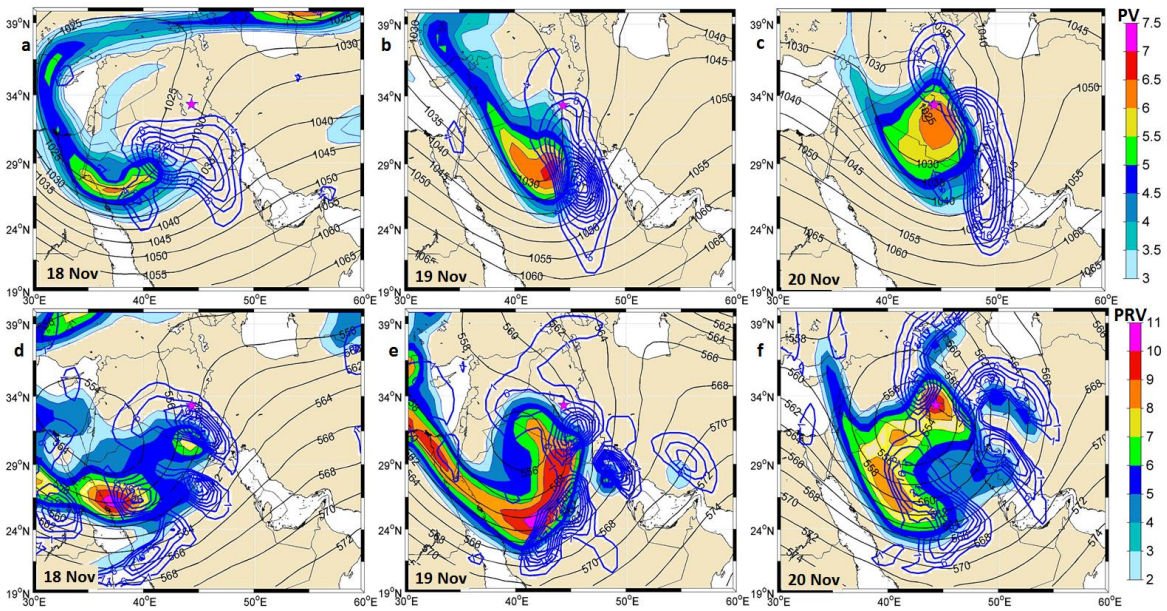

Figure 4.2. (Top panels) PV (colored with intervals of 0.5 PVU), PV advection (blue contours with intervals of 10^{-5} PVU s^{-1}) and geopotential height (black contours with intervals of 5 dam) at 250 hPa for 17-20 November 2013, 1200 UTC. (Bottom panels) Positive RV (colored shaded with intervals of 10^{-5} s^{-1}), advection of positive RV (blue contours with intervals of 10^{-5} s^{-2}) and geopotential height (black contours with intervals of 5 dam) at 500 hPa.

The horizontal velocity divergence at 250 and 850 hPa helps identify the coupling between the upper and lower atmospheric levels (Fig. 4.3, top and bottom panels). High absolute positive and negative values, respectively at 250 hPa and 850 hPa, match over central and eastern Iraq on 19 November (Figs. 4.3b,h). Such correspondence points at the existence of dynamical forcing from the upper to the lower levels, confirmed by intense upward motions in the middle atmosphere (700 hPa) (Fig. 4.3e). These high values remained on 20 November but had moved over Iran (Figs. 4.3c,f,i).

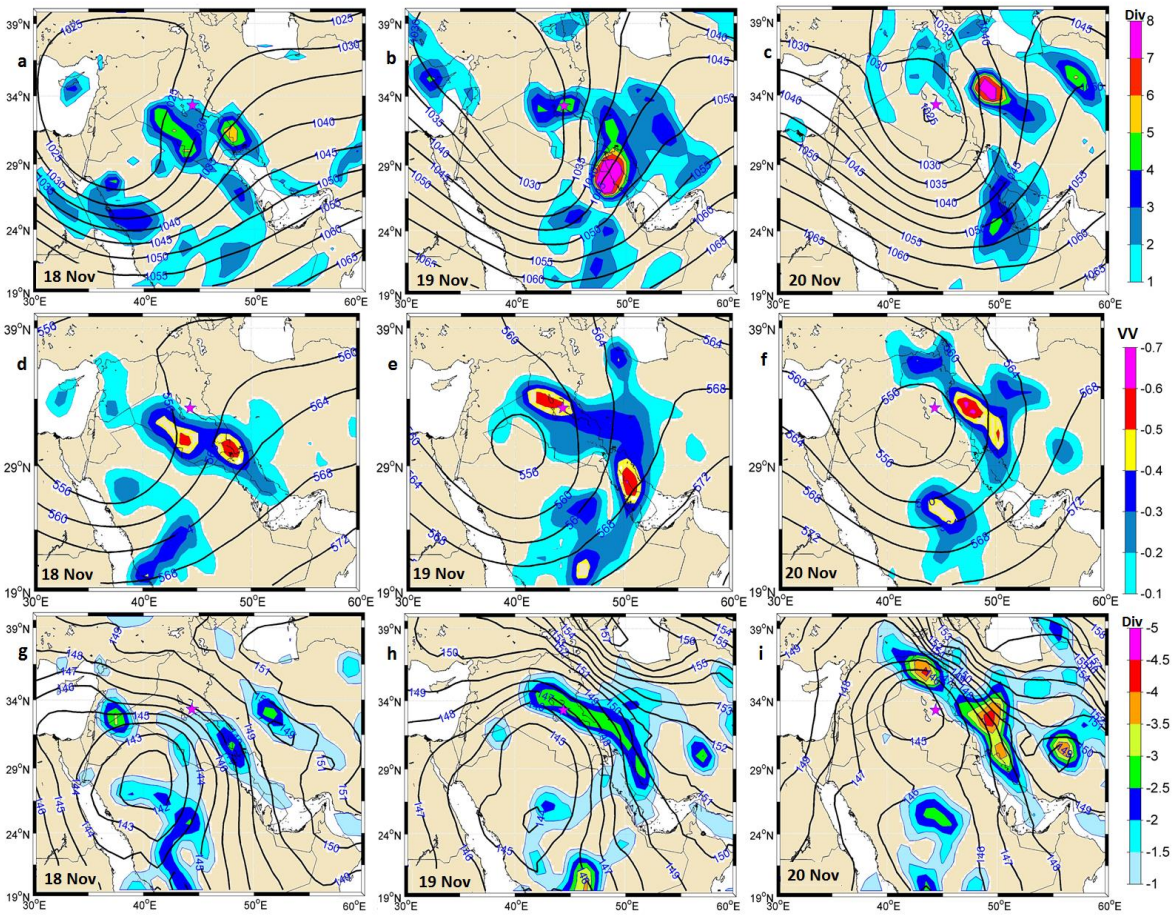

Figure 4.3. (Top panels) Horizontal divergence (colored with intervals of 10^{-5} s^{-1}) and geopotential height (black contours with intervals of 5 dam) at 250 hPa, for 18-20 November 2013, 1200 UTC. (Middle panels) Pressure vertical velocity (colored with intervals of 0.2 Pa s^{-1}) at 700 hPa and geopotential height (black contours with intervals of 4 dam) at 500 hPa, for 18-20 November 2013, 1200 UTC. (Bottom panels) Horizontal divergence (colored with intervals of 0.5 × 10^{-5} s^{-1}) and geopotential height (black contours with intervals of 1 dam) at 850 hPa for 18-20 November 2013, 1200 UTC; note the change in the color bar as compared with the top panels, with the reddish colors now representing negative convergent values.

The existence of deep vertical motion in central Iraq during the November 2013 event is confirmed by the 700-400 hPa mean horizontal distributions of both vertical velocities and Q-vector divergence (Fig. 4.4). Peak vertical velocities developed in regions of high RV and PV advection (Fig. 4.2) and intense horizontal divergence (Fig. 4.3).

The Q-vector divergence was patchy (Fig. 4.4), yet high negative values (convergent regions) coincided with low/high level convergence/divergence and upward motions (negative pressure vertical velocities) (Fig. 4.4), as expected to occur ahead of a cyclone (Sanders and Hoskins, 1990).

A vertical section along 44.5°E, almost right over Baghdad, helps appreciate the vertical extension of the convective motions (Fig. 4.5). Between 0000 UTC of 19 November and 0000 UTC of 20 November (Figs. 4.5c,d,e) the velocities reached maximum upward values, all the way from near the surface to the 250 hPa level, precisely over the Baghdad area.

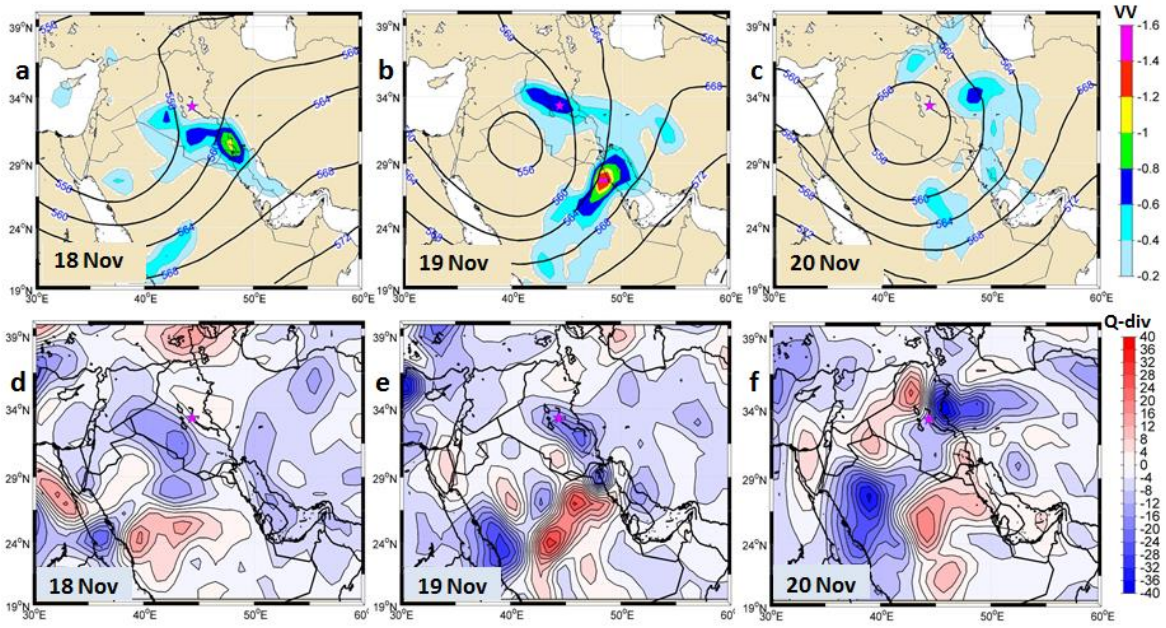

Figure 4.4. (Top panels) Mean pressure vertical velocity (colored with intervals of 0.2 Pa s^{-1}) over the 700-400 hPa interval and geopotential height (black contours with intervals of 4 dam) at 500 hPa, for 18-20 November 2013, 1200 UTC. (Bottom panels) Q-vector divergence (colored with intervals of 2 □ 10^{-18} m kg^{-1} s^{-1}) over the 700-400 hPa interval for 18-20 November 2013, 1200 UTC.

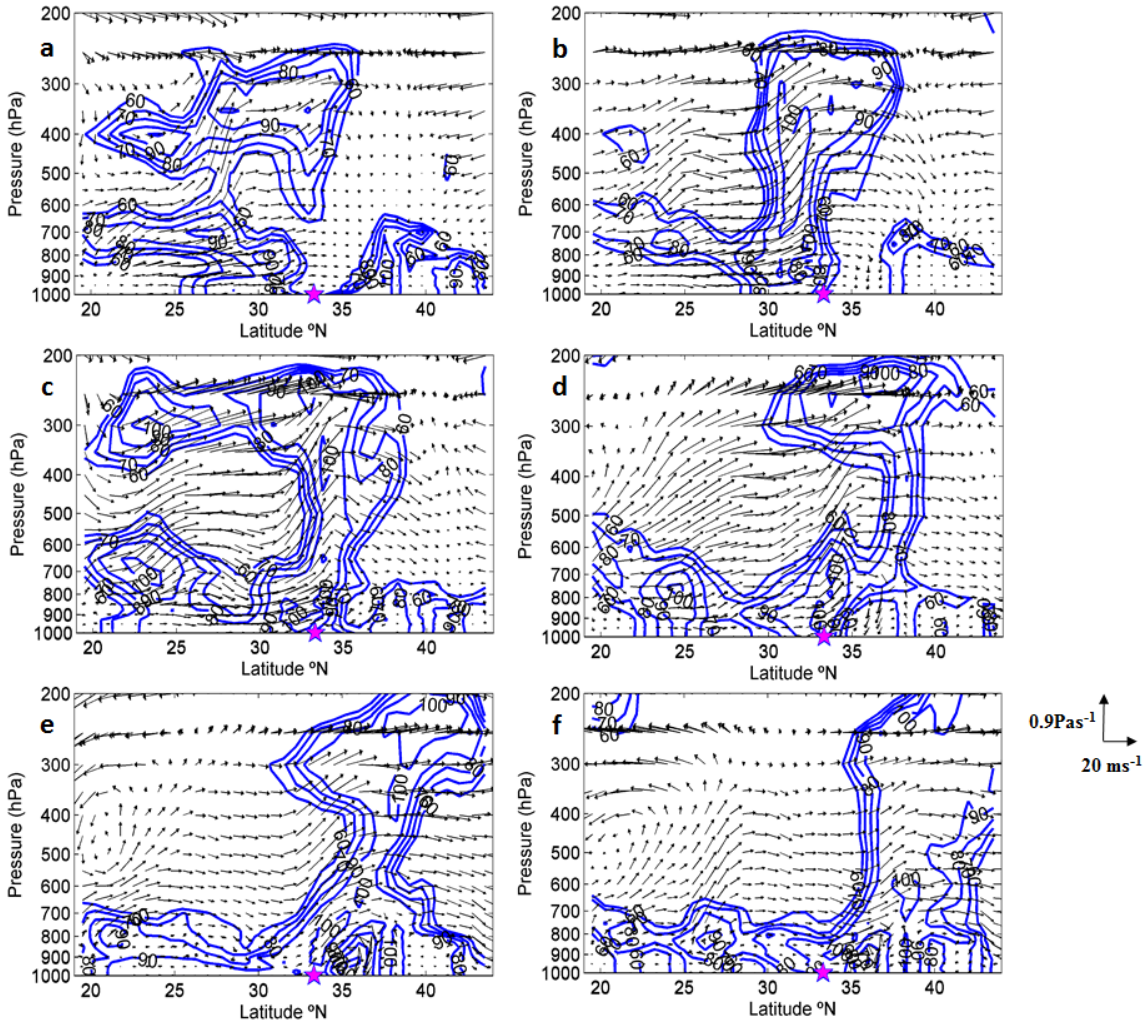

Figure 4.5. Relative humidity (values ≥ 60% with intervals of 10%, blue line) and wind velocity (horizontal velocity in m s^{-1} and pressure vertical velocity in Pa s^{-1}, black arrows) for (a, b) 18, (c, d) 19 and (e, f) 20 November 2013 at 0000 UTC (left panels) and 1200 UTC (right panels), respectively. The velocity scale is shown in panel f.

4.2.3 Convective instability

We complete the dynamic analysis by assessing whether the conditions over Iraq at the time of the November 2013 event had caused convective instability. For this purpose we compute several atmospheric instability indexes, calculated with the daily radiosonde data from the Baghdad station and the ERA-Interim reanalysis, and compare them with thresholds for the development of storm conditions (Section 3.2.2).

Figure 4.6 presents skew-T log-P diagrams for Baghdad at 1200 UTC for the 17, 19 and 20 November 2013. Using these figures, and the ERA-Interim data, we compute the instability indexes for the period 17-20 November 2013 (Table 4.1) and compare them with the Lorente et al. (2008) thresholds, which were developed for another Mediterranean region (Table 3.1).

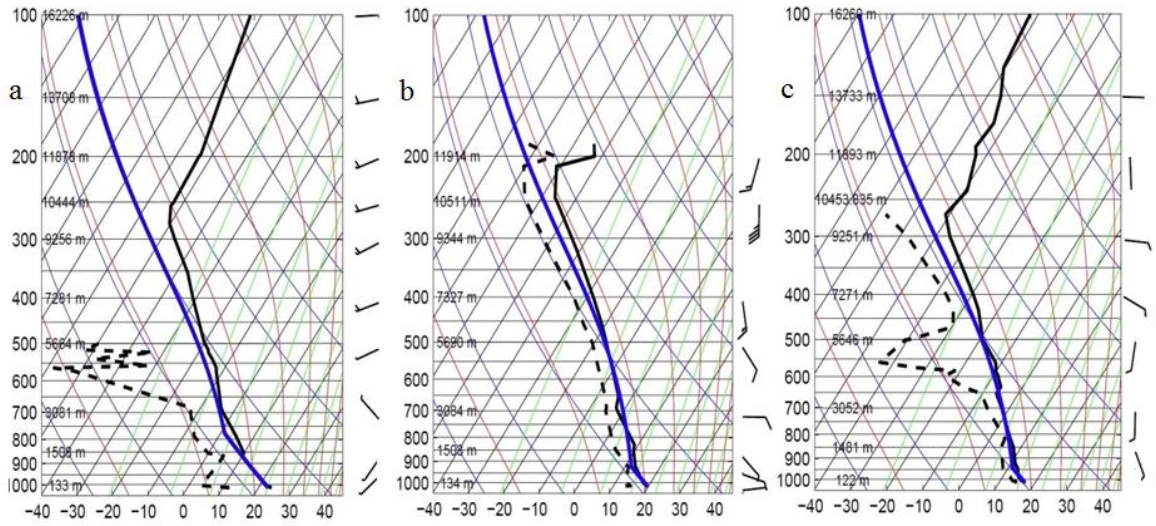

Figure 4.6. Skew-T log-P diagrams for Baghdad station at 1200 UTC (1500 local time) for (a) 17, (b) 19 and (c) 20 November 2013. The blue line represents the temperature of the air parcel when lifted adiabatically from the surface, the black solid line represents the environmental temperature, and the black dashed line is the dew point temperature.

The instability conditions associated with the positive buoyant air parcels are assessed through the K index and, even better, the CAPE index (Table 4.1 and Fig. 4.7). Other indexes may not be as adequate for our analysis but are included for the sake of completeness: TT is more relevant for elevated regions, and LI, SWEAT and SI are commonly used to discriminate the potential for severe events, such as tornados. The indexes using the local soundings are presented in Table 4.1, and the spatial distributions of SWEAT and LI from the ERA-Interim data are shown in the. (Fig. 4.8).

The skew-T log-P diagrams help assess the likelihood of vertical convection (Fig. 4.6). On 17 November the profile was stable. In contrast, on 19 November the profile indicated weak (marginal conditional) vertical instability; this is confirmed by the moderate K and CAPE figures, as well as by the positive LI value (Table 4.1). PW remained moderate, below the threshold for high moisture content (Tables 3.1 and 4.1).

Table 4.1. Precipitable water and convective indices as deduced from the sounding at Baghdad station (33.33° N, 44.43° E; elevation 34m) at 1200 UTC (1500 local time) for 17, 19 and 20 of November 2013. The CAPE, K and SWEAT indexes from the ERA Interim reanalysis data set are shown between brackets.

SKEW-T INDICES	17/11/2013	18/11/2013	19/11/2013	20/11/2013
Precipitable water (PW, mm)	15.4 (15)	(18)	28.1 (22)	23.8 (20)
K (KI, °C)	19.5 (20)	(26.8)	27.4 (36.8)	27.3 (24.2)
Convective available potential energy (CAPE, J kg^{-1})	0 (139.1)	(21.9)	61.8 (777)	13.6 (300.2)
SWEAT	33.4 (45.9)	(135.4)	136 (253.4)	135.3 (178.1)
Lifted index (LI, °C)	2.01 (-2.5)	(-1.0)	0.45 (-0.5)	0.34 (-3.2)
Showalter index (SI, °C)	-0.21		1.4	0.17
Total totals (TT, °C)	48.6		47.6	50.6

The soundings are characteristic of a relatively small region over Baghdad so the indexes calculated from these data are only indicative of local convective instability conditions (Table 4.1). For the conditions over central Iraq we may use instead the ERA-Interim reanalysis (Figs. 4.7 and 4.8). In all cases, the local soundings produce indexes indicating more stable conditions than as inferred from the ERA-Interim reanalysis, with the less stable conditions corresponding to 19 November 2013.

On 19 November, the local sounding gave a K index of 27.4°C, increasing to almost 37°C when using the ERA-Interim data, which is above the 25°C threshold proposed by Lorente et al. (2008). However, the local CAPE index was only 62 J kg-1, reaching 777 J kg-1 with the Era-Interim data, in this case well below the 1000 J kg-1 instability threshold (Lorente et al., 2008). These relatively small values indicate the existence of marginally unstable convection. It is worth pointing that similarly small values have been reported to occur during flooding events in other Mediterranean regions (Iturrioz et al., 2007; Lorente et al., 2008).

The maps for CAPE and K display the penetration of unstable conditions from the Red Sea and Persian Gulf on the 18 and 19 November (Figs. 4.7c,g). The patterns of the SWEAT distribution were alike those for CAPE, particularly on 18 November, while the peak LI values were more scattered (Fig. 4.8). The SI, LI and SWEAT values never exceeded the threshold values (Table 4.1 and Fig. 4.8). In contrast, the TT index surpassed the thresholds – 44 according to NOAA (2017) and 45 for Lorente et al. (2008) – during the entire event. Its largest value over Baghdad, however, took place on 20 November rather than 19 November.

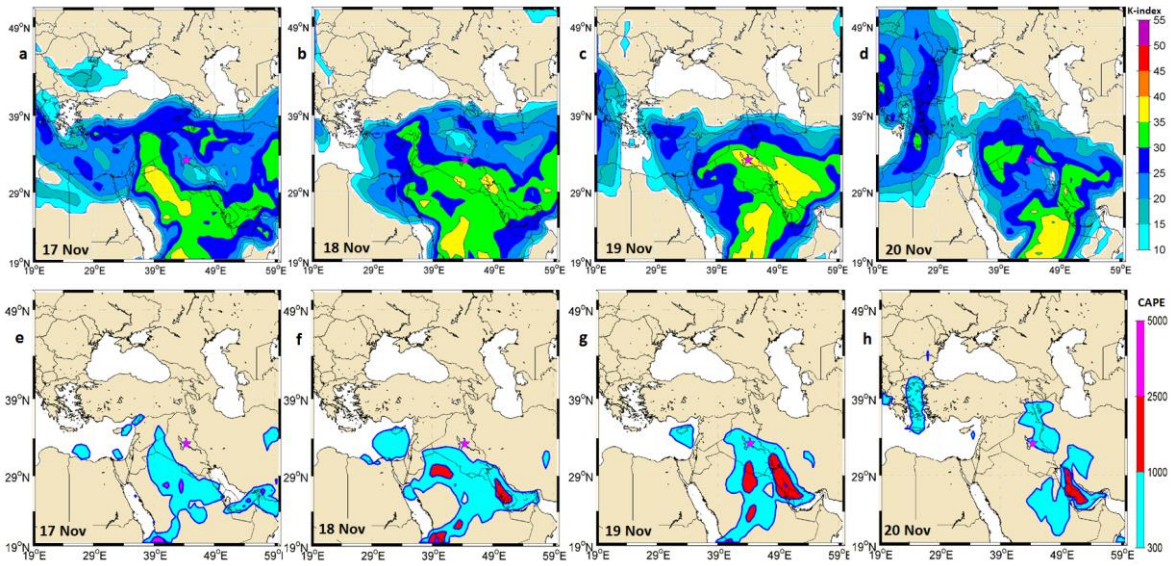

Figure 4.7. (Top panels) K index (colored, units of ℃) and (bottom panels) CAPE index (colored, units of J kg^{-1}) for 17-20 November 2013, 1200 UTC.

A relevant variable is PW, the amount of water between 1000 and 700 hPa (Tables 3.1 and 4.1) (Kassomenos and McGregor, 2006). This variable attained peak values on 19 November but never exceeded the 1.25 inches (31.8 mm) threshold for low moisture content (NOAA, 2017). In this case, however, the values deduced from the local soundings (28 mm) were larger than the values inferred from the ERA-interim data (22 mm), reflecting relatively large humidity values in the low-level atmosphere. This humidity translated in the progressive appearance of clouds over the Middle East between 17 and 19 November 2013 (Fig. 3.5).

In summary, the convective instability indexes show that the atmosphere was only marginally unstable over Iraq during the November 2013 event. The amount of water in the 1000-700 hPa vertical range reached maximum values on 19 November but the indexes did not exceed the

thresholds for intense storm events. Hence, marginal instability was a secondary player in the flooding, which would have assisted the intense upward dynamical forcing.

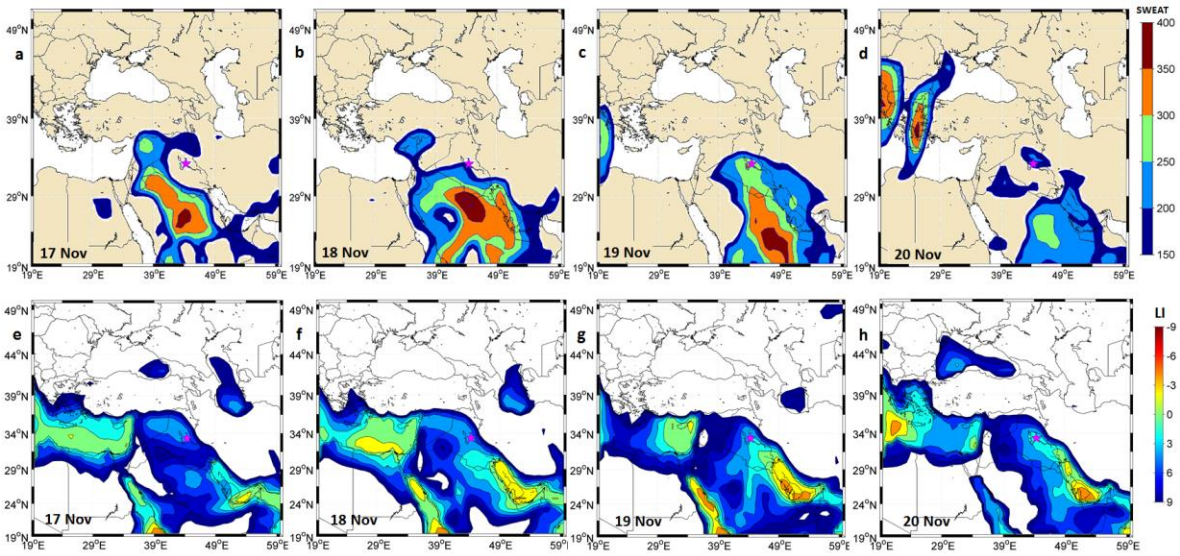

Figure 4.8. (Top panels) severe weather threat index (SWEAT) (colored) and (bottom panels) lifted index (LI) (colored, ℃) for 17-20 November 2013, 1200 UTC.

4.3 Moisture source

The establishment of the November 2013 upper-level cut-off low over Iraq led to the reinforcement of the lower-level cyclonic circulation and the generation of southerly winds from the Red Sea and the Persian Gulf. Further, the cut-off low caused intense upward dynamical forcing ahead of the cyclone, with low-level wind convergence and upward motion. These factors favor rainfall but yet require a source of moisture.

Krichak et al. (2015) carried out a detailed analysis of the tropical and subtropical sources of moisture for high precipitation events in the Mediterranean region. They found that over most of the Mediterranean the source was in the North Atlantic, except for the easternmost region where moisture was associated with the Red Sea Trough – a low-level center linking the Red and eastern Mediterranean Seas (Krichak et al., 1997) – with humid air arriving from the Arabian and Red Seas. The arrival of these air masses often takes place as a relatively narrow plume converging vapor at middle latitudes, what they named an atmospheric river, the sort of warm conveyor belt that ascends and saturates near a warm front (Carlson, 1980).

In this section we first explore the moisture conditions during the November 2013 episode, followed by an analysis of the source of moisture that led to extreme precipitation. Two key variables to assess the occurrence of precipitation are the availability of water in the lower atmosphere (precipitable water, PW) and the horizontal source of this water (vertically integrated moisture flux convergence, VIMFC) (Section 3.2.3). In particular, the VIMFC has often been used for predicting the initiation of convection (van Delden, 2001; Banacos and Schultz, 2005; Zomeren and van Delden, 2007; Ukkonen, 2015). We may expect that heavy precipitation will occur when and where these variables are high and accompanied by upward air motions.

The horizontal distribution of VIMFC and PW over the Middle East prior and during the 19 November 2013 episode is illuminating (Fig. 4.9). On 17 November there was relatively little PW over Iraq (less than 16 kg m-2) (Fig. 4.9e). At this time, the vertically-integrated moisture flux (VIMF) was moderate and the corresponding horizontal convergence values (VIMFC) were generally less than 4×10^{-4} kg m^{-2} s^{-1} (Fig. 4.9a); these values may be compared with figures reported by Krichak et al. (2015), whom noted that most intense rain events in Mediterranean regions take place when the VIMFC exceeds 5×10^{-4} kg m-2 s^{-1}.

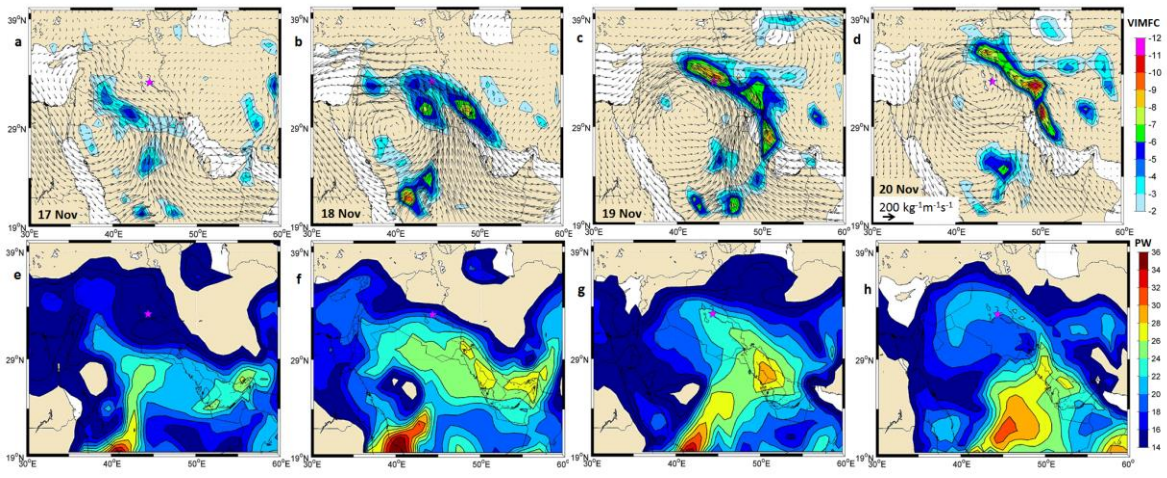

Figure 4.9. (Top panels) Mean vertically integrated moisture flux (VIMF) (arrows, units of kg m^{-1} s^{-1}; the reference arrow denotes 200 kg m^{-1} s^{-1}) and mean vertically integrated moisture flux convergence (VIMFC) (colored with intervals of 10^{-4} kg m^{-2} s^{-1}) over the 1000-700 hPa band for 17-20 November 2013, 1200 UTC. (Bottom panels) Precipitable water (PW) (colored with intervals of kg m^{-2}) integrated over the 1000-700 hPa band for 17-20 November 2013, 1200 UTC.

On 18 November, coinciding with the formation of the cut-off low over Iraq, the situation changed drastically. The southeasterly winds intensified significantly, bringing wet air from the Persian Gulf and Arabian Sea into the region. This moisture converged over Iraq and led to much larger VIMFC values, in excess of 8×10^{-4} kg m^{-2} s^{-1} in the southern part of the country and near 5×10^{-4} kg m^{-2} s^{-1} over Baghdad (Fig. 4.9b). The result was a doubling of the PW values over southern Iraq as compared with the previous day (Fig. 4.9f).

This situation continued and increased on 19 November, with the VIMFC reaching peak values (above 10×10^{-4} kg m^{-2} s^{-1}) precisely over Baghdad and the high-PW area stretching from the Persian Gulf into central Iraq. Finally, on 20 November, the winds and, consequently, the amount of moisture transported north, weakened considerably (Fig. 4.9d). There was still a region of high VIMFC values but this had moved north of Baghdad. The amount of PW over central Iraq also decreased, with maximum values in the southern portion of the Arabian Peninsula (Fig. 4.9h).

The analysis of the November 2013 event shows that the cyclone over the Arabian Peninsula brought air masses initially from the Red Sea and later from the Persian Gulf (Figs. 4.3 and 4.9), in agreement with the observation that intense rainfall began in southern Iraq one day before the Baghdad area (Fig. 3.4).

A marine origin of the air masses can also be identified for most cut-off low extreme rain events (e.g. six cases in Fig. 3.8). An analysis of all 14 cut-off low cases (not shown) clarifies that the low level southerly winds arrive into central Iraq from the Red Sea and the Persian Gulf, typically with the Red Sea being the initial and main source of humidity and the Persian Gulf acting as a secondary source 2-3 days later. In a few cases there is also an additional moisture source from the Mediterranean Sea (e.g. March 2016, Fig. 3.8)

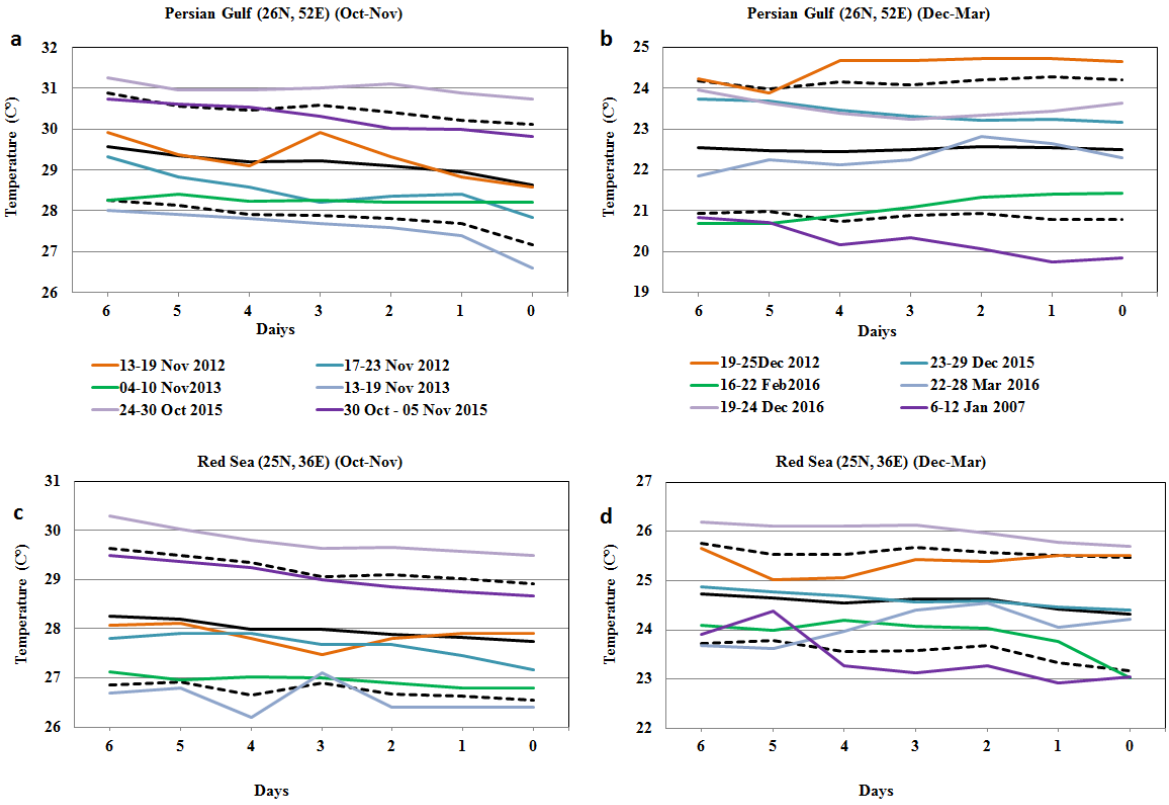

Figure 4.10. Evolution of the SST (a, b) in the central part of the Persian Gulf (26°N, 52°E) and (c, d) in the northern part of the Red Sea (25°N, 36°E) during the six days previous to the cut-off low extreme flooding in the Baghdad area. The left panels (a, c) show the episodes during October and November, while the right panels (b, d) correspond to events between December and March. Time runs backwards, with day zero corresponding to the flooding time.

It is reasonable to assume that the moisture arriving to central Iraq is associated with the release of latent heat from the ocean to the atmosphere, arising when the cool cyclonic winds blow over the Red Sea and the Persian Gulf. This heat release would cool these surface waters, which should show up in the SST evolution previous to rainfall over Baghdad. Considering the distances between the Persian Gulf and the Red Sea to the Baghdad area and using characteristic surface winds of 6 m s^{-1}, we may estimate that the SST would decrease a few days before the flooding: 1-2 days over the Persian Gulf and 3-5 days over the Red Sea. The SSTs previous to each extreme-rain cut-off low confirms this evolution, with temperature changes of 1-2°C in just a few days, with the single exception of the March 2016 event (Fig. 4.10).

For the November 2013 event, for example, the main SST decrease in the Red Sea took place four days before the event and the SST in the Persian Gulf decreased the entire week with a maximum change one day before the event (Fig. 4.10). The last-day change in the Persian Gulf did coincide with high VIMFC and PW values on 18 November, stretching from the Persian Gulf into central Iraq (Figs. 4.10b,f).

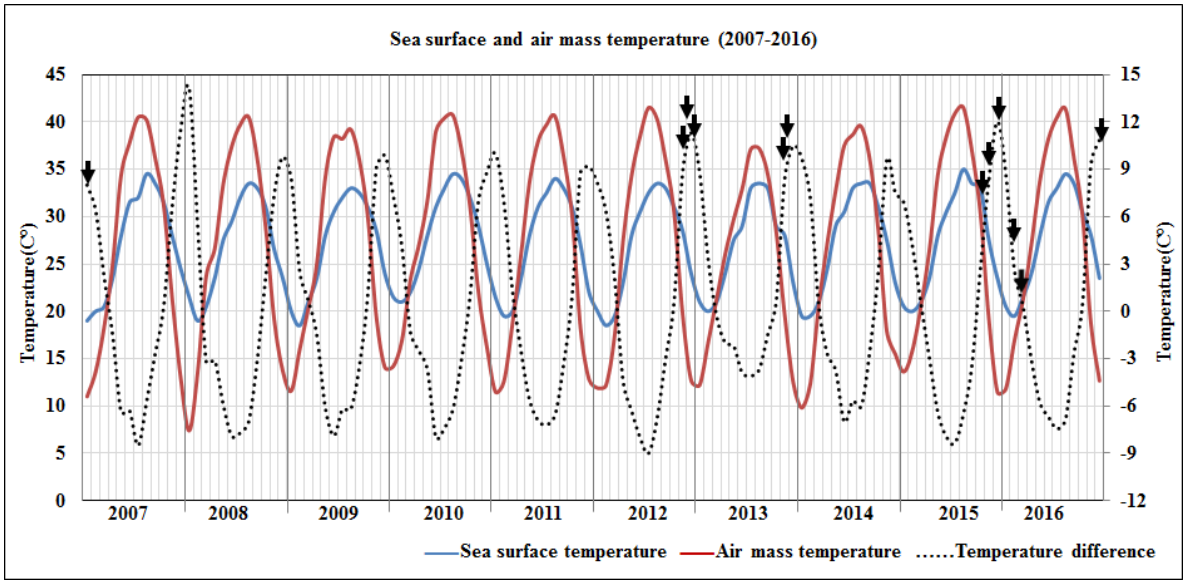

Figure 4.11. Mean SST west of the Strait of Hormuz (56°E) (blue line, left ordinate), mean AST in the northern Red Sea (29°N, 48°E) (red line, left ordinate) and the difference between SST and AST (black dotted line, right ordinate). The arrows indicate the time of occurrence of the extreme cut-off lows (over 20 mm) between 2007 and 2016.

The essential requirement for latent heat (and hence moisture) transfer to the atmosphere is that the AST be less than the SST. This only happens during late fall and early winter, with maximum temperature differences (9.8 ± 2.2°C) precisely in November-December (Fig. 4.11). If this requirement takes place at times of intense southeasterly surface winds then water vapor is first incorporated to the lower atmosphere and later transported to central Iraq. This happened during the November 2013 event, as reflected by the rapid SST decrease in the Persian Gulf (Fig. 4.10) and the advent of high northward fluxes of PW (Fig. 4.9), as well as in most cut-off lows that brought extreme rain to the Baghdad area (Fig. 3.8).

4.4 Concluding remarks

We have carefully analyzed the synoptic conditions of the cut-off low leading to the largest flood event, taking place 18-20 November 2013. The middle and upper atmospheric conditions arose from the development of an omega block and its evolution into a Rex block, with substantial frontogenesis in the eastern portion of the cyclonic structure of the Rex block. This region was experiencing horizontal divergence and the associated upward motions extended all the way from 1000 to 250 hPa. Simultaneously, the low-level atmosphere (1000 to 700 hPa) displayed substantial winds from the Red Sea: the surface waters cooled likely as a result of substantial heat and water release to the atmosphere and the southerly winds brought substantial amounts of water that converged into central Iraq.

The 19 November 2013 event is a remarkable case of vertical motions driven dynamically by a cut-off low pattern, at a time when surface moisture arose thanks to the southerly cool winds blowing over the still warm Red Sea. During the entire event the thermodynamic conditions were only marginally unstable, hence playing a relatively minor role. The conditions leading to this event developed very swiftly, in only 1-2 days, making very difficult a proper forecast. Our results, pointing at the harsh consequences from the interaction of high-latitude upper-level perturbations with local low-level forcing, shall help identify and timely predict analogous future situations.

Chapter 5

Extreme Precipitation Events over Iraq

5.1 Introduction

We close the dissertation with an introductory description of all extreme precipitation events over Iraq between 2005 and 2016. We do not aim at providing an exhaustive analysis of the dynamics behind these events but rather we will make an orderly presentation of those infrequent weather phenomena over the Middle East with direct impact on Iraq. The episodes will be classified as corresponding to either one of following four types of upper-atmosphere situations: jet streak, upper-air trough, cut-off low and Rex block.

For our description we first identify the extreme events and then follow the same approach, though much less exhaustive, used for the 19 November 2013 episode (Chapter 4). We will provide a short description of the synoptic situation and moisture fluxes for all these extreme episodes. This will be completed by a more complete narrative of three particularly intense events, each of them respectively belonging to the jet streak, upper-air trough and cut-off low types (the Rex block event will not be considered as it was carefully described in last chapter).

5.2 Data

Four our analysis we again use the daily precipitation records for the Baghdad weather station, ran by the Iraqi Meteorological and Seismology Organization, combined with ECMWF (ERA-Interim) reanalysis data from January 2005 to December 2016. The Baghdad records are employed to identify when an extreme precipitation event takes place and the ERA-Interim data are then used to establish the weather patterns, horizontal and vertical flows, moisture source and instability conditions during these extreme episodes.

5.3 Brief synoptic characterization of all extreme precipitation events

5.3.1. Definition of extreme events

How is an extreme event defined? One simple way is to obtain the probability density function for precipitation and choose some percentile that corresponds to high precipitation. Values above this percentile are then taken as representing episodes that bring unusual amounts of rain to the study site. In this work we have chosen this threshold to be the 90 percentile.

The 90-percentile condition allows identifying 20 extreme precipitation events where rainfall precisely exceeded 20 mm. These events, identified in Table 3.2, contributed to a total of 805.2 mm (51.3%) of the total precipitation for the entire period. They have been classified as belonging to either one of four weather patterns: jet streak, upper air trough, cut-off low or Rex block. This has been possible through the scrutiny of the geopotential and velocity fields at 500 hPa and 250 hPa, as inferred from the ERA-Interim reanalysis.

The analysis shows the following grouping of events: 7 related with Rex block conditions (causing the highest precipitation, 324.1 mm or 40.3% of the total extreme-event precipitation), 7 happenings related with cut-off-lows (252.6 mm or 31.4%), 2 episodes related with jet streak occurrences (95.3 mm or 11.8%), and 4 events related with upper-air troughs (133.2 mm or 16.5%). The cut-off lows and Rex block together accounted for 576.7 mm (71.6%) out of the total 805.2 mm of rainfall associated with the 20 extreme events.

Five out of the 20 extreme events caused flash floods in Baghdad, with one of them (related with a Rex block) being the most dramatic heavy rain event in Iraq in the last 30 years. This maximum-rain event (18-20 November 2013) was carefully analyzed in Chapter 4. In this chapter we will proceed with a brief exploration of three other extreme episodes, each belonging to one of the other three types of weather patterns (jet streak, upper-air trough and cut-off low).

5.3.2 Classification in different synoptic patterns

The high-precipitation episodes require some favourable atmospheric conditions: lower level convergence of humid air, vertical ascending motions and upper level divergence. The specific way these conditions are achieved allows us to classify the episodes as belonging to one out of four different types of weather patterns: jet streak, upper-air trough, cut-off low and Rex block.

In this section we will classify each of the 20 extreme events as belonging to one single weather pattern, though we recognize that this separation is often quite subtle. We could imagine an unstable jet stream as continuously evolving into different weather patterns: a relatively elongated jet streak may meander into a trough, which can eventually detach as single cut-off lows or double vortex (Rex block) structures.

To set up this classification we use the horizontal divergence and geopotential height in the upper atmosphere (250 hPa), the mean pressure vertical velocity (over the 700-400 hPa interval) and geopotential height (500 hPa) in the middle atmosphere, and the horizontal divergence and geopotential height in the lower atmosphere (850 hPa).

5.3.2.1 Jet streak

The jet stream is a relatively thin (a few kilometers) and narrow (several hundred kilometers) intense eastward air flow, with peak speeds in excess of 100 m s^{-1}, located in the upper troposphere in both hemispheres. There are two main jet streams: the polar jet, which forms near the border of the Polar and Ferrel meridional circulation cells, and the subtropical jet, which sets in the edge between the Ferrel and Hadley meridional circulation cells. The polar jet usually exceeds 75 m s^{-1} and is located at 9–12 km high, while the subtropical jet surpasses 50 m s^{-1} and is found 10–16 km high.

The nuclei or core of the jet stream, where the swiftest air masses are found, is named the jet streak. It has an important role in the generation of mid-latitude cyclones, often with high precipitation and intense vertical wind-shear. The two back or rear quadrants of the jet streak are called the entrance region while the two frontal quadrants are named the exit region (Bluestein 1993). Cyclogenesis and harsh weather conditions get enhanced in the divergent areas – the right-entrance and left-exit quadrants – of the jet streak (Clark et al., 2009).

Only two out of the 20 extreme episodes belong to the jet streak category (Fig. 5.1). One event occurred between 7 and 11 March 2005, accounting for 60.6 mm of rainfall, and the second event lasted between 6 and 11 March 2006, providing for 34.7 mm of precipitation (Table 3.2).

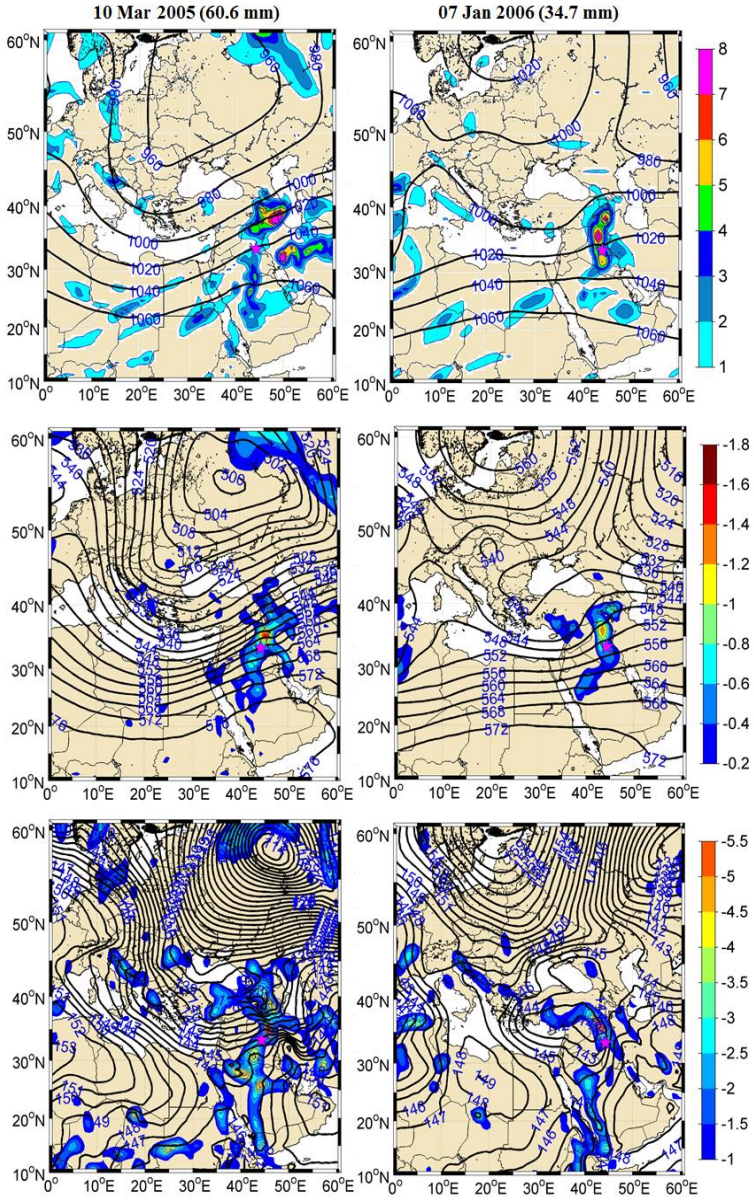

Figure 5.1. Dynamic conditions during jet-streak extreme precipitation events over Iraq. Left: 10 March 2005, 1200 UTC; right: 7 January 2006, 1200 UTC. (Top panels) Horizontal divergence (colored with intervals of 10^{-5} s^{-1}) and geopotential height (black contours with intervals of 5 dam) at 250 hPa. (Middle panels) Mean pressure vertical velocity (colored with intervals of 0.2 Pa s^{-1}) over the 700-400 hPa interval and geopotential height (black contours with intervals of 4 dam) at 500 hPa. (Bottom panels) Horizontal divergence (colored with intervals of 0.5 × 10^{-5} s^{-1}) and geopotential height (black contours with intervals of 1 dam) at 850 hPa; note the change in the color bar as compared with the top panels, with the reddish colors now representing negative convergent values.

5.3.2.2 Upper-air through

An upper-air trough is characterized by a sharp equatorward extension of the geopotential jet stream contours. This elongation appears as a trough in the meandering pattern of the jet stream: the height of an equal-pressure surface (geopotential) decreases or, alternatively, at constant height the pressure decreases. Considering the centre of the upper-air trough – as where a certain geopotential finds its maximum equatorward position – the exit quadrants are characterized by divergence and upward motions, causing an unstable atmosphere where colder air masses form clouds and cause rain; in contrast, the entrance quadrants are distinguished by downward air motions, bringing more stable weather.

Four out of the 20 extreme episodes belong to the upper-air trough category (Fig. 5.2). These events are the following: 1-3 February 2006 (33.4 mm), 19-22 April 2011 (29.1 mm), 27-28 January 2013 (49.7 mm) and 20 January to 1 February 2013 (21.0 mm) (Table 3.2).

5.3.2.3 Cut-off low

A cut-off low is a synoptic-scale closed-circulation pattern that forms when a trough deepens and eventually separates (cuts off) from the main jet stream. This separated low lies to the south of the main middle and upper troposphere westerly winds, as an independent rotating feature that slowly loses angular momentum. Cut-off lows usually remain for a few days over a certain site may, typically 2-3 days and in some cases 5 days.

Severe convective events, with unstable weather and heavy rainfall, can occur under cut-off lows when there is sufficient moisture, as bands of clouds are triggered by the slow motion of the cut-off lows. Severe weather episodes that affect southern Europe and northern Africa are often associated with cut-off lows.

Seven out of the 20 extreme episodes belong to the cut-off low category (Fig. 5.3). These events are the following: 21-24 January 2005 (20.4 mm), 1-2 April 2006 (20.8 mm), 11-12 January 2007 (24.6 mm), 24-25 December 2012 (67.5 mm), 7-10 November 2013 (74.3 mm), 29 December to 1 January 2015 (23.7 mm) and 21-23 February 2016 (21.3 mm) (Table 3.2).

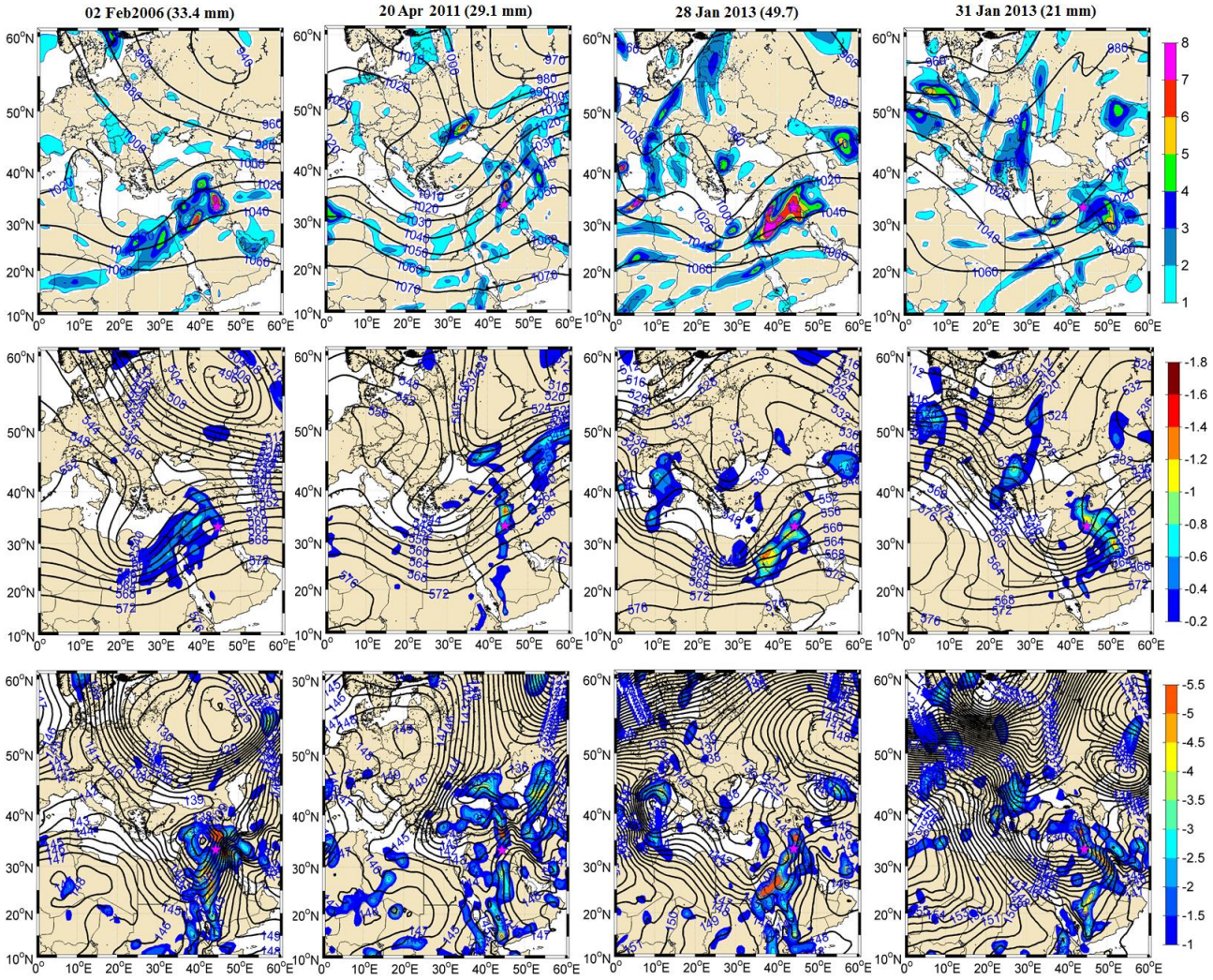

Figure 5.2. Dynamic conditions during upper-air trough extreme precipitation events over Iraq. From left to right: 2 February 2006, 20 April 2011, 28 January 2013 and 31 January 2013, all times are 1200 UTC. (Top panels) Horizontal divergence (colored with intervals of 10^{-5} s^{-1}) and geopotential height (black contours with intervals of 5 dam) at 250 hPa. (Middle panels) Mean pressure vertical velocity (colored with intervals of 0.2 Pa s^{-1}) over the 700-400 hPa interval and geopotential height (black contours with intervals of 4 dam) at 500 hPa. (Bottom panels) Horizontal divergence (colored with intervals of 0.5 × 10^{-5} s^{-1}) and geopotential height (black contours with intervals of 1 dam) at 850 hPa; note the change in the color bar as compared with the top panels, with the reddish colors now representing negative convergent values.

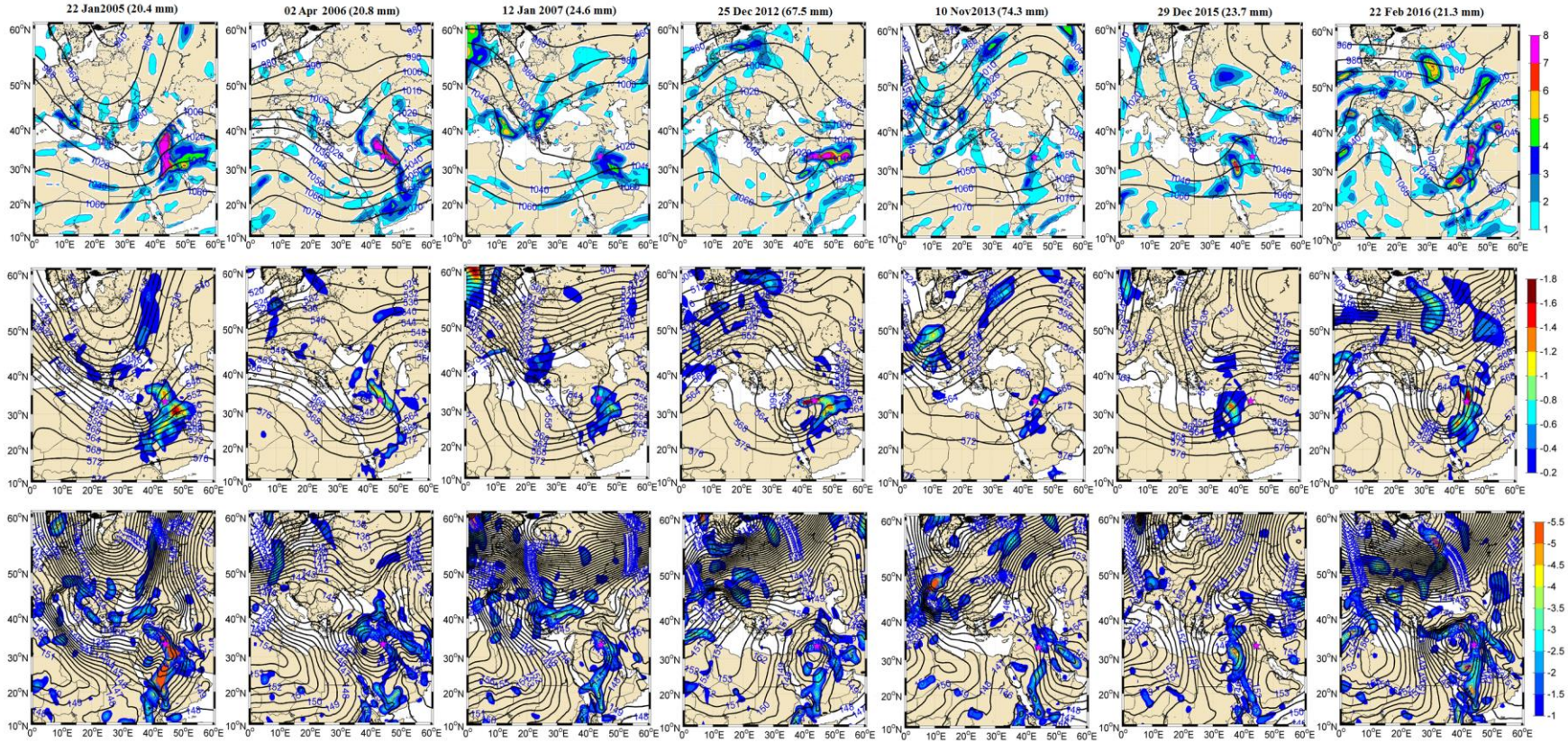

Figure 5.3. Dynamic conditions during cut-off low extreme precipitation events over Iraq. From left to right: 22 January 2005, 02 April 2006, 12 January 2007, 25 December 2012, 10 November2013, 29 December 2015 and 22 February 2016, all times are 1200 UTC. (Top panels) Horizontal divergence (colored with intervals of 10^{-5} s^{-1}) and geopotential height (black contours with intervals of 5 dam) at 250 hPa. (Middle panels) Mean pressure vertical velocity (colored with intervals of 0.2 Pa s^{-1}) over the 700-400 hPa interval and geopotential height (black contours with intervals of 4 dam) at 500 hPa. (Bottom panels) Horizontal divergence (colored with intervals of 0.5 × 10^{-5} s^{-1}) and geopotential height (black contours with intervals of 1 dam) at 850 hPa; note the change in the color bar as compared with the top panels, with the reddish colors now representing negative convergent values.

5.3.2.4 Rex block

When a large scale pattern remains stationary for some time, ranging from days to weeks, we say that it is blocked (Huang et al., 2007). There are several types of block patterns, among them one consisting of a closed high-pressure region situated poleward from a closed low-pressure centre. As this pattern was first studied by the meteorologist Daniel F. Rex (Rex, 1950), it has been named Rex block pattern. It conforms a high-low pattern; when the low is englobed by another high, hence forming a low-high-low pattern, we refer to it as an omega block.

In some cases the Rex block may last only a few days but this is enough to substantially lower the temperature and produce extreme rainfall; high precipitation variance in temperate regions has often been attributed to Rex block phenomena (Davini, 2013).

Seven out of the 20 extreme episodes belong to the Rex block category (Figs. 4.1 and 5.4). These events are the following: 17-19 November 2012 (35.0 mm), 22-23 November 2012 (37.3 mm), 18-20 November 2013 (89.6 mm), 25-29 October 2015 (84.9 mm), 4-6 November 2015 (21.8 mm), 23-25 December 2016 (29.6 mm) and 25-28 March 2016 (25.9 mm) (Table 3.2). A detailed discussion of the 18-20 November 2013 event, the peak rainfall episode for the entire 12-year period, is provided in Chapter 4.

5.4 Moisture fluxes for all 20 extreme precipitation events

For the sake of completeness, in Figure 5.5 we present the vertically integrated moisture fluxes and moisture fluxes convergence for all 20 extreme episodes, at the time of the reported maximum precipitation in the Baghdad station. All 20 cases, with no exception, are characterized by a flux of moisture heading toward central Iraq where it converges and large amounts of precipitable water (PW) accumulate. A summary of these extreme cases by season and pattern is presented in Tables 5.1 and 5.2, respectively.

In next section we proceed to a more detailed description of one case study for each type of atmospheric pattern. For the jet streak this will be the 7-11 March 2015 event (60.6 mm), for the upper-air trough we will focus on the 27-28 January 2013 event (49.7 mm), and for the cut-off low we will consider the 24-25 December 2012 episode (67.5 mm). The event that characterizes the Rex block pattern (18-20 November 2013, 89.6 mm) has already been examined in Chapter 4.

Table 5.1. Summary of all extreme precipitation episodes according to season, the summer months are not indicated because they had no extreme events.

Winter (40.5%)			**Spring (16.9%)**			**Autumn (42.6%)**		
Dec (120.8 mm, 15%)	Jan (150.4 mm, 19%)	Feb (54.7 mm, 7%)	Mar (86.5 mm, 11%)	Apr (49.9 mm, 6%)	May (0%)	Sep (0%)	Oct (84.8 mm, 11%)	Nov (258.0 mm, 32%)
25 Dec2012 (67.5 mm) Cut off low	22 Jan 2005 (20.4 mm) Cut-off low	22 Feb 2016 (21.3mm) Cut-off low	27 Mar 2016 (25.9mm) Rex block	2 Apr 2006 (20.8 mm) Cut-off low			28 Oct 2015 (84.9mm) Rex block	10 Nov 2013 (74.3 mm) Cut-off low
29 Dec 2015 (23.7 mm) Cut off low	12 Jan 2007 (24.6 mm) Cut-off low	2 Feb 2006 (33.4 mm) Upper air trough	10 Mar 2005 (60.6 mm) Jet streak	20 Apr 2011 (29.1mm) Upper air trough				19 Nov 2013 (89.6 mm) Cut-off low
24 Dec 2016 (29.6 mm) Rex block	07 Jan 2006 (34.7 mm) Jet streak							19 Nov 2012 (35.0 mm) Rex block
	28 Jan 2013 (49.7 mm) Upper air trough							23 Nov 2012 (37.3 mm) Rex block
	31 Jan 2013 (21 mm) Upper air trough							05 Nov 2015 (21.8 mm) Rex block

Table 5.2. Summary of all extreme precipitation episodes according to synoptic pattern.

	Jet streak 95.3 mm (11.8%)	**Upper-air trough** 133.2 mm (16.5%)	**Cut-off low** 252.4 mm (31.4%)	**Rex-block** 324.1 mm (40.3%)
1	10 Mar 2005 (60.6 mm)	2 Feb 2006 (33.4 mm)	22 Jan 2005 (20.4 mm)	19 Nov 2012 (35.0mm)
2	7 Jan 2006 (34.7 mm)	20 Apr 2011 (29.1 mm)	2 Apr 2006 (20.8 mm)	23 NOV 2012 (37.3 mm)
3		28 Jan 2013 (49.7 mm)	12 Jan 2007 (24.6 mm)	19 Nov 2013 (89.6 mm)
4		31 Jan 2013 (21 mm)	25 Dec 2012 (67.5 mm)	28 Oct 2015 (84.9mm)
5			10 Nov 2013(74.3mm)	5 Nov 2015 (21.8mm)
6			29 Dec 2015 (23.7mm)	27 Mar 2016 (25.9mm)
7			22 Feb 2016 (21.3mm)	24 Dec2016 (29.6mm)

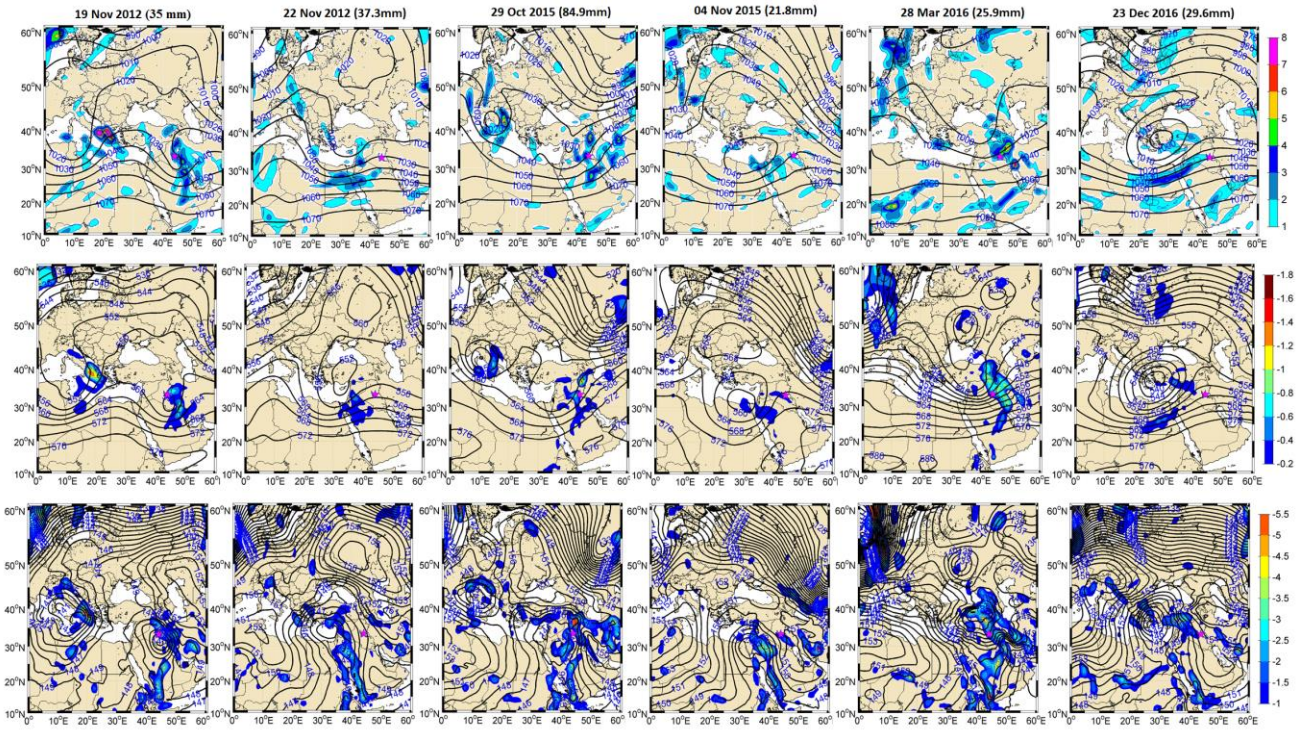

Figure 5.4. Dynamic conditions during Rex block extreme precipitation events over Iraq. From left to right: 19 November 2012, 22 November 2012, 29 October 2015, 4 November 2015, 28 March 2016 and 23 December 2016 , all times are 1200 UTC. (Top panels) Horizontal divergence (colored with intervals of 10^{-5} s^{-1}) and geopotential height (black contours with intervals of 5 dam) at 250 hPa. (Middle panels) Mean pressure vertical velocity (colored with intervals of 0.2 Pa s^{-1}) over the 700-400 hPa interval and geopotential height (black contours with intervals of 4 dam) at 500 hPa. (Bottom panels) Horizontal divergence (colored with intervals of 0.5 × 10-5 s^{-1}) and geopotential height (black contours with intervals of 1 dam) at 850 hPa; note the change in the color bar as compared with the top panels, with the reddish colors now representing negative convergent values.

It is important to emphasize that the forecoming description of these selected events is entirely preliminary and fully descriptive, no detailed analysis of the dynamics will be included. We simply draw the main characteristics of these extreme episodes both for the sake of completeness and in order to provide the basic elements of future works. For the sake of clarity, we will present the observations for each event in four different parts: synoptic situation, horizontal divergence and vertical flow, moisture source and convective instability.

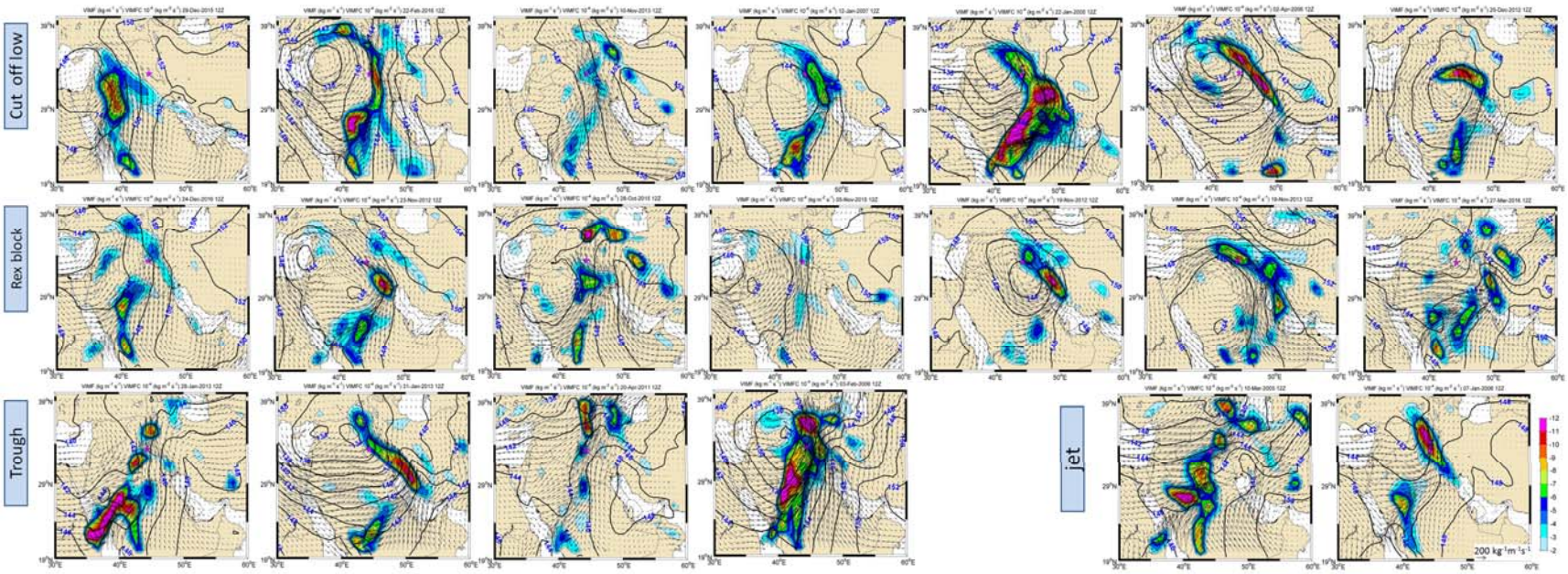

Figure 5.5. Mean vertically integrated moisture flux (VIMF) (arrows, units of kg m^{-1} s^{-1}; the reference arrow denotes 200 kg m^{-1} s^{-1}) and mean vertically integrated moisture flux convergence (VIMFC) (colored with intervals of 10^{-4} kg m^{-1} s^{-1}, see Figure 4.9 for the color bar) over the 1000-700 hPa band for all extreme precipitation episodes, grouped into the four different weather patterns.

5.5 Jet streak case study: 7-11 March 2005

The rainfall during the 7-11 March 2005 extreme event was distributed as follows: 0.2 mm on 7 March, 2.3 mm on 9 March, 34.1 mm on 10 March and 24.0 mm on 11 March, for a total of 60.6 mm. The precipitation during this event represented 56.0% of the total annual precipitation for the calendar 2013 year, with 31.5% in one single day.

5.5.1 Synoptic situation

The synoptic situation is presented in Figure 5.6. The 250 and 500 hPa geopotentials display an upper air trough pattern over Europe and the northern Mediterranean Sea. The PV and temperature fields illustrate the penetration of high PV and cold streaks along the upper air trough on 8 March 2005. The 850 hPa geopotential height indicates the coincidence of a low-level trough with the 500 and 250 upper air trough, so that low-level air flows from the Mediterranean Sea into central Iraq.

On 9 March, the geopotential and PV middle- and upper-atmosphere contours show that the trough, together with its cold air mass, shifted slightly east but remained still far from Iraq, which continued affected by warm air masses. The 850-hPa geopotential contours are similar to those during the previous day.

During the extreme precipitation day, 10 March (34 mm), the upper air trough had moved further east tough remained far from Iraq. The low level trough also moved east, closely correlated with the upper air trough, causing intense westerlies from the Mediterranean Sea. On 11 March (24 mm), the upper-air trough became more pronounced and moved further east into Turkey, with westerlies connecting the Mediterranean Sea with central Iraq. Finally, on 12 March, the 250 hPa upper air trough had moved further east into Central Asia, and a pool of cold air entered Iraq.

For the jet streak event it is useful to observe the upper-atmosphere velocity field (Fig. 5.6, bottom panels). Several days prior to the event (not shown), the 250 hPa isotachs illustrate the existence of two jet stream cores: the first one located on (30°N, 15°E) and the second one, closer to Iraq, located on (40°N, 30°E). On 8-9 March the two jet cores overlap in one single high-speed core, with Iraq being on the entrance area of this jet. On 11 March, following the extreme precipitation, the jet speed has decreased and Iraq is left on the exit sector of the jet.

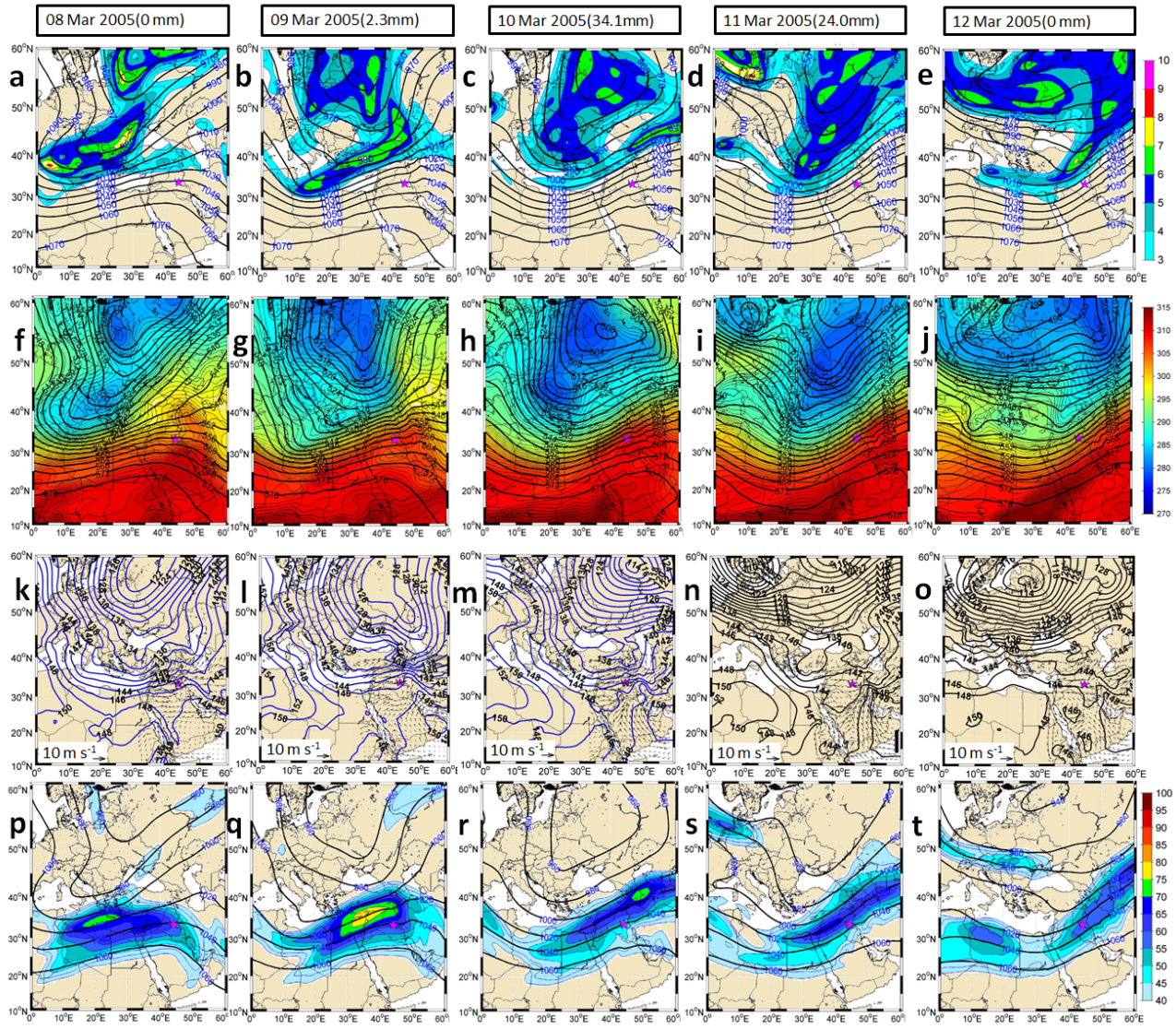

Figure 5.6. Distribution of variables, from left to right, between 8 and 12 March 2005, 1200 UTC. (Top panels) PV (colored with intervals of 1 PVU) and geopotential height (solid contours with intervals of 10 dam) at 250 hPa for. (Middle panels) EPT (colored with intervals of 5K) and geopotential height (solid contours with intervals of 4 dam) at 500 hPa. (Bottom panels) Geopotential height (solid contours with intervals of 2 dam) and wind vectors solely for the Iraq region (arrows, units of m s^{-1}; the reference arrow denotes 1 m s^{-1}) at 850 hPa. (Bottom panels) Wind speed (colored with intervals of 5 m s^{-1}) and geopotential height (solid contours with intervals of 20 dam) at 250 hPa.

5.5.2 Horizontal divergence and vertical flow

The horizontal divergence maps in the upper and lower atmosphere are presented in Figure 5.7. The association of upper horizontal divergence with lower convergence has a fundamental role in the onset of the extreme episode. On 8 March, the areas of the upper-level (250 hPa) horizontal divergence remain west from Iraq, and low-level (850 hPa) horizontal convergence develops in central Iraq. On 9 March and specially 10 March, an intense upper-level horizontal divergence collocates with the low-level horizontal convergence. After these days, the upper-lower level inverted correlation decrease sharply.

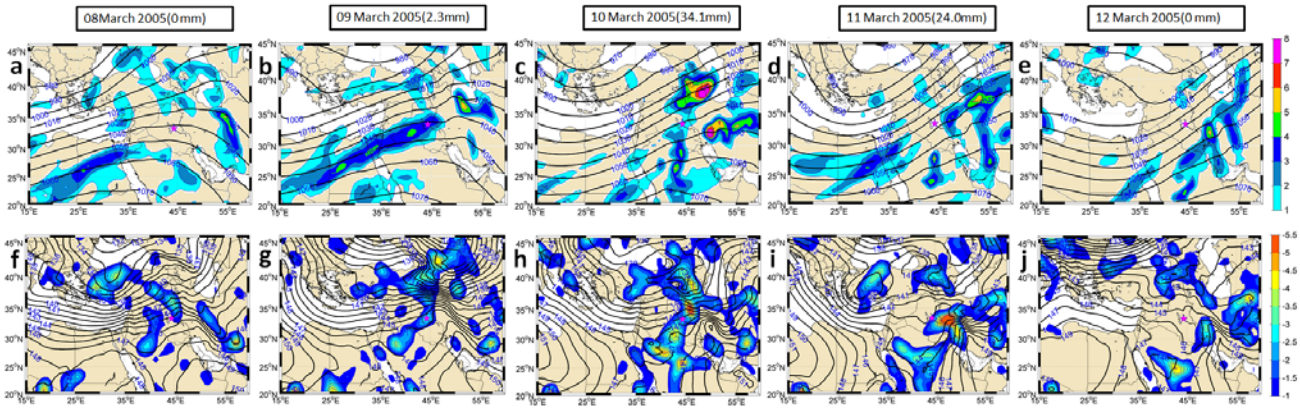

Figure 5.7. Distribution of variables, from left to right, between 8 and 12 March 2005, 1200 UTC. (Top panels) Horizontal divergence (colored with intervals of 10^{-5} s^{-1}) and geopotential height (black contours with intervals of 5 dam) at 250 hPa. (Bottom panels) Horizontal divergence (colored with intervals of 0.5×10^{-5} s^{-1}) and geopotential height (black contours with intervals of 1 dam) at 850 hPa; note the change in the color bar as compared with the top panels, with the reddish colors now representing negative convergent values.

The distribution of both vertical velocities and Q-vector divergence between 700-400 hPa is presented in Figure 5.8. Once again, both variables exhibit peak values and maximum spatial correlation at the time of the flood, on 10 March. In Figure 5.9 we include the temporal evolution of the maps of RV, PV and PV advection, illustrating their location over central Iraq on 10 March.

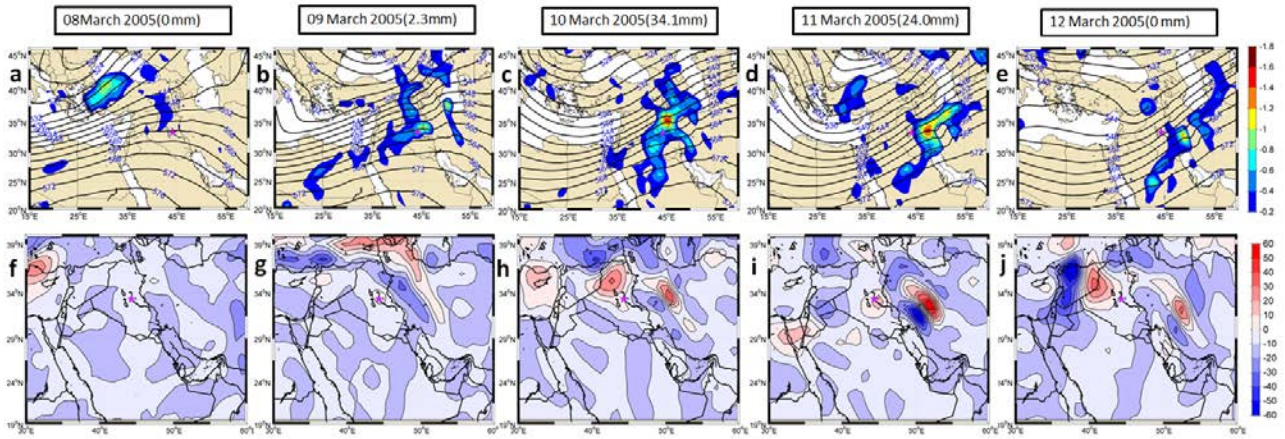

Figure 5.8. Distribution of variables, from left to right, between 8 and 12 March 2005, 1200 UTC. (Top panels) Mean pressure vertical velocity (colored with intervals of 0.2 Pa s^{-1}) over the 700-400 hPa interval and geopotential height (black contours with intervals of 4 dam) at 500 hPa. (Bottom panels) Q-vector divergence (colored with intervals of 2 × 10^{-18} m kg^{-1} s^{-1}) over the 700-400 hPa interval.

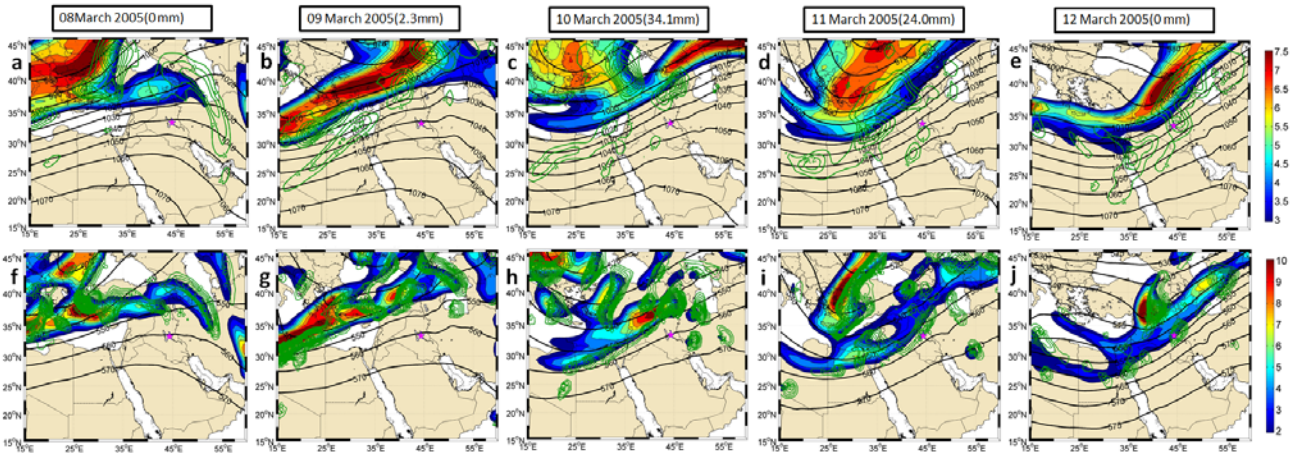

Figure 5.9. Distribution of variables, from left to right, between 8 and 12 March 2005, 1200 UTC. (Top panels) PV (colored with intervals of 0.5 PVU), PV advection (green contours with intervals of 10^{-5} PVU s^{-1}) and geopotential height (black contours with intervals of 5 dam) at 250 hPa. (Bottom panels) Positive RV (colored shaded with intervals of 10^{-5} s^{-1}), advection of positive RV (blue contours with intervals of 10^{-5} s^{-1}) and geopotential height (black contours with intervals of 5 dam) at 500 hPa.

The vertical extension of the convective motions in central Iraq is shown in Figure 5.10. A latitudinal section along 44.5°E illustrates the temporal evolution of the vertical velocities and the vertical extension of humid air between 9 and 12 March. The maximum vertical velocities and humidity values over Baghdad, all the way from near the surface to the 250 hPa level, took place on 10 March.

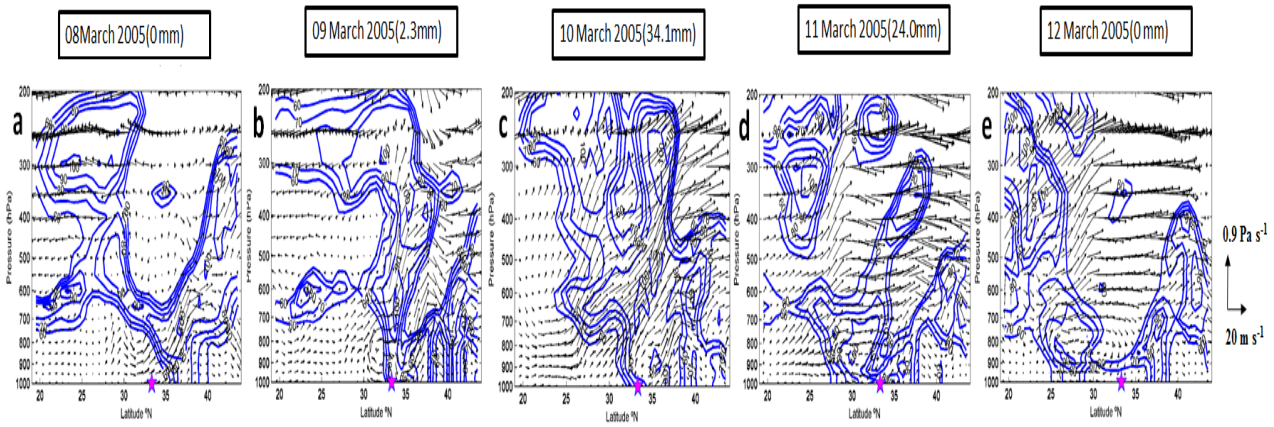

Figure 5.10. Distribution of variables, from left to right, between 8 and 12 March 2005, 1200 UTC. Relative humidity (values ≥ 60% with intervals of 10%, blue contours) and wind velocity (horizontal velocity in m s^{-1} and pressure vertical velocity in Pa s^{-1}, black arrows).

5.5.3 Moisture source

The ERA-Interim variables show that the jet streak over Iraq was associated with intense low-level wind convergence, upward motions and upper-level divergence, at a time of low-level easterly winds from the Mediterranean Sea. These factors favor rainfall but yet require a source of moisture. We may explore what was this source through the distributions of three variables – the 1000-700 hPa vertically-integrated moisture flux (VIMF), its convergence (VIMFC) and the precipitable water (PW) – over the Middle East previous and during the 10 March 2005 extreme event (Fig. 5.11).

We observe that there was little PW over Iraq on 8 and 9 March (less than 16 kg m^{-2}). At this time, however, the westerly and southerly winds brought wet air from the Mediterranean Sea and Persian Gulf, respectively, so the VIMFC reached 9×10^{-4} kg m^{-2} s^{-1} in northern Iraq, which are values larger than those reported by Krichak et al. (2015) during intense-rain events in Mediterranean regions. The VIMFC over central Iraq remained high during 10 March and, consequently, the PW rose to more than 20 kg m^{-2}. On 11 March (24 mm of rain in Baghdad) there was still a region of

high VIMFC values in eastern Iraq and the amount of PW over central Iraq had decreased to some 16 kg m^{-2}. Finally, on 12 March, the winds weakened and the high VIMFC and PW values remained constrained to south of Iraq.

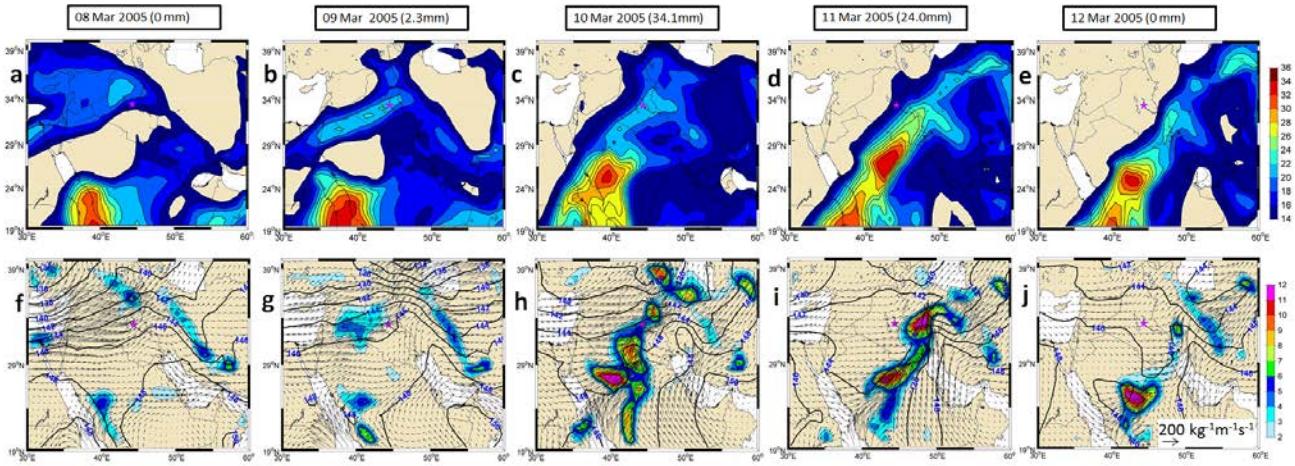

Figure 5.11. Distribution of variables, from left to right, between 8 and 12 March 2005, 1200 UTC. (Top panels) Precipitable water (PW) (colored with intervals of kg m^{-2}) integrated over the 1000-700 hPa band. (Bottom panels) Vertically integrated moisture flux (VIMF) (arrows, units of kg m^{-1} s^{-1}) and vertically integrated moisture flux convergence (VIMFC) (colored with intervals of 10^{-4} kg m^{-1} s^{-1}) over the 1000-700 hPa band.

5.5.4 Convective instability

We finally explore the relevance of convective instability through the distributions of the K, SWEAT, LI and CAPE indices (Figs. 5.12 and 5.13). Regarding the LI, CAPE and K indices, they were low on 7 and 8 of March, increased to maximum values on 9 and 10 March (yet below the instability threshold) and decreased afterwards. An analogous evolution occurred with the SWEAT index, though in this case it did exceed the instability threshold on 9 March.

5.6 Upper air through case study: 27-28 January 2013

The 27-28 January 2013 extreme rainfall was distributed between 2.4 mm on 27 January and 47.3 mm on 28 January, for a total of 52.1 mm. This was a sudden episode that represented 81.1% of the January precipitation and 20.8% of the total precipitation during the 2013 natural year.

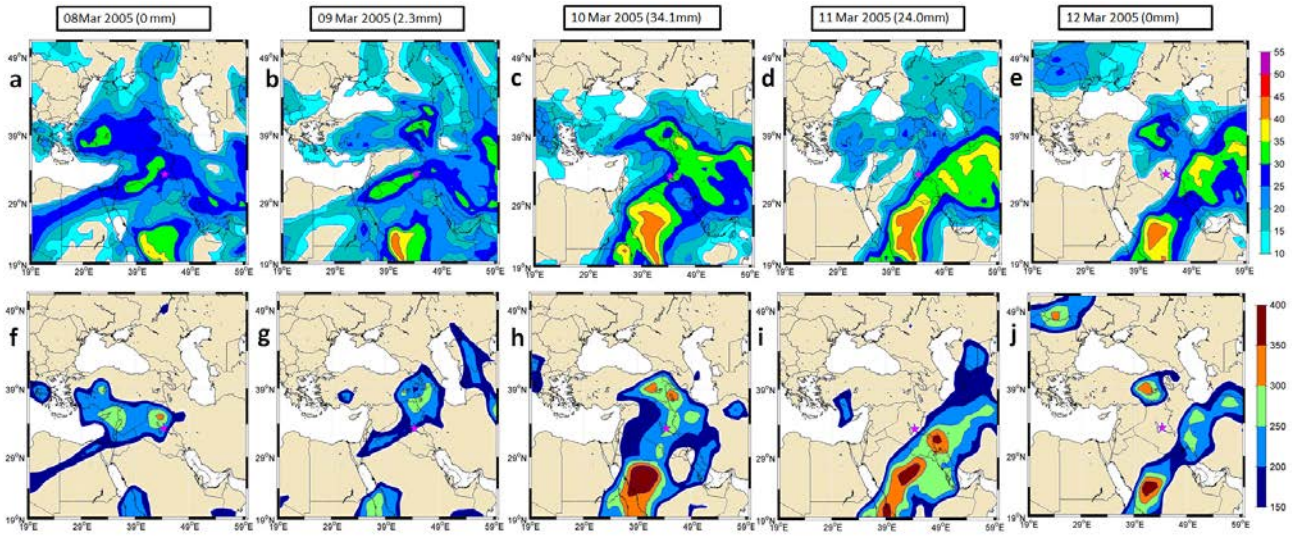

Figure 5.12. Distribution of variables, from left to right, between 8 and 12 March 2005, 1200 UTC. (Top panels) K index (colored, °C) and (bottom panels) severe weather threat index (SWEAT) (colored, dimensionless).

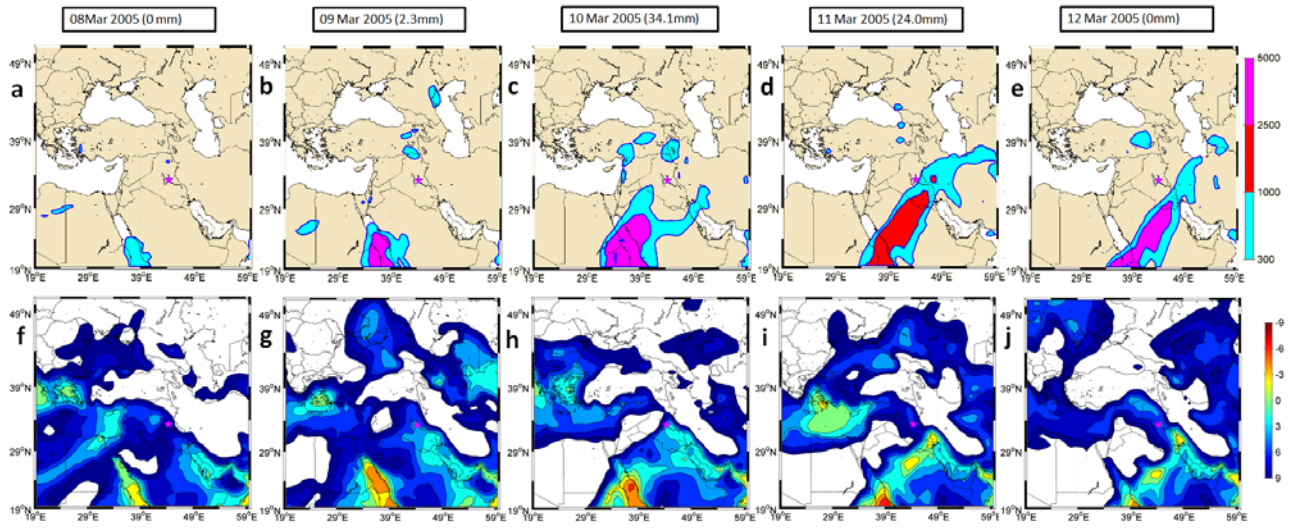

Figure 5.13. Distribution of variables, from left to right, between 8 and 12 March 2005, 1200 UTC. (Top panels) CAPE index (colored, J kg^{-1}) and (bottom panels) lifted index (LI) (colored, °C).

5.6.1 Synoptic situation

The synoptic situation during the 27-28 January 2013 episode is shown in Figure 5.14. The 250 and 500 hPa geopotentials display an intense upper-air trough over Europe and the northern Mediterranean Sea. This upper-air trough is reflected by a tongue of high PV and cold air masses, with PV values greater than 8 PVU, extending longitudinally over the Mediterranean Sea as early as 26 January. The 850 hPa geopotential height indicates a cyclonic lower-atmosphere circulation over the central Mediterranean Sea, which was associated with the 500 and 250 upper-air trough. As a consequence, low-level air flew from the Mediterranean Sea into central Iraq during the episode. Further, a lower-atmosphere anticyclonic feature, centered on the Arabian Peninsula, induced south-westerly winds that brought moisture from the Arabian Sea and the Persian Gulf over southern Iraq.

The upper-level trough intensified and shifted east between 26 and 27 January. The tongue of high-PV values extended south covering southeast Europe and penetrating into northern Africa (Tunisia, Algeria and Libya) but without reaching Iraq. The 850 hPa low propagated slightly eastwards and increased the southwesterly winds from the Arabian Sea and Persian Gulf.

On 28 January, the flooding day, the upper-level trough continued its slow eastward propagation, with the trough axis over east Africa and peak PV values over Libya. On 29 January, one day after the maximum rainfall, the upper level air trough reached Iraq, with peak PV values over Baghdad.

5.6.2 Horizontal divergence and vertical flow

With the purpose of identifying the coupling between the upper and lower atmosphere, we present the horizontal divergence maps at 250 and 850 hPa (Fig. 5.15). On 26 January, relatively high values of horizontal divergence covered much of Iraq at high atmospheric levels while convergence occurred at low levels. On 27 January, coinciding with the slow eastward propagation of the upper-level trough and lower-level low, the upper/lower horizontal divergence/convergence increased. On 28 January, the upper-level trough moved towards Iraq and led to more intense upper and lower level divergence. These high values remained on 29 January but moved northeast of Baghdad.

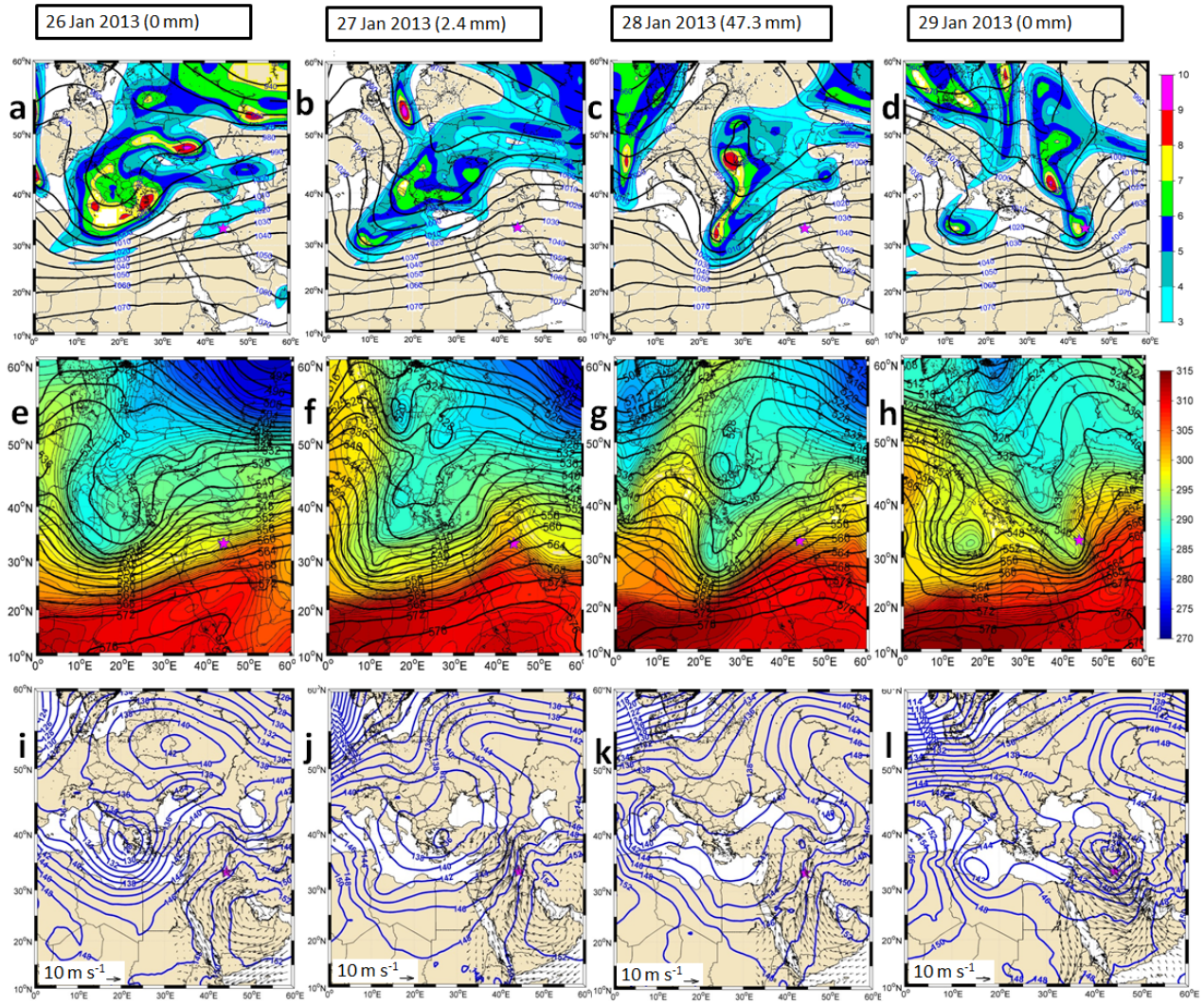

Figure 5.14. Distribution of variables, from left to right, between 26 and 29 January 2013, 0600 UTC. (Top panels) PV (colored with intervals of 1 PVU) and geopotential height (solid contours with intervals of 10 dam) at 250 hPa. (Middle panels) EPT (colored with intervals of 5K) and geopotential height (solid contours with intervals of 4 dam) at 500 hPa. (Bottom panels) Geopotential height (solid contours with intervals of 2 dam) and wind vectors solely for the Iraq region (arrows, units of m s^{-1}; the reference arrow denotes 1 m s^{-1}) at 850 hPa.

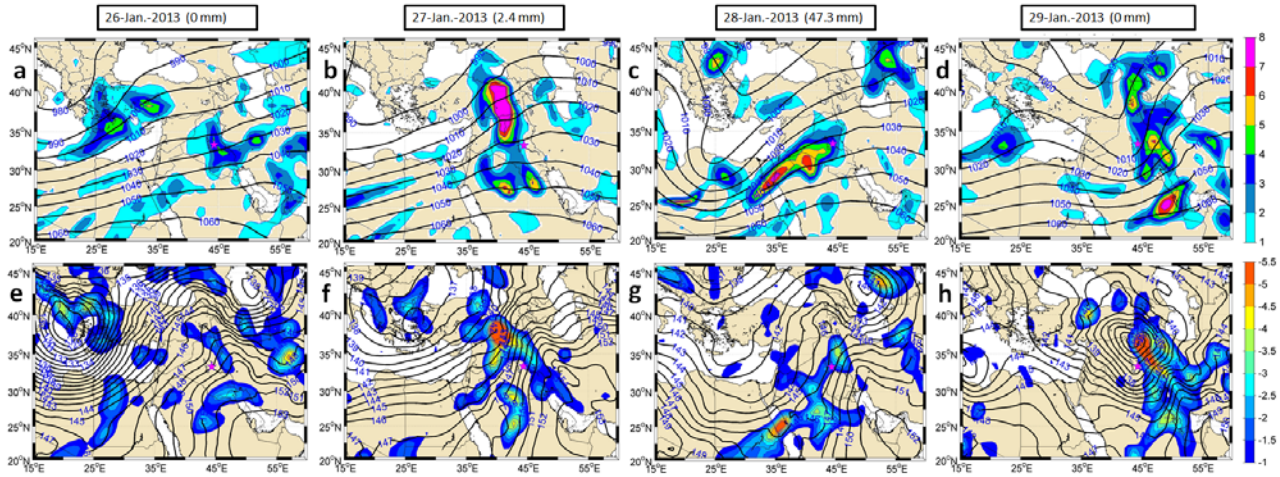

Figure 5.15. Distribution of variables, from left to right, between 26 and 29 January 2013, 1200 UTC. (Top panels) Horizontal divergence (colored with intervals of 10^{-5} s^{-1}) and geopotential height (black contours with intervals of 5 dam) at 250 hPa. (Bottom panels) Horizontal divergence (colored with intervals of 0.5×10^{-5} s^{-1}) and geopotential height (black contours with intervals of 1 dam) at 850 hPa; note the change in the color bar as compared with the top panels, with the reddish colors now representing negative convergent values.

The distribution of the 700-400 hPa vertical velocities and Q-vector divergence fields is shown in Figure 5.16. The evolution of the vertical velocities again illustrates the slow eastward propagation and expansion of the region with high upward vertical velocities, though surprisingly the values are moderate over central Iraq on 28 January, the day of maximum flooding. In Figure 5.17 we include the temporal evolution of the maps of RV, PV and PV advection, which clearly exemplify the eastward propagation of the perturbation and its associated rainfall.

The temporal development of relative humidity and upward velocities between 26 and 29 January is illustrated for a latitudinal section along 44.5°E (Fig. 5.18). The relative humidity and upward velocities changed substantially during this period, from low values on 26 January to peak values on 28 January over Baghdad, extending all the way from the surface to the 200 hPa level.

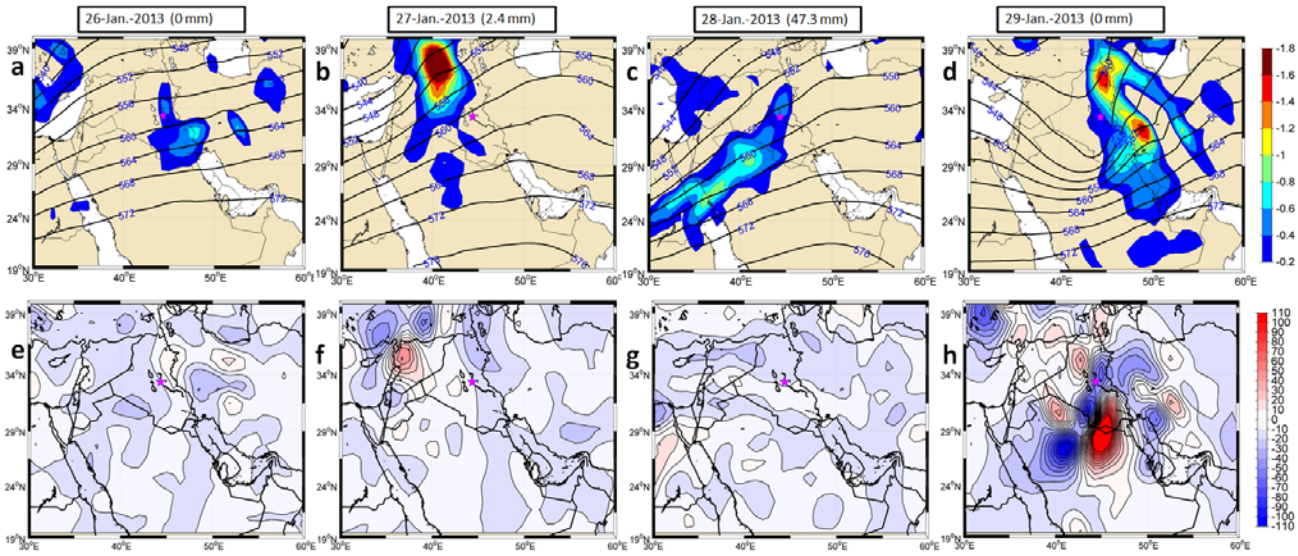

Figure 5.16. Distribution of variables, from left to right, between 26 and 29 January 2013, 0600 UTC. (Top panels) Mean pressure vertical velocity (colored with intervals of 0.2 Pa s^{-1}) over the 700-400 hPa interval and geopotential height (black contours with intervals of 4 dam) at 500 hPa. (Bottom panels) Q-vector divergence (colored with intervals of 2 × 10^{-18} m kg^{-1} s^{-1}) over the 700-400 hPa interval.

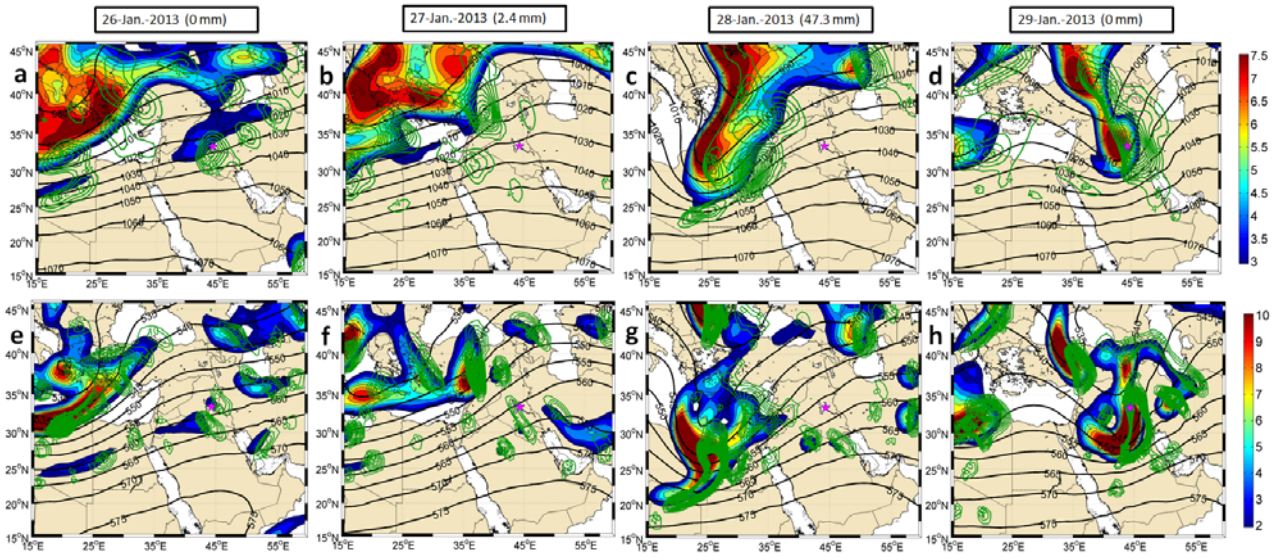

Figure 5.17. Distribution of variables, from left to right, between 26 and 29 January 2013, 0600 UTC. (Top panels) PV (colored with intervals of 0.5 PVU), PV advection (green contours, intervals of 10^{-5} PVU s^{-1}) and geopotential height (black contours, intervals of 5 dam) at 250 hPa. (Bottom panels) Positive RV (colored shaded with intervals of 10^{-5} s^{-1}), advection of positive RV (blue contours, intervals of 10^{-5} s^{-1}) and geopotential height (black contours, 5 dam intervals) at 500 hPa.

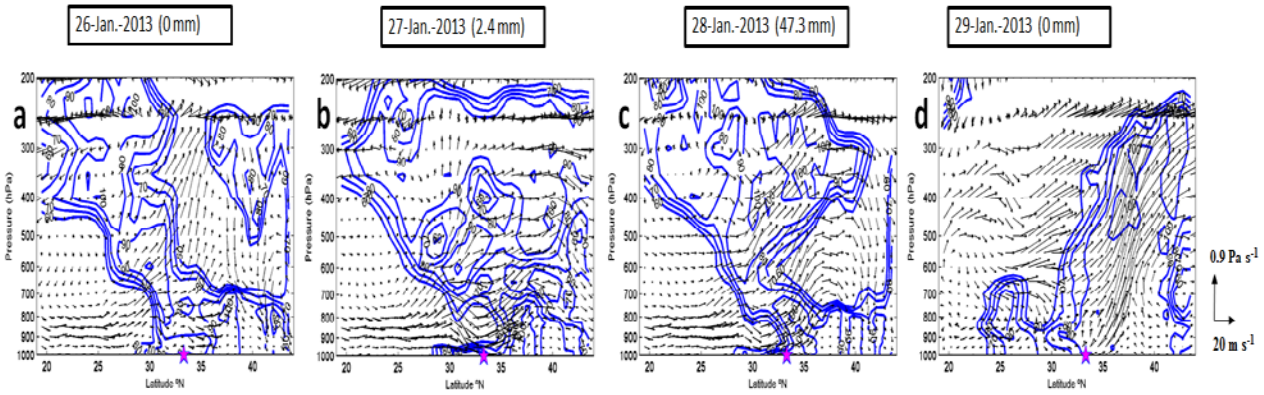

Figure 5.18. Distribution of variables, from left to right, between 26 and 29 January 2013, 0600 UTC. Relative humidity (values ≥ 60% with intervals of 10%, blue contours) and wind velocity (horizontal velocity in m s^{-1} and pressure vertical velocity in Pa s^{-1}, black arrows).

5.6.3 Moisture source

The ERA-Interim reanalysis shows that the establishment of the upper-level trough led to the reinforcement of the lower level cyclonic circulation and the generation of southerly winds from the Red Sea and Persian Gulf. Further, the upper-level trough caused intense upward dynamical forcing ahead of the cyclone, with low-level wind convergence and upward motion. These factors favor rainfall but require a source of moisture. We next look at the distributions of three variables – the 1000-700 hPa vertically-integrated moisture flux (VIMF), its convergence (VIMFC) and the precipitable water (PW) – over the Middle East in order to investigate what was the source of moisture (Fig. 5.19).

On 26 January, we observe the input of PW from the Red Sea into Iraq, accompanied by moderate values of VIMF and VIMFC (less than 2×10^{-4} kg m^{-2} s^{-1}). On 27 January, coinciding with the evolution of the upper level trough, the winds from the west and southwest intensified, bringing wet air from the Mediterranean and Red Sea into central Iraq. This moisture converged over Iraq, with VIMFC values above 8×10^{-4} kg m^{-2} s^{-1} in northern Iraq and near 3×10^{-4} kg m^{-2} s^{-1} over Baghdad. In contrast the amount of PW over southern Iraq was reduced as compared with the previous day.

The westerly and southwesterly winds increased on 28 January, with the VIMFC exceeding 3×10^{-4} kg m^{-2} s^{-1} and the PW reaching more than 20 kg m^{-2} precisely over Baghdad, and the high-PW area

stretching from the Red and Arabian Seas into central Iraq. Finally, on 29 January, the southerly winds remained intense so the moisture northward transport remained large though the PW over central Iraq decreased, with maximum values in the southern portion of the Arabian Peninsula.

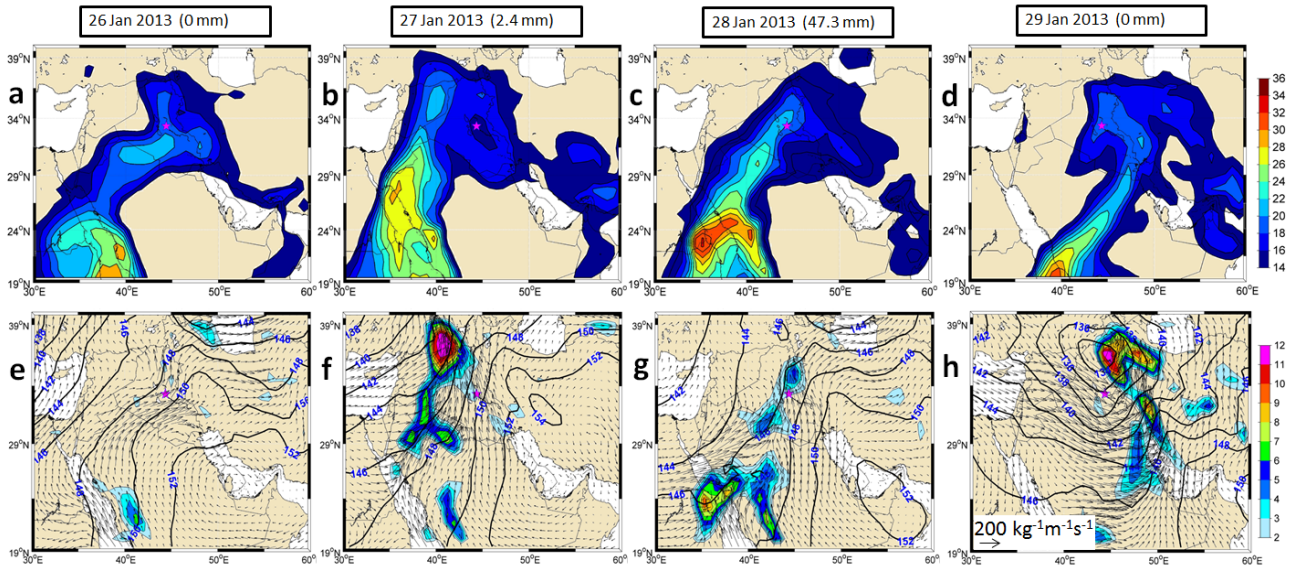

Figure 5.19. Distribution of variables, from left to right, between 26 and 29 January 2013, 0600 UTC. (Top panels) Precipitable water (PW) (colored with intervals of kg m^{-2}) integrated over the 1000-700 hPa band. (Bottom panels) Vertically integrated moisture flux (VIMF) (arrows, units of kg m^{-1} s^{-1}) and vertically integrated moisture flux convergence (VIMFC) (colored with intervals of 10^{-4} kg m^{-1} s^{-1}) over the 1000-700 hPa band.

5.6.4 Convective instability

We finally briefly look at the importance of convective instability through the distributions of the K, SWEAT, LI and CAPE indices (Figs. 5.20 and 5.21). The K and SWEAT indices did exceed the instability thresholds, and the LI did become negative (<0°C) though it happened on 29 January rather than 28 January. The local CAPE index, however, was always well below the instability threshold.

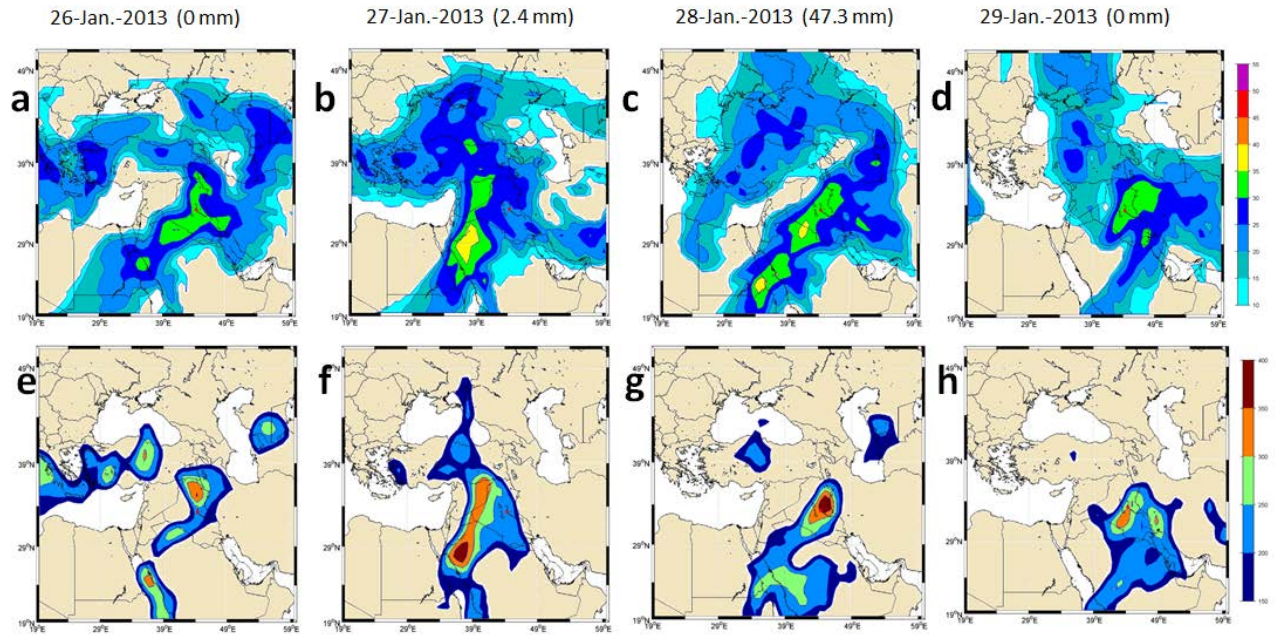

Figure 5.20. Distribution of variables, from left to right, between 26 and 29 January 2013, 0600 UTC. (Top panels) K index (colored, °C) and (bottom panels) severe weather threat index (SWEAT) (colored, dimensionless).

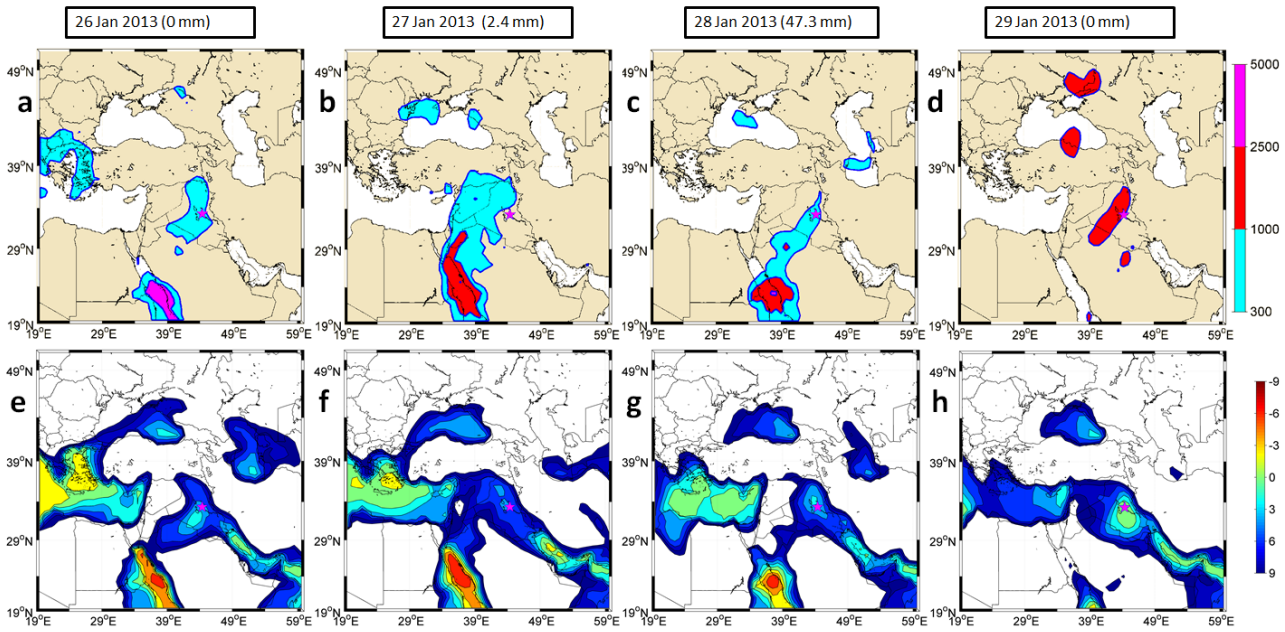

Figure 5.21. Distribution of variables, from left to right, between 26 and 29 January 2013, 0600 UTC. (Top panels) CAPE index (colored, J kg^{-1}) and (bottom panels) lifted index (LI) (colored, °C).

5.7 Cut-off low case study: 24-25 December 2012

The December 2012 extreme episode was distributed between 3.1 mm on 24 December and 67.5 mm on 25 December. The precipitation during December 2012 (70.6 mm) represented 26.8% of the total annual precipitation for the natural 2013 year (38.3% of the calendar 2012 year). Further, 95.6% of the December precipitation (67.5 mm) took place on 25 December, representing 25.6% of Baghdad's rainfall during the 2013 natural year (36.6% of the calendar 2012 year).

5.7.1 Synoptic situation

The synoptic situation between 23 and 26 December 2012 is revealed in Figure 5.22. On 23 December, the geopotential height hints at the transformation of a sharp upper-level trough into a cut-off low – with PV above 8 PVU – centered south of the eastern Mediterranean Sea (30°N, 25°E), which is accompanied by a ridge over central Iraq. An intense PV maximum is associated with this cut-off low, with values above 8 PVU. Simultaneously, in the lower atmosphere (850 hPa), the geopotential height displays a dipole, made up by a cyclone in the eastern Mediterranean Sea (32°N, 25°E) and anticyclonic over most of Iraq, eastern Saudi Arabia and western Iran. This dipole induces south-easterly winds that bring moisture from the Arabian Sea and Persian Gulf into the central regions of Iraq.

On 24 December, the upper-level trough intensified and shifted east. At low levels, the Mediterranean cyclone and Middle East anticyclone propagated east, causing Iraq to be affected by the south-easterly winds from Arabian Sea, Persian Gulf and the Red Sea.

On the flooding day, 25 December, the cut-off low had already formed, showing up as a well-defined depression over western Iraq, with maximum PV values (9 PVU). The cut-off low had propagated east, centred near (30°N, 40°E), reaching north of Saudi Arabia and western Iraq, and coinciding with the 250-hPa low-pressure centre. This low-level depression, in turn, caused south-easterly winds from the Persian Gulf and Red Sea.

On 26 December, the upper-level low turned back into a pronounced trough and the low-level cyclone moved southeast but kept influencing Iraq, now with intense north-westerly winds. Remarkably, the upper- and lower-level features remained vertically aligned during the entire temporal sequence.

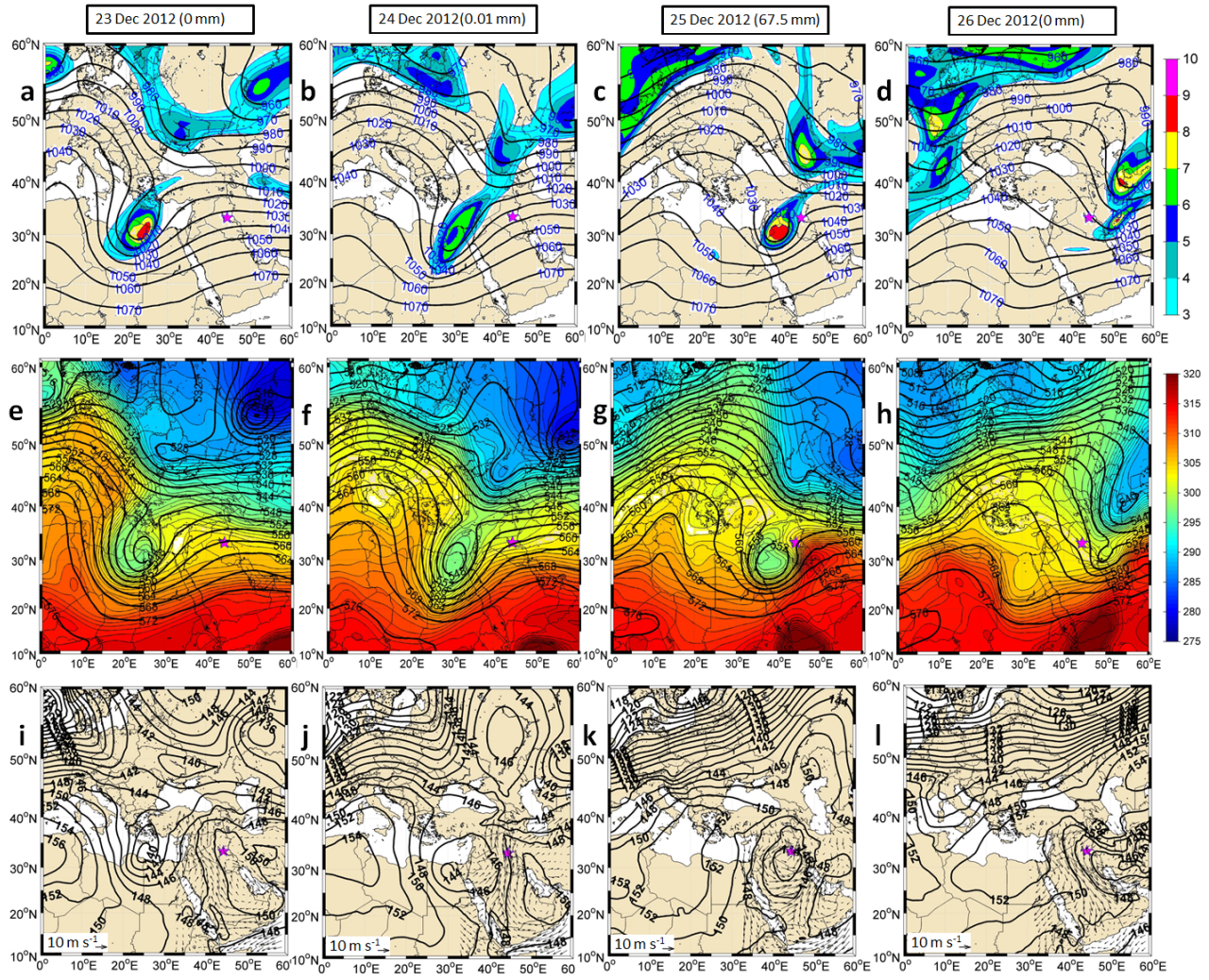

Figure 5.22. Distribution of variables, from left to right, between 23 and 26 December 2012, 1200 UTC. (Top panels) PV (colored with intervals of 1 PVU) and geopotential height (solid contours with intervals of 10 dam) at 250 hPa. (Middle panels) EPT (colored with intervals of 5K) and geopotential height (solid contours with intervals of 4 dam) at 500 hPa. (Bottom panels) Geopotential height (solid contours with intervals of 2 dam) and wind vectors solely for the Iraq region (arrows, units of m s^{-1}; the reference arrow denotes 1 m s^{-1}) at 850 hPa.

5.7.2 Horizontal divergence and vertical flow

As for the jet streak and upper-level trough, we turn now to explore the association between the upper (250 hPa) and lower (850 hPa) horizontal-divergence fields (Fig. 5.23). On 23 December, a small region of high-level divergence can be distinguished near Baghdad (2×10^{-5} s^{-1}), coinciding with the presence of a ridge, while nothing remarkable is observed at low levels. On 24 December,

the 250-hPa level shows a distinct area of horizontal divergence (over 3×10^{-5} s^{-1}) but yet without affecting Baghdad.

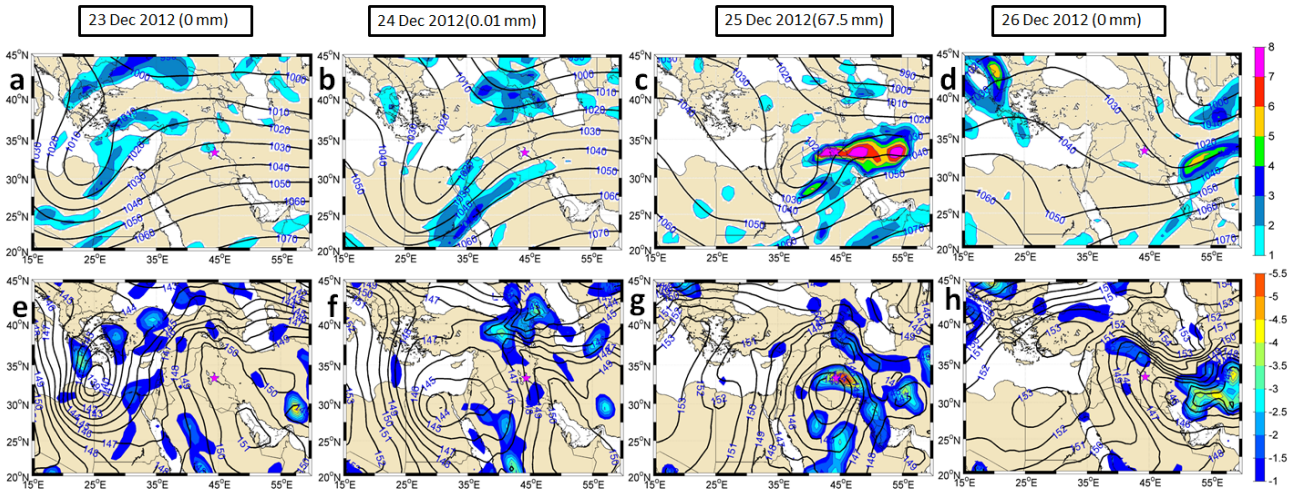

Figure 5.23. Distribution of variables, from left to right, between 23 and 26 December 2012, 1200 UTC. (Top panels) Horizontal divergence (colored with intervals of 10^{-5} s^{-1}) and geopotential height (black contours with intervals of 5 dam) at 250 hPa. (Bottom panels) Horizontal divergence (colored with intervals of 0.5 × 10^{-5} s^{-1}) and geopotential height (black contours with intervals of 1 dam) at 850 hPa; note the change in the color bar as compared with the top panels, with the reddish colors now representing negative convergent values.

On 25 December, the flooding day, the area of upper-level divergence was situated both in central Iraq, with maximum values (7×10^{-5} s^{-1}) coinciding with the eastern sector of the cut-off low, and in the northern Arabian Peninsula, with maximum values of 4×10^{-5} s^{-1}. Simultaneously, the lower atmosphere (850 hPa) shows high convergence values (-4.5×10^{-5} s^{-1}), which are collocated with the northern upper-level divergent areas.

On 26 December, the upper-level divergent region moved east, following the displacement of the upper-level low, leaving Baghdad behind its influence. Concurrently, the low-level convergent region moved east, coupled with the upper-level low, towards Iran.

The distribution of the 700-400 hPa vertical velocity and Q-vector divergence fields is shown in Figure 5.24. The region of high upward velocities coincides with areas of high RV and PV advection, following the displacement of the upper-level low. During the flooding day, the negative values of the Q-vector (700-400 hPa) in central Iraq coincide with regions of low-level convergence

and high vertical velocities, as expected to occur in the region ahead of a cyclone (Sanders and Hoskins, 1990).

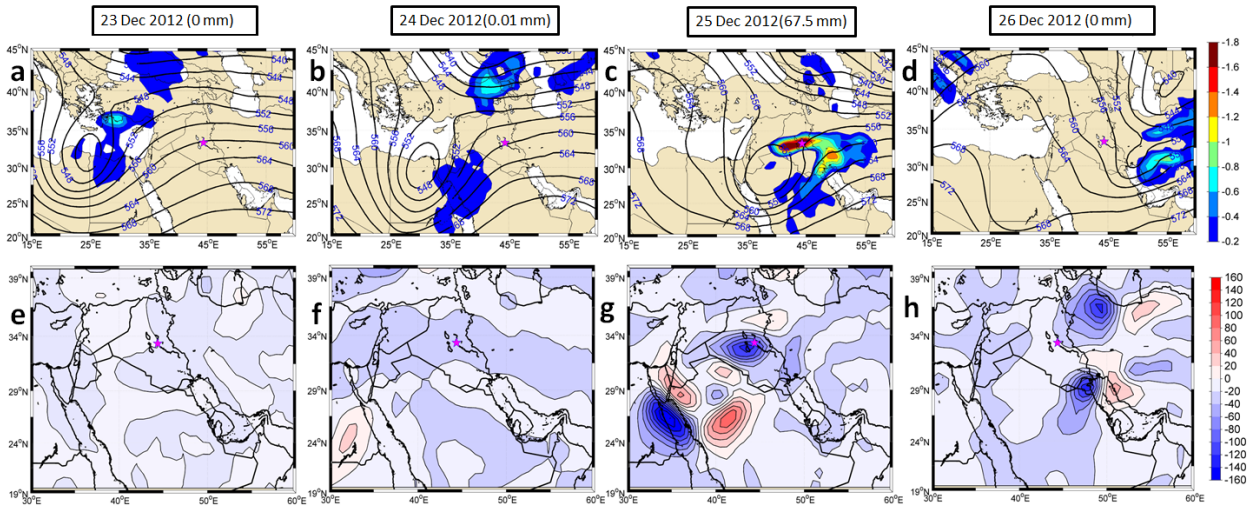

Figure 5.24. Distribution of variables, from left to right, between 23 and 26 December 2012, 1200 UTC. (Top panels) Mean pressure vertical velocity (colored with intervals of 0.2 Pa s^{-1}) over the 700-400 hPa interval and geopotential height (black contours with intervals of 4 dam) at 500 hPa. (Bottom panels) Q-vector divergence (colored with intervals of 2 × 10-18 m kg^{-1} s^{-1}) over the 700-400 hPa interval.

The temporal development of relative humidity and upward velocities between 23 and 26 December is illustrated for a latitudinal section along 44.5°E (Fig. 5.25). The region is affected by the vertical rise of moist air, with a remarkably deep column of high relative humidity and upward velocities over Baghdad on the flooding day, reaching all the way from the surface to 300 hPa

5.7.3 Moisture source

We look at the source of moisture for the December 2012 extreme episode with the help of the distributions of the vertically-integrated moisture flux (VIMF), its convergence (VIMFC) and the precipitable water (PW) over the Middle (Fig. 5.27).

On 23 December, a tongue of high PW stretches north from the Red Sea and Persian Gulf, associated with high values of VIMF in the western part of the low, although they remain far south from Iraq. On 24 December, the VIMF and PW reach further north but the values remain moderate over central Iraq.

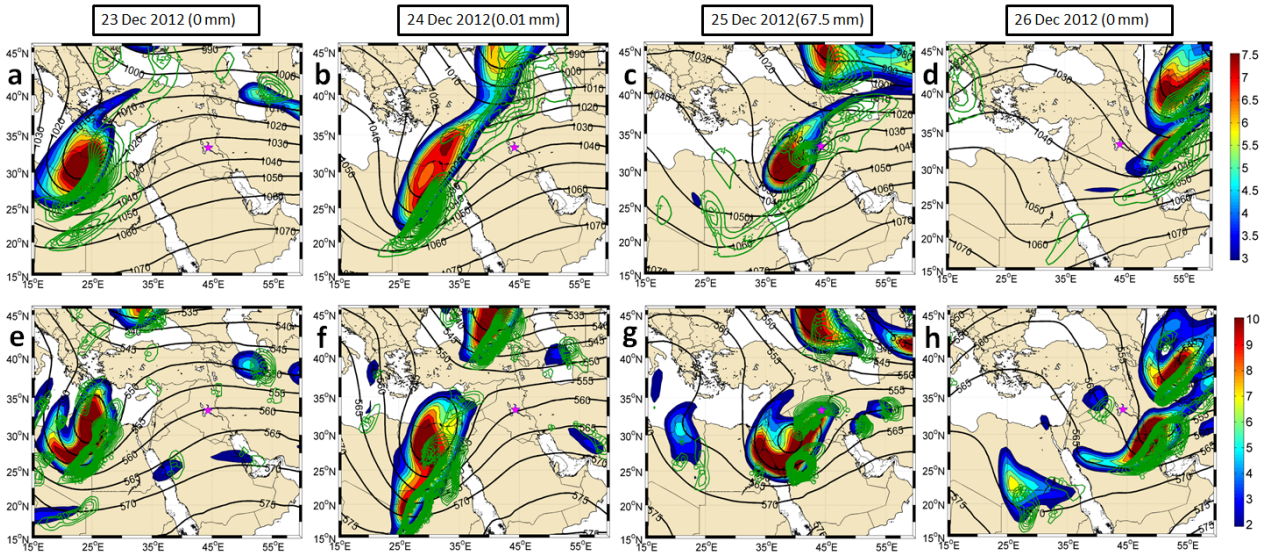

Figure 5.25. Distribution of variables, from left to right, between 23 and 26 December 2012, 1200 UTC. (Top panels) PV (colored with intervals of 0.5 PVU), PV advection (green contours with intervals of 10^{-5} PVU s^{-1}) and geopotential height (black contours with intervals of 5 dam) at 250 hPa. (Bottom panels) Positive RV (colored shaded with intervals of 10^{-5} s^{-1}), advection of positive RV (blue contours with intervals of 10^{-5} s^{-1}) and geopotential height (black contours with intervals of 5 dam) at 500 hPa.

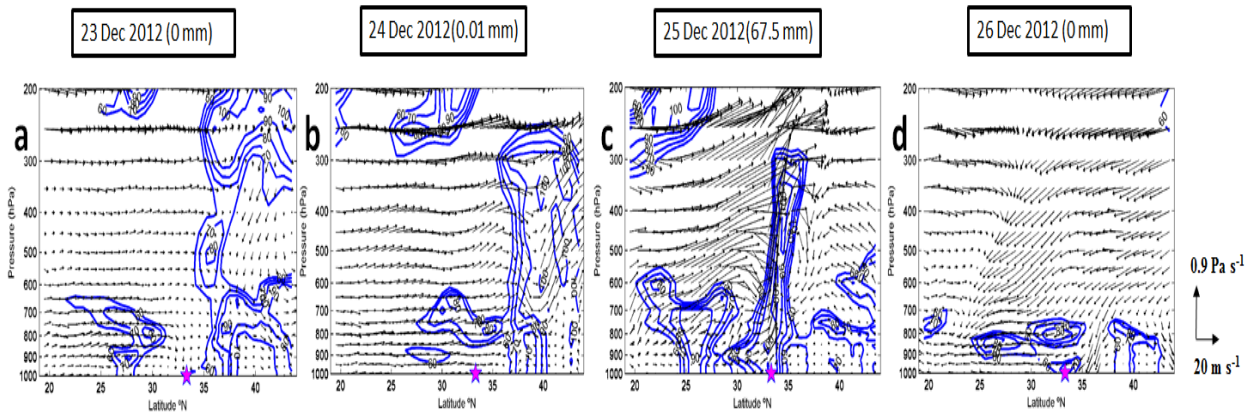

Figure 5.26. Distribution of variables, from left to right, between 23 and 26 December 2012, 1200 UTC. Relative humidity (values ≥ 60% with intervals of 10%, blue contours) and wind velocity (horizontal velocity in m s^{-1} and pressure vertical velocity in Pa s^{-1}, black arrows).

On 25 December, the flooding day, a high moisture flux (12 kg m^{-1} s^{-1}) from the Persian Gulf and the Red Sea has reached central Iraq, associated with the western part of the low-level cyclonic circulation, causing a large increase in the amount of PW. On 26 of December, the cyclonic circulation has moved east and the band of moisture convergence is now far from Iraq.

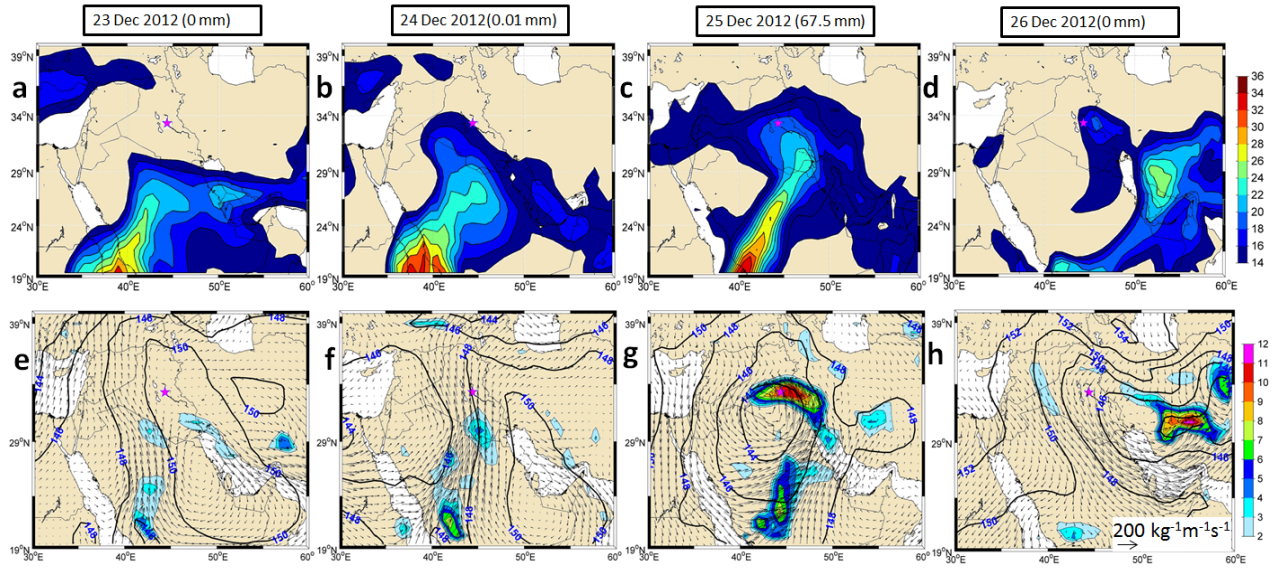

Figure 5.27. Distribution of variables, from left to right, between 23 and 26 December 2012, 1200 UTC. (Top panels) Precipitable water (PW) (colored with intervals of kg m^{-2}) integrated over the 1000-700 hPa band. (Bottom panels) Vertically integrated moisture flux (VIMF) (arrows, units of kg m^{-1} s^{-1}) and vertically integrated moisture flux convergence (VIMFC) (colored with intervals of 10^{-4} kg m^{-1} s^{-1}) over the 1000-700 hPa band.

5.7.4 Convective instability

We finally use the ERA-Interim data to calculate the convective instability indices (Figs. 5.28 and 5.29). On 23 December, all instability indices indicated stable weather in central Iraq. In contrast, on 25 December, all indices attain values that suggest the development of vertical instability: high values of KI, SWEAT and CAPE and low positive values of LI (Fig. 19 and 20). However, the only index that exceeds the instability threshold is KI.

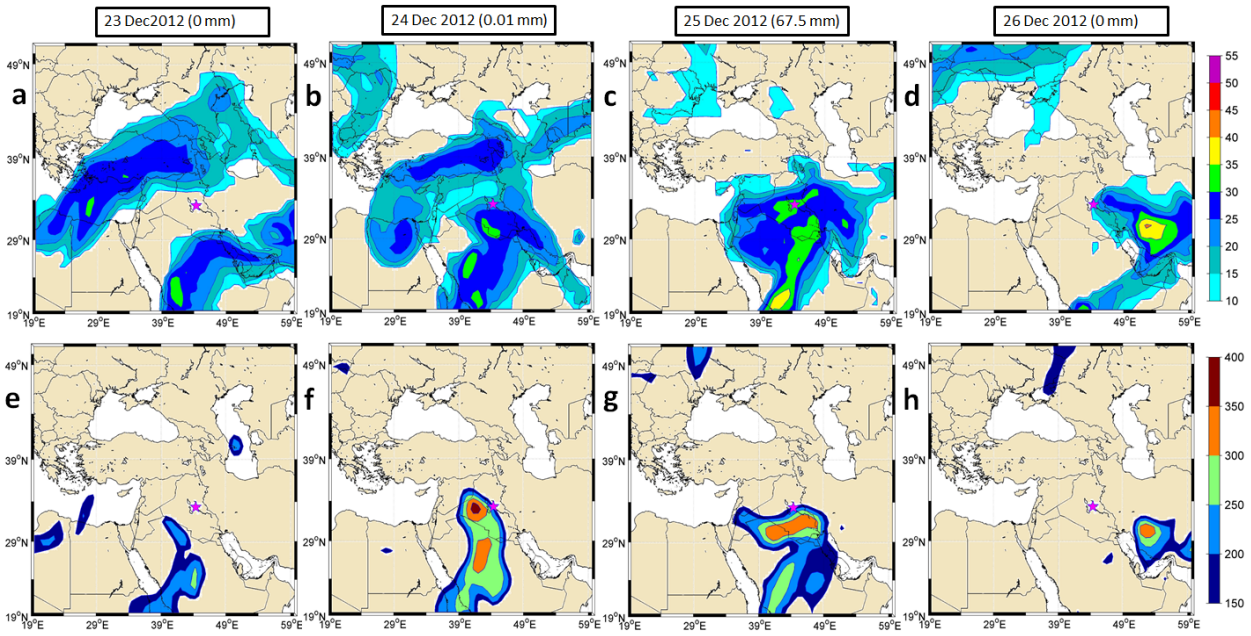

Figure 5.28. Distribution of variables, from left to right, between 23 and 26 December 2012, 1200 UTC. (Top panels) K index (colored, °C) and (bottom panels) severe weather threat index (SWEAT) (colored, dimensionless).

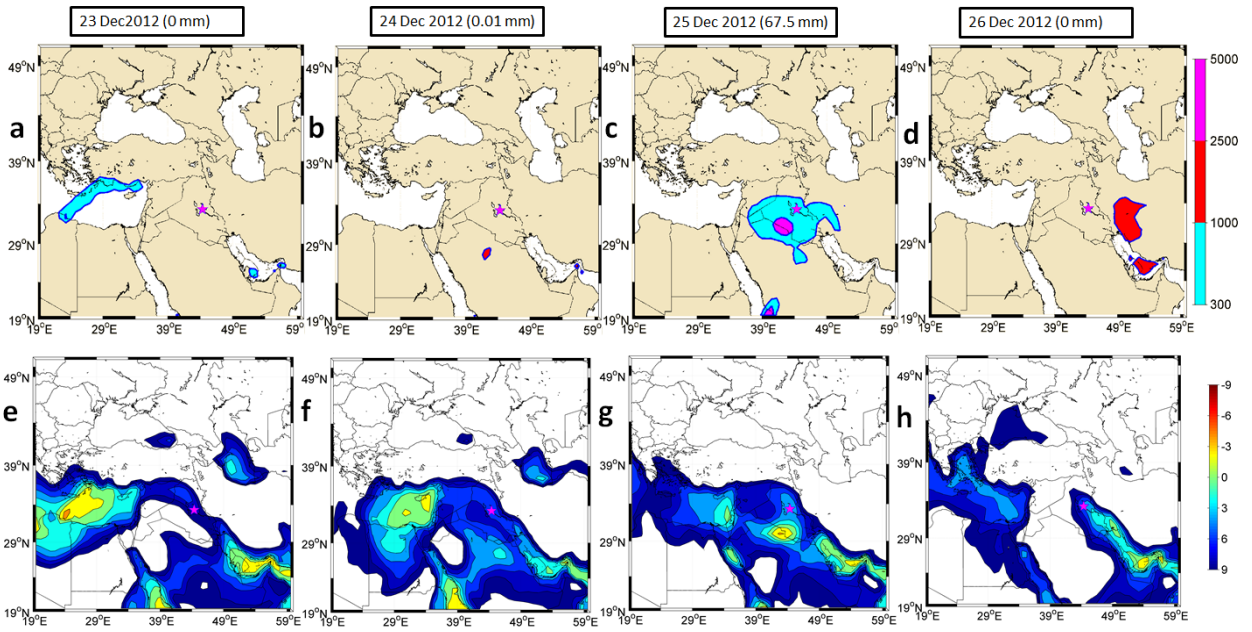

Figure 5.29. Distribution of variables, from left to right, between 23 and 26 December 2012, 1200 UTC. (Top panels) CAPE index (colored, J kg^{-1}) and (bottom panels) lifted index (LI) (colored, °C).

Chapter 6

Conclusions and Future Work

6.1 Conclusions

Rainfall over Iraq is characterized by high temporal and spatial variability, with intermittent flooding episodes. There are several studies that have explored the temporal distribution of rain over Iraq but very few have explored what are the weather patterns behind the extreme precipitation events, what is their seasonal and inter-annual variability and how much they contribute to the total annual rainfall. In this dissertation we have precisely examined these last aspects, identifying the extreme rainy episodes and exploring their contribution to the total annual precipitation in average as well as during arid and wet years, and exploring the dynamics and thermodynamics that leads to these extreme occurrences, with special emphasis on the November 2013 episode, the rainiest event over Baghdad since 1980.

For our study we have used monthly (1938-2016 period) and daily (2005-2016 period) data from the Baghdad meteorological station, ran by the Iraqi Meteorological Organization and Seismology, and reanalysis ERA-Interim global atmospheric data from the European Centre for Medium-Range Weather Forecasts (ECMWF). Our statistical analysis strictly applies to data from one single station. However, the fact that this station is located in the central plains of Iraq, in a low-elevation (34 m) location with very little topographic relief, and the circumstance that the ERA-Interim data shows good agreement with these observations, grants us confidence to extrapolate our results to the entire central Iraq and possibly also to large regions of the Middle East.

Because of the lack of summer precipitations – no rain was ever reported for June, July and August – we introduce the concept of a natural year, as corresponding to the period running from 1 July to 30 June and labeled by the final year. Hence, we analyze the annual data in terms of natural years, which decreases the time series to only 75 years, but retain all available months (77 years) for the monthly analysis. Additionally, our daily data starts in January 2005 so we can only identify the event-contributions for the last 12 years. There is also ERA-Interim reanalysis data for this period so, with the help of a cut-off detection numerical algorithm, we combine both data sets to assess the

contribution of cut-off lows to the annual precipitation, and to further describe the dynamic and thermodynamic conditions behind these rainy episodes.

We will next respond to the questions behind each of the specific objectives we posed at the start of the thesis:

1- What are the mean conditions and temporal variability of precipitation over central Iraq? The analysis of 77 years of monthly rainfall (January 1938 to December 2016 without 2003 and 2004) give a mean-annual precipitation of 135.9 ± 61.9 mm, with 43/32 years with rainfall below/above this mean value. The mean monthly precipitation for the entire period was 11.3 ± 18.7 mm. This value increases to 17.1 ± 20.9 mm if we ignore the three dry summer months (June-August), which never recorded any rainfall. Disregarding the summer months, there are 391 months (63.3%) with monthly rainfall below the mean and 223 months (36.3%) with monthly precipitation above the mean.

2- How these conditions change at inter-decadal scales? Can we talk of arid and wet periods? We indeed find very significant inter-annual and inter-decadal variations in annual and seasonal rainfall. The 75-yr annual-precipitation time series shows a small linear trend (-0.5 mm/yr), which decreases even further when we separately consider the winter and spring seasons (-0.13 and -0.11 mm/yr, respectively) but switches sign when only analyzing the autumn season (0.08 mm/yr). However, these trends are very much dependent on the period considered, with relatively wet 1950-1969 (150-170 mm/year) and arid 1990- 2009 (100-120 mm/yr) periods.

3- What do we learn from the annual-precipitation histograms? How does precipitation changes between average, arid and wet years? The years with highest precipitation were 1974, 2014 and 2013 (307.7, 278.1 and 263.6 mm), while those with the least rainfall were 2012, 1997 and 2008 (29.3, 36.6 and 37.6 mm), with 43/32 years below/above the annual average. We calculate the annual-precipitation histograms and use the 25- and 75-percentiles (88 and 174 mm) to select the arid and wet years (19 years for either one). The arid years provide a total of 1227 mm of rain (64.6 mm/yr) or 12.0% of the total precipitation; the wet years represent 4181 mm of rain (220.1 mm/yr) or 41% of the total rainfall.

4- What do we learn from the monthly-precipitation histograms? How these histograms change between average, arid and wet years? In average, January is the wettest month (29.5 mm/month) and also the one that experiences the largest inter-annual variations; November-December and February-April represent intermediate conditions and May and October correspond to low rainfall. During the arid years, the December-February period receives the largest amount of rain (10-15 mm/month) and experiences the highest variability. During the wet years, November-April collects the maximum precipitation (30-40 mm/month), with March, April and November showing the greatest variability.

5- Is there any relation between monthly precipitation in central Iraq and the El Niño-Southern Ocean (ENSO) oscillation? A careful analysis of the correlations between monthly values of precipitation in Baghdad and the NINO3.4 index shows no significant correlation. This strongly suggests that the inter-annual development of the Red Sea Trough responds to either regional or large-scale patterns that bear no relation with the ENSO global pattern.

6- What is the contribution of extreme precipitation cut-off lows to annual precipitation? During the 2005-2016 period there were a total of 94 cut-off lows that affected Iraq, with 38 of them causing rain over Baghdad and 14 producing precipitation over 20 mm. These rainy cut-off lows are very short, typically 1-3 days, for a total of only 118 days (21.6% of the total number of rainy days); however, they brought as much as 43.4% of the rainfall for the entire period. Autumn holds the highest frequency of extreme events (42.6%), followed by winter (40.5%) and spring (16.9%); however, the contribution of rainy cut-off lows to total rainfall was largest in autumn (24.2%), followed by winter (15.0%) and spring (5.5%).

7- How does the contribution of rainy cut-off lows to the total annual precipitation change between arid and wet years? The fraction of rain caused by cut-off lows did not change markedly between arid and wet years but the total amount of rain associated with these events increased by a 16 factor, from 31.3 mm during the three arid years to 512.3 mm during the three wet years (with nearly 400 mm corresponding to six extreme cut-off lows, each discharging over 30 mm). This is because rainy cut-off lows bring little water (< 10 mm) during arid years while they cause high rainfall (> 14 mm) during wet years. These data confirm that extreme-rain cut-off lows are a main factor turning an arid into a wet year.

8- What are the physical processes in the lower, middle and upper atmosphere necessary for the occurrence of extreme precipitation events? The cut-off lows take place all year long, more frequently in May-June and October-November, when a low-level cyclonic center linking the Red and eastern Mediterranean Seas (the Red Sea Trough) grows over the Middle East, and less frequently between July and September, when the Atlantic subtropical high-pressure system influences the Arabian Peninsula. During the November 2013 extreme episode, the middle and upper atmospheric conditions developed from a cut-off low into an omega block and eventually a Rex block. The eastern portion of the cyclonic structure of the Rex block experienced horizontal divergence and the associated upward motions extended all the way from 1000 to 250 hPa. During the entire event the thermodynamic conditions were only marginally unstable, hence playing a relatively minor role.

9- During severe rainfall incidents, where does the moisture come from and how it gets to central Iraq? The amount of rain associated with cut-off lows between October and December – when the surface waters of the Red Sea and Persian Gulf remain warm and can transfer water vapor to the atmosphere – accounts for about one third of the total annual rainfall (41.0 out of 130.8 mm). The 19 November 2013 event is a remarkable case of vertical motions driven dynamically by a cut-off low pattern, at a time when surface moisture arrived to central Iraq thanks to the southerly cool winds blowing over the still warm Red Sea. The surface Red Sea waters cooled likely as a result of substantial heat and water release to the atmosphere, and the low-level (1000 to 700 hPa) southerly winds converged large amounts of precipitable water into central Iraq.

10- Besides cut-off lows, are there other meteorological patterns involved in the extreme precipitation episodes? There is no unique synoptic pattern leading to high precipitation. The analysis of all extreme rainy episodes (above the 90-percentile) shows that there were 7 events related with Rex block conditions (causing 324.1 mm or 40.3% of the total extreme-event precipitation), 7 happenings associated with cut-off-lows (252.6 mm or 31.4%), 2 episodes during jet streak conditions (95.3 mm or 11.8%), and 4 events related with upper-air troughs (133.2 mm or 16.5%). All extreme rainfall episodes require low-level convergence of humid air, vertical ascending motions and upper-level divergence.

1.2 Future work

Chapters 3 and 4 of this dissertation have been submitted to a high-impact journal as an article entitled "Cut-off lows over Iraq: contribution to annual precipitation and synoptic description of extreme events", by Ali Raheem Al-Nassar, Pablo Sangrà, Marta Alarcon, Agusti Jansa and Josep L. Pelegrí. The revision and completion of this manuscript is currently work in progress.

As part of our work, we have applied the cut-off low detection algorithm in order to trace back in time the origin and evolution of the extreme episodes. Some preliminary results have been obtained but they have not been included in this dissertation, further research is currently in progress. This detection and backtracking technique could also be applied to identify the origin and evolution of the low-atmosphere cyclones and associated winds.

Our work has opened many additional questions, which may become the subject of future research. A short list of some of these questions, that we plan to explore as an extension of the work carried out during this dissertation, is the following:

a- Is there a global index that correlates significantly with the monthly precipitation records over the Middle East?

b- Could we identify the lower- and upper-atmosphere developments that precede the vertical coupling during extreme precipitation episodes?

c- What is the main coupling mechanism between the lower- and upper-atmosphere patterns and how does it operate?

d- Could we develop a predictor index that combines lower and upper atmospheric conditions with the sea surface temperature in the Red Sea and Persian Gulf?

References

Al-Ameri BY. 2014. Using remote sensing techniques on the study to analyze the rain on 25/12/2012 over Iraq and its relationship with lightning strokes. *Al-Mustansiriyah Journal of Science* **25**: 83-94

Al-Ansari NA. 2013. Management of water resources in Iraq: perspectives and prognoses, *Engineering* **5**: 667-684.

Al-Ansari NA, Knutsson S. 2011. Toward prudent management of water resources in Iraq. *Journal of Advanced Science and Engineering Research* **1**: 53-67.

Aldsaa SA, Shalal IH. 2007. The relationship between the amount of rainfall and the number of rainy days in Iraq. *Al-Mustansiriyah Journal of Science* **18**: 49-62.

Al-Dulimi A. 2005. *Variation Quantity of Rainfall in Iraq and its Role in Determination the Scope of Rainfed-Farming for the Cultivation of Sun flower*. Master degree in Geography, College of Education, University of Baghdad (in Arabic).

Alghazali N, Alawadi D. 2014. Fitting statistical distributions of monthly rainfall for some Iraqi stations. *Civil and Environmental Research* **6**: 40-46.

Al-Mansory HB. 2005. Statistical analysis of extreme monthly rainfall in Basrah City, South of Iraq. *Marina Mesopotamica* **20**: 283-296.

Al-Rijabo W, Salih H. 2013. Spatial and temporal variation of rainfall in Iraq. *IOSR Journal of Applied Physics* **4**: 1-7.

Al-Salihi1 AM, Mohammed TH. 2015. The effect of dust storms on some meteorological elements over Baghdad , Iraq: Study Cases. *IOSR Journal of Applied Physics* **7**: 1-7.

Al-Salihi A, Al-lami A, Altemimi Y. 2014. Spatio-temporal analysis of annual and seasonal rainfall trends for Iraq. *Al-Mustansiriyah Journal of Science* **1**: 153-168.

Al-Suhili R, Khanbilvardi R. 2014. Frequency analysis of the monthly rainfall data at Sulaimania region, Iraq. *American Journal of Engineering Research* **5**: 212-222.

Al-Timimi Y. 2012. *Assessment of Drought in Iraq Using Standardized Precipitation Index (SPI) and Satellite Data*. Doctoral dissertation, Al-Mustansiriya University.

Al-Timimi Y, Al-Jiboori M. 2013. Assessment of spatial and temporal drought in Iraq during the period 1980-2010. *International Journal of Energy and Environment* **2**: 291-302.

Asakereh H. 2017. Trends in monthly precipitation over the northwest of Iran (NWI). *Theoretical and Applied Climatology* **130**: 443–451.

Babu CA, Samah AA, Varikoden H. 2011. Rainfall climatology over Middle East region and its variability. *International Journal of Water Resources and Arid Environments* **1**: 180-192.

Banacos PC, Schultz DM. 2005. The use of moisture flux convergence in forecasting convective initiation: Historical and operational perspectives. *Weather and Forecasting* **3**: 351-366.

Barlow M, Wheeler M, Lyon B, Cullen H. 2005. Modulation of daily precipitation over Southwest Asia by the Madden-Julian Oscillation. *Monthly Weather Review* **133**: 3579-3594.

Barth HJ, Steinkohl F. 2004. Origin of winter precipitation in the central coastal lowlands of Saudi Arabia. *Journal of Arid Environments* **57**: 101-115

Bitan A, Sa'aroni H. 1992. The horizontal and vertical extension of the Persian Gulf trough. *International Journal of Climatology* **12**: 733-747.

Columbia. 2018. *North Atlantic Oscillation*. Lamont-Doherty Earth Observatory, Columbia Univesity, http://www.ldeo.columbia.edu/res/pi/NAO/, last accessed 21 May 2018.

Cullem HM, Kaplan A, Arkin PA, Demenocal PB. 2002. Impact of the North Atlantic Oscillation on Middle Eastern climate and streamflow. *Climatic Change* **55**: 315–338.

Davini P. 2013. *Atmospheric Blocking and Winter Mid-latitude Climate Variability*. Doctoral Dissertation, Universitá Ca' Foscari, 141 pp.

Easterling DR, Meehl GA, Parmesan C, Changnon SA, Karl TR, Mearns LO. 2009. Climate extremes: observations, modeling, and impacts. *Science* **289**: 2068-2074.

Galway JG. 1956. The lifted index as a predictor of latent instability. *Bulletin of the American Meteorological Society* **37**: 528–529.

George JJ. 1960. *Weather Forecasting for Aeronautics*. Academic Press, 673 pp.

Ghulam A, Qin Q, Kusky T, Li ZL. 2008. A re-examination of perpendicular drought indices. *International Journal of Remote Sensing* **29**: 6037-6044.

Hadi AS. 2013. Analysis pressure system for low and high rainy year in Iraq during trims 1970/1971- 1998/1999. *Diyala Journal For Human Science* **60**: 573-614 (in Arabic).

Hanson C, 2007. *Long-range Operational Military Forecasts for Iraq*. MSc Thesis, Department of Meteorology, Naval Postgraduate School, 77 pp.

Hurrell JW, Kushnir Y, Otterson G, Visbeck M. 2003. An overview of the North Atlantic Oscillation. In: *The North Atlantic Oscillation: Climatic Significance and Environmental Impact*, pp. 1-34, edited by JW Hurrell, Y Kushnir, G Otterson and M Visbeck, Geophysical Monography, 134, American Geophysical Union.

Hussein M, Awad M, Jabbar A. 2005. Distribution of rainfall, runoff and soil moisture storage in the low rainfall zone of northern Iraq. *Journal of Environmental Hydrology* **13**: 26.

IAU. 2012. *Climate change in Iraq*. Fact sheet June 2012, Inter-Agency Information and Analysis Unit, https://reliefweb.int/map/iraq/iraq-climate-change-iraq-june-2012, last accessed 5 November 2017.

Jassim SZ, Goff JC. 2006. *Geology of Iraq*. Dolin Prague and Moravian Museum, Brno, distributed by Geological Society of London, 486 pp.

Karamouz M, Razavi S, Araghinejad S. 2008. Long-lead seasonal rainfall forecasting using time-delay recurrent neural networks: a case study. *Hydrological. Processes* 22, 229–241.

Kassomenos PA, McGregor GR. 2006. The interannual variability and trend of precipitable water over southern Greece. *Journal of Hydrometeorology* **6**: 271-284.

Khidher SA, Pilesjö P. 2015. The effect of the North Atlantic Oscillation on the Iraqi climate 1982–2000. *Theoretical and Applied Climatology* **122**: 771-782.

KNMI. 2018. *Time Series Monthly NINO3.4*. KNMI Climate Explorer, https://climexp.knmi.nl, last accessed 25 June 2018.

Krichak SO, Barkan J, Breitgand JS, Gualdi, Feldstein SB. 2015. The role of the export of tropical moisture into midlatitudes for extreme precipitation events in the Mediterranean region. *Theoretical and Applied Climatology* **121**: 499-515.

Lionello P. 2012. *The climate of the Mediterranean region: from the past to the future*. Elsevier, Amsterdam, 592 pp.

Lorente P, Hernández E, Queralt S, Ribera P. 2008. The flood event that affected Badajoz in November 1997. *Advances in Geosciences* **16**: 73-80.

Malinowski JC. 2002. *Iraq: A Geography*. Department of Geography and Environmental Engineering, United States Military Academy, West Point, NY.

Mariotti A. 2007. How ENSO impacts precipitation in southwest central Asia. *Geophysical Research Letters* **34**, L16706.

McKee B, Doesken NJ, Kleist N. 1993. The relationship of drought frequency and duration to time scales. *Proceedings of 8th Applied Meteorology*, pp. 179-184, Anaheim, CA, American Meteorological Society, Boston.

Miller JA. 1972. *Notes on analysis and severe storms forecasting procedures of the Air Force global weather central*. AWS–USAF Tech. Rep. 200, Headquarters Air Weather Service, Scott Air Force Base, IL, 102 pp.

Mohammed T. 2009. Variations and Probabilities of annual rainfall in the Wavy Region of Iraq, *Journal of Al-Adab Baghdad University* **90**: 263-291 (in Arabic).

Mohammed T, Hadi A. 2012. Deviations in the amount of annual Rainfall on Iraq, compared with the general rates during the period 1970/1971-1999/2000. *Journal of Research Diyala University* **54**: 456-485 (in Arabic).

NOAA. 2017. *National Weather Service Glossary*. National Oceanic and Atmospheric Administration, http://forecast.weather.gov/glossary.php, last accessed 5 November 2017.

Omer TM. 2011. *Country Pasture/Forage Resource Profiles Ira*q, FAO, Rome, 34 pp.

Peixoto JH, Oort AH. 1992. *Physics of Climate*. American Institute of Physics, 520 pp.

Philander GS. 1990. *El Nino, La Nina, and the Southern Oscillation*. Academic Press, San Diego.

Ropelewski F, Halpert MS. 1987. Global and regional scale precipitation patterns associated with the El Niño/Southern Oscillation. *Monthly Weather Review* 115: 1602-1626.

Salehvand S, Montazeri M, Gandomkar A, Moemeni M, Ataei H. 2015. Study Pressure Fields Affecting Cyclone Rainfall: Case Study of Iran. *Atmospheric and Climate Sciences* **5**, 129-136.

Sanders F, Hoskins BJ. 1990. An easy method for estimation of Q-vectors from weather maps. *Weather and Forecasting* **2**: 346-353.

Scherrer S, Croci-Maspoli M, Schwierz C, Appenzeller C. 2006. Two-dimensional indices of atmospheric blocking and their statistical relationship with winter climate patterns in the Euro-Atlantic region. *International Journal of Climatology* **26**: 233-249.

Showalter AK. 1953. A stability index for thunderstorm forecasting. *Bulletin of the American Meteorological Society* **6**: 250–252.

Sissakian VK, Al-Ansari N, Knutsson S. 2013. Sand and dust storm events in Iraq. *Natural Science* **5**: 1084-1094.

Terink W, Immerzeel W, Droogers P. 2013. Climate change projections of precipitation and reference evapotranspiration for the Middle East and Northern Africa until 2050. *International Journal of Climatology* **14**: 3055-3072.

Tibaldi S, Molteni F. 1990. On the Operational Predictability of Blocking. *Tellus* **42A**: 343-365.

Tsvieli Y, Zangvil A. 2007. Synoptic climatological analysis of Red Sea Trough and non-Red Sea Trough rain situations over Israel. *Advances in Geosciences* **12**: 137-143.

Ukkonen P. 2015. Evaluation of thunderstorm predictors for Finland using reanalysis and neural networks. *Journal of Applied Meteorology and Climatology* **56**: 2821-2844.

UN-Iraq. 2010. *Drought Impact Assessment, recovery and mitigation framework and regional project design in Kurdistan region (KR)*. United Nations Development Programme Iraq, December 2010, 77 pp.

UN-Iraq. 2013. *Water in Iraq*. Fact sheet March 2013, Joint Analysis and Policy Unit, United Nations, https://reliefweb.int/sites/reliefweb.int/files/resources/Water-Factsheet.pdf, last accessed 5 November 2017.

Van Delden A. 2001. The synoptic setting of thunderstorms in western Europe. *Atmospheric Research* **1**: 89-110.

Van Zomeren J, van Delden A. 2007. Vertically integrated moisture flux convergence as a predictor of thunderstorms. *Atmospheric Research* **2**: 435-445.

Vojtesak MJ, Martin KP, Myles G, Gilford MT. 1991. *SWANEA (Southwest Asia-Northeast Africa) – A climatological study, Vol II – The Middle East peninsula*. USAFETAC TN-91/002, USAF Environmental Technical Applications Center, 246 pp.

Vorhees D. 2006. *The impacts of global scale climate variations on Southwest Asia*. MSc Thesis, Department of Meteorology, Naval Postgraduate School.

Walker, M. 2005. *Iraq – A full year study*. Report AFCCC/CCD-05/002, Air Force Combat Climatology Center, 112 p.

Walters KR, Sjoberg WF. 1988. The Persian Gulf region a climatological study. USAF Environmental Technical Applications Center, pp. 1-62.

Weisman ML, Klemp JB. 1986. Characteristics of isolated convective storms, In *Mesoscale Meteorology and Forecasting*, pp. 331-358, edited by PS Ray, American Meteorological Society.

Xoplaki E, González-Rouco JF, Luterbacher J, Wanner H. 2004. Wet season Mediterranean precipitation variability: influence of large-scale dynamics and trends. *Climate Dynamics* **23**: 63–78

Yao F. 2008. *Water Mass Formation and Circulation in the Persian Gulf and Water Exchange with the Indian Ocean*. PhD Dissertation, University of Miami.

Zakaria S, Al-Ansari N, Ezz-Aldeen M., Knutsson S. 2012. Rain water harvesting at eastern Sinjar Mountain, Iraq. *Geoscience Research* **3**, 100.

Zangana LM. 2007. *The Location of the Jet Stream and its Impact in the Depressions and Rain in Iraq*. Kurdistan Center for Strategic Studies Salmaniya (in Arabic).

Zangvil A. 2005. Synoptic climatological analysis of 'wet' and 'dry' Red Sea Troughs over Israel. *International Journal of Climatology* **25**: 1997-2015.

Projects and Publications

Participation in competitive projects

- New TEChnologies for the study of the diversity and dynamics of aeroBiOlogical components and for their forecast based on METeorology (TECBIOMET, reference number CTM2017-89565-C2-2-P), Ministerio de Economía, Industria y Competitividad, January 2018 to December 2020, PI Marta Alarcón Jordán.

- Atmospheric bio-aerosols: levels, transport and impacts (BATMAN, reference number CGL2012-39523-C02-02), Ministerio de Economía y Competitividad, January 2013 to May 2016, PI Marta Alarcón Jordán.

Communications at international meetings

- Al-Nassar A, Sangrà P, Alarcón M, Jansà A, Ramis C. 2015. The flood event that affected Iraq on November 2013: a synoptic approach. 5th METMED International Conference on Meteorology and Climatology of the Mediterranean, Istanbul, Turkey, March 2-4 2015.

- Al-Nassar A, Sangrá P, Alarcón M. 2016. Extreme precipitation events and related weather patterns over Iraq. *Geophysical Research Abstracts* 18, EGU2016-7423, EGU General Assembly, Vienna, Austria, 23-28 April 2017.

Publications in Journals

- Al-Nassar AR, Sangrà P, Alarcon M, Jansa A, Pelegrí JL. 2018. Cut-off lows over Iraq: contribution to annual precipitation and synoptic description of extreme events. *International Journal of Climatology*, under revision.